Establishment and characterisation of tumour-bearing mouse models for evaluation of biodistribution of a radiopharmaceutical

PC Koatale

orcid.org/ 0000-0002-2659-0454

Dissertation submitted in fulfilment of the requirements for the degree Master of Science in Pharmaceutical Sciences at the North West University

Supervisor:	Prof R Hayeshi
Co-supervisor:	Prof AM Engelbrecht
Assistant supervisor:	Dr C Driver

Graduation: May 2019

Student number: 29438853

DECLARATION

I, Palesa Caroline Koatale, hereby declare that the dissertation submitted by me is my own independent work and has not previously been submitted by me at another university.

Signature:

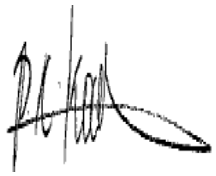

Date: 12/11/2018

PREFACE

This dissertation is submitted in accordance with the requirements for a Master of Science degree in Pharmaceutical Sciences, at the North-West University, Potchefstroom Campus. Chapters 3 and 4 are written in an article format (unpublished) and include: the abstract, introduction, methods and materials, results, discussion and conclusion. NWU Harvard referencing style is used throughout this thesis and the references are provided at the end of each chapter.

ACKNOWLEDGEMENTS

Firstly, my utmost gratitude goes to my Holy Father in Heaven. Father I have seen your glory in my life, and your peace and comfort have sustained me through this journey.

I would like to acknowledge the following people for their contributions and support in making this project a success.

- **Prof Rose Hayeshi**, thank you for your guidance and for always believing in me more than I believed in myself. For all the contributions you made towards my personal and professional development, words can never be enough to express my gratitude. You are the best supervisor one could ever have and I count myself among the most fortunate to have had an opportunity to work with you.

- **Prof Anna-Maart**, we never met but thank you for the time and effort you put into my thesis. To work with someone who has made an enormous contribution in the field of cancer research, was a privilege.

- **Dr Cathryn Helena Driver**, thank you for giving me an opportunity to be part of your project, it was the most exciting part of my research. I highly appreciate your expertise and the contribution you made during the writing process.

- **Dr Ambrose Okem**, thank for your constant guidance and support from the beginning to the end of this journey. Your valuable input and expertise makes part of the skeleton of this project.

- **Mr Kobus Venter**, **Mr Cor Bester** and **Ms Antoinette Fick**, thank you for your assistance and for always availing yourself when I had to inoculate the mice.

- **Prof Che Weldon**, thank you for providing me with histology training and for your constant assistance in the laboratory when I was struggling. It was a privilege to work with you and the atmosphere in your lab made it most exciting place in which to work.

- **Dr Louis De Jager**, thank you for assisting me with the histology interpretation. This was the most difficult section of my project but your input made it the most exciting section to write.

- **Dr Adrienne Leussa,** thank you for helping me with confocal imaging. Your enthusiasm encouraged me through those long hours of frustration.

- **Prof Lissinda Du Plessis**, thank you for providing me with flow cytometry training.

- **The Nesca staff**, thank you for your expertise and the time you contributed during the imaging study.

- **Dr John Takyi-Williams**, thank you for your friendship and words of encouragement when things were not working. There were times when I was struggling to construct my ideas and our long discussions helped me to have a better perspective.

- To my cousin, **Goitsemang Prudance Mngomezulu**, thank you for being my pillar of strength. I am grateful to have you in my life.

- To my friend, **Mamello Mathebula**, thank you for your support and for always cheering me up. Research can be a very lonely journey, but having friends like you makes it bearable.

- To my family, **Selobelwang**, **Tebogo** and **Molebatsi Koatale**, thank you for always supporting me, your love for me is comforting.

- To the staff of the DST/NWU Preclinical Drug Development Platform (PCDDP), thank you for your support and for creating a conducive working environment.

"No eye has seen, no ear has heard, and no mind has imagined what God has prepared for those who love him." **1 Corinthians 2:9**

ABSTRACT

Introduction: To improve early detection of breast and ovarian cancer, characterised animal models of cancer are required for screening novel tumour-specific imaging radiopharmaceuticals. The purpose of this study was to establish and characterise allograft and xenograft tumour mouse models of breast and ovarian malignancies, respectively, for evaluation of ^{64}Cu-GluCAB, a novel imaging radiopharmaceutical intended to target tumours through their high expression of glucose receptor (GLUT-1) and their increased vascularisation.

Methods: The breast tumour allograft model was established by subcutaneous inoculation of E0771 cells suspended in Matrigel into the mammary fat pad of female C57BL/6 mice. The ovarian tumour xenograft model was established by subcutaneous inoculation of OVCAR-3 cells, with and without Matrigel, above the proximal tibia of the female athymic nude (nu/nu) mice. Tumour growth was monitored using a digital calliper and the tumours were excised after reaching the end-point tumour volume (≥300 mm^3) to determine the tumour growth rate and confirm malignancy using haematoxylin and eosin (H &E) staining.

To illustrate the application of the tumour models established, the E0771 derived allograft model was used for investigation of the *ex vivo* biodistribution and *in vivo* imaging of ^{64}Cu-GluCAB. The mice were administered intravenously with ^{64}Cu-GluCAB precursor (without albumin) and images acquired at 1, 2, 6 and 24 hours using microPET/CT. After 24 hours, blood, tumours and several organs and tissues were collected to determine the compound biodistribution using a gamma counter. Flow cytometry and immunofluorescence staining were conducted in order to evaluate the expression of the GLUT-1 receptor in E0771 cells and E0771 derived tumours.

Results: Palpable tumours were detected within one-week post inoculation for the E0771 derived allograft model, with a tumour take rate of 100% (26/26) and average tumour growth rate of 0.03 g/day based on the final *ex vivo* tumour weight. For the OVCAR-3 derived xenograft model, tumours were palpable within approximately one month and two months with and without Matrigel, respectively, however, the tumour growth rate (based on the final *ex vivo* tumour weight) with or without Matrigel was statistically insignificant ($p>0.05$). Histological analysis revealed that the tumours of both models were malignant and actively proliferating.

The biodistribution profile of ^{64}Cu-GluCAB illustrated high accumulation of radioactivity in the plasma (4.07 ± 0.21%ID/g), confirming that ^{64}Cu-GluCAB precursor (without albumin) bound to albumin *in vivo* thereby increasing the biological half-life of the compound. In correlation with the microPET/CT images, high uptake was observed in the liver (3.63 ± 0.80 %ID/g) and large intestine (2.82 ± 1.29 %ID/g), suggesting hepatobiliary excretion of the compound. In contrast, uptake of ^{64}Cu-GluCAB by tumours (0.95 ± 0.30 %ID/g) and other organs was minimal. Moreover,

the tumours could not be visualised using microPET/CT. Evaluation of GLUT-1 receptor expression in E0771 cells and E0771 derived tumour, yielded inconclusive results.

Conclusion: The tumour-bearing mouse models of breast and ovarian cancers were successfully developed and characterised. Although the expression of the GLUT-1 receptor could not be confirmed, the biodistribution profile of ^{64}Cu-GluCAB indicated a minimal amount of uptake by the tumour. The low radioactivity signal could however not be used for localisation and visualisation of the tumour by microPET/CT.

Key words: Breast cancer; Ovarian cancer; Allograft; Xenograft; E0771 cells; OVCAR-3 cells; radiopharmaceutical; ^{64}Cu-GluCAB; microPET/CT

TABLE OF CONTENTS

LIST OF TABLES

CHAPTER 2

CHAPTER 3

CHAPTER 4

LIST OF FIGURES

CHAPTER 2

CHAPTER 3

CHAPTER 4

ABBREVIATIONS

ADH	Atypical ductal hyperplasia
ANOVA	Analysis of variance
ATCC	American Type Culture Collection
β	Beta decay
BC-G	Breast cancer group
BFCA	Bifunctional chelating agent
BSE	Breast cancer self-examination
BRCA	Breast cancer Susceptibility gene
CA	Cancer antigen
CBE	Breast cancer examination
CO_2	Carbon dioxide
CT	Computational tomography
^{64}Cu	Copper-64
DCI	Ductal carcinoma *in situ*
DMEM	Dulbecco's modified eagle medium
E0771	Murine mammary adenocarcinoma
EGFR	Epidermal growth factor receptor
EPR	Enhanced permeability and retention
^{18}F	Fluorine-18
FDG	Fluoro-2-deoxyglucose
FBS	Foetal bovine serum
FITC	Fuorescein isothiocyanate
GETM	Genetically engineered tumour models
GluCAB	Glucose-cyclam-albumin
GLUT	Glucose transporter
H & E	Haematoxylin and eosin
HEPES	4-(2-hydroxyethyl)-1-piperazineethanesulfonic acid

H + L	Heavy and light specificity
IgG	Immunoglobulin
IVC	Individually ventilated cages
MRI	Magnetic resonance imaging
Nesca	South African Nuclear Energy Corporation
NWU	North-West University
OSE	Ovarian surface epithelium
OVCAR-3	Human ovarian adenocarcinoma cell line
OV-G	Ovarian cancer group
PBS	Phosphate buffered saline
PCDDP	DST/NWU Preclinical Drug Development Platform
PET	Positron emitting tomography
RPMI	Roswell Park Memorial Institute
SCID	Severe combined immune-deficient
SD	Standard deviation
SPECT	Single photon emission computed tomography
TDLU	Terminal duct lobular units
TVUS	Transvaginal ultrasonography

UNITS

˚C	degree Celsius
g	gram
hr	hour(s)
kDa	kilodation
keV	kiloelectron volt
M	molar
mg	milligram
min	minutes(s)
ml	millilitre
mm^3	cubic millimetre
ng	nanogram
nm	nanometre
Pa	Pascal
rpm	rotations per minute
$t_{1/2}$	half-life
µg	microgram
µl	microliter
µm	micrometre
%	percentage
%ID/g	percentage of the injected dose per gram of tissue

CHAPTER 1: INTRODUCTION, PROBLEM STATEMENT AND AIMS

1.1 Introduction

Cancer is a heterogeneous disease characterised by the accumulation of genetic mutations at cellular level leading to uncontrolled cell growth and proliferation, which ultimately progresses into a population of cells that can invade tissues and metastasise (Chen *et al.*, 2014; Li & Wang, 2014). These genetic mutations affect various pathways, such as proliferation, signalling, metabolism, apoptosis and angiogenesis that are necessary for the regulation of normal biological activities (Hanahan & Weinberg, 2000). Cancer is predicted to rank as the leading cause of death worldwide in the 21st century, with approximately 9.6 million deaths and 18.1 million newly diagnosed cases estimated in 2018 (Bray *et al.*, 2018). Among the malignancies affecting women, a significant increase of deaths was observed for breast and ovarian cancer from 2005 to 2015 (Wang *et al.*, 2016), with a global estimate of 626 679 and 184 799 deaths in 2018, respectively (Bray *et al.*, 2018).

Currently, one of the significant challenges contributing to the high mortality rate of breast and ovarian cancer is a late diagnosis (Gu *et al.*, 2016; Latha *et al.*, 2014). If the cancer is accurately detected and a diagnosis made early enough, the treatment outcome may be greatly improved and the number of mortality cases reduced (Kramer-Marek & Capala, 2012). The most routinely used diagnostic imaging techniques for cancer include mammography, ultrasound, X-ray computed tomography (CT) and magnetic resonance imaging (MRI). These techniques however often fall short in that they only provide anatomical information from which to make a diagnosis (Lu, 2017). Unlike conventional imaging, single photon emission computed tomography (SPECT) and positron-emission tomography (PET) imaging are newer techniques capable of imaging the entire tumour and possible metastases. These techniques work on the principle of administration and detection of radiolabeled compounds known as radiopharmaceuticals (Aerts *et al.*, 2014). Recently, there has been an increased interest in the development of target-specific diagnostic radiopharmaceuticals for the early and precise diagnosis of cancers, such as malignancies of the breast and ovaries (Aerts *et al.*, 2014). The Nuclear Energy Corporation of South Africa (Necsa) has recently developed a radiopharmaceutical called GluCAB, which is labelled with the positron- emitting isotope copper-^{64}[Cu], and applies these tumour-targeting principles in an attempt to improve cancer diagnosis.

In cancer drug development, animal models of cancer play a crucial role in the study of the molecular mechanisms of the disease, and are a prerequisite for the clinical evaluation of any anticancer or imaging radiopharmaceutical agent that has shown potential *in vitro* (Cekanova & Rathore, 2014). *In vivo* cancer models are categorised as either *in situ,* occurring spontaneously or by induction, or transplantable, occurring by implantation of cancer cells. *In situ* tumour models

are also subcategorised according to the method of tumour induction, either by chemical or genetic means and are frequently used to investigate factors responsible for triggering cancer initiation and development (Shields & Price, 2007). Transplantable tumour models are subcategorised based on the site of implantation and the species in which the tumour originated. More commonly, transplantable tumour models are established by subcutaneous or orthotopic implantation of tumour cells, or biopsies, into a similar (termed allograft) or different (termed xenograft) species from that of origin (Workman *et al.*, 2010). Contrary to *in situ* tumour models, transplantable tumour models are preferable for drug efficacy evaluation due to ease of establishment and monitoring of tumour growth (Navale, 2013; Shields & Price, 2007).

The focus of this study was to develop characterised breast cancer allograft and ovarian cancer xenograft models using immune-competent and immune-compromised mice, respectively. Furthermore, the study aimed to determine if the breast tumour can be detected, and imaged, using a microPET/CT scanner through localisation of the radiopharmaceutical ^{64}Cu-GluCAB in the tumour.

1.2 Problem statement

Although there have been improvements in treating breast and ovarian malignancies, the death rates remain high due to late diagnosis and failure to identify metastases. ^{64}Cu-GluCAB, a target-specific radiopharmaceutical, is intended to solve this problem by combining a dual targeting approach for localisation in the tumour leading to early detection of the cancer. However, successful evaluation and validation of radiopharmaceuticals such as ^{64}Cu-GluCAB for targeted imaging of malignancies, including breast and ovarian cancers, requires the establishment and provision of animal models of cancer.

1.3 Research aim and objectives

1.3.1 Research aim

The primary aim of this study was to establish and characterise ovarian cancer xenograft and breast cancer allograft models. In addition, the study aimed to use the breast cancer allograft model for first time pre-clinical evaluation of ^{64}Cu-GluCAB and its effectiveness for cancer imaging.

1.3.2 Research objectives

The following objectives were set to achieve the above mentioned aim of the study:

- To grow and maintain OVCAR-3 and E0771 cancer cells *in vitro.*
- To grow OVCAR-3 and E0771 derived tumours *in vivo* in immune-compromised (nu/nu) and immune-competent mice (C57BL/6) respectively.
- To determine the tumour growth pattern.
- To describe the histology of the tumours using haematoxylin and eosin (H & E) staining.
- To quantify expression of glucose transport (GLUT-1) receptor in the E0771 cancer cell line using flow cytometry.
- To evaluate E0771 derived tumours for the expression of GLUT-1 receptor using immunofluorescence.
- To evaluate uptake and biodistribution of ^{64}Cu-GluCAB in the E0771 breast cancer allograft model using microPET/CT imaging.

REFERENCES

Aerts, A., Impens, N.R., Gijs, M., D'huyvetter, M., Vanmarcke, H., Ponsard, B., Lahoutte, T., Luxen, A. & Baatout, S. 2014. Biological carrier molecules of radiopharmaceuticals for molecular cancer imaging and targeted cancer therapy. *Current pharmaceutical design*, 20(32):5218-5244.

Bray, F., Ferlay, J., Soerjomataram, I., Siegel, R.L., Torre, L.A. & Jemal, A. 2018. Global cancer statistics 2018: GLOBOCAN estimates of incidence and mortality worldwide for 36 cancers in 185 countries. *CA: A cancer journal for clinicians*, 0(0):3-31.

Cekanova, M. & Rathore, K. 2014. Animal models and therapeutic molecular targets of cancer: utility and limitations. *Drug design development therapy*, 8:1911-1921.

Chen, Y., Williams, V., Filippova, M., Filippov, V. & Duerksen-Hughes, P. 2014. Viral carcinogenesis: Factors inducing DNA damage and virus integration. *Cancers*, 6(4):2155.

Gu, B., Cai, J., Zhang, J., Xu, X., Luo, J., Zhou, X., Zheng, Y. & Zhang, Y. 2016. 99m Tc-labeled and gadolinium-chelated transferrin enhances the sensitivity and specificity of dual-modality SPECT/MR imaging of breast cancer. *RSC Advances*, 6(25):20532-20541.

Hanahan, D. & Weinberg, R.A. 2000. The hallmarks of cancer. *Cell*, 100(1):57-70.

Kramer-Marek, G. & Capala, J. 2012. The role of nuclear medicine in modern therapy of cancer. *Tumor biology*, 33(3):629-640.

Latha, T.S., Panati, K., Gowd, D.S.K., Reddy, M.C. & Lomada, D. 2014. Ovarian cancer biology and immunotherapy. *International reviews of immunology*, 33(5):428-440. (Abstract).

Li, C. & Wang, J. 2014. Quantifying the underlying landscape and paths of cancer. *Journal of The Royal Society Interface*, 11(100):0774.

Lu, Z.-R. 2017. Magnetic resonance molecular imaging for non-invasive precision cancer diagnosis. *(In* Millan, J.D.R. & Rollins, A., *eds*. Current Opinion in Biomedical Engineering. Elsevier. p. 67-73).

Navale, A.M. 2013. Animal models of cancer: a review. *International journal of pharmaceutical sciences and research*, 4(1):19.

Shields, A.F. & Price, P. 2007. *In vivo* imaging of cancer therapy: Humana Press. Available: https://books.google.co.za/books?hl=en&lr=&id=WqZjZppx5KUC&oi=fnd&pg=PR5&dq=Shields,+A.F.+%26+Price,+P.++2007 Date of access 03 Aprl.2017.

Wang, H., Naghavi, M., Allen, C., Barber, R.M., Bhutta, Z.A., Carter, A., Casey, D.C., Charlson, F.J., Chen, A.Z., Coates, M.M., Coggeshall, M., Dandona, L., Dicker, D.J., Erskine, H.E., Ferrari, A.J., Fitzmaurice, C., Foreman, K., Forouzanfar, M.H., Fraser, M.S., Fullman, N., Gething, P.W., Goldberg, E.M., Graetz, N., Haagsma, J.A., Hay, S.I., Huynh, C., Johnson, C.O., Kassebaum, N.J., Kinfu, Y., Kulikoff, X.R., Kutz, M., Kyu, H.H., Larson, H.J., Leung, J., Liang, X., Lim, S.S., Lind, M., Lozano, R., Marquez, N., Mensah, G.A., Mikesell, J., Mokdad, A.H., Mooney, M.D., Nguyen, G., Nsoesie, E., Pigott, D.M., Pinho, C., Roth, G.A., Salomon, J.A., Sandar, L., Silpakit, N., Sligar, A., Sorensen, R.J.D., Stanaway, J., Steiner, C., Teeple, S., Thomas, B.A., Troeger, C., VanderZanden, A., Vollset, S.E., Wanga, V., Whiteford, H.A., Wolock, T., Zoeckler, L., Abate, K.H., Abbafati, C., Abbas, K.M., Abd-Allah, F., Abera, S.F., Abreu, D.M.X., Abu-Raddad, L.J., Abyu, G.Y., Achoki, T., Adelekan, A.L., Ademi, Z., Adou, A.K., Adsuar, J.C., Afanvi, K.A., Afshin, A., Agardh, E.E., Agarwal, A., Agrawal, A., Kiadaliri, A.A., Ajala, O.N., Akanda, A.S., Akinyemi, R.O., Akinyemiju, T.F., Akseer, N., Lami, F.H.A., Alabed, S., Al-Aly, Z., Alam, K., Alam, N.K.M.,

Alasfoor, D., Aldhahri, S.F., Aldridge, R.W., Alegretti, M.A., Aleman, A.V., Alemu, Z.A., Alexander, L.T., Alhabib, S., Ali, R., Alkerwi, A.a., Alla, F., Allebeck, P., Al-Raddadi, R., Alsharif, U., Altirkawi, K.A., Martin, E.A., Alvis-Guzman, N., Amare, A.T., Amegah, A.K., Ameh, E.A., Amini, H., Ammar, W., Amrock, S.M., Andersen, H.H., Anderson, B.O., Anderson, G.M., Antonio, C.A.T., Aregay, A.F., Ärnlöv, J., Arsenijevic, V.S.A., Artaman, A., Asayesh, H., Asghar, R.J., Atique, S., Avokpaho, E.F.G.A., Awasthi, A., Azzopardi, P., Bacha, U., Badawi, A., Bahit, M.C., Balakrishnan, K., Banerjee, A., Barac, A., Barker-Collo, S.L., Bärnighausen, T., Barregard, L., Barrero, L.H., Basu, A., Basu, S., Bayou, Y.T., Bazargan-Hejazi, S., Beardsley, J., Bedi, N., Beghi, E., Belay, H.A., Bell, B., Bell, M.L., Bello, A.K., Bennett, D.A., Bensenor, I.M., Berhane, A., Bernabé, E., Betsu, B.D., Beyene, A.S., Bhala, N., Bhalla, A., Biadgilign, S., Bikbov, B., Abdulhak, A.A.B., Biroscak, B.J., Biryukov, S., Bjertness, E., Blore, J.D., Blosser, C.D., Bohensky, M.A., Borschmann, R., Bose, D., Bourne, R.R.A., Brainin, M., Brayne, C.E.G., Brazinova, A., Breitborde, N.J.K., Brenner, H., Brewer, J.D., Brown, A., Brown, J., Brugha, T.S., Buckle, G.C., Butt, Z.A., Calabria, B., Campos-Nonato, I.R., Campuzano, J.C., Carapetis, J.R., Cárdenas, R., Carpenter, D.O., Carrero, J.J., Castañeda-Orjuela, C.A., Rivas, J.C., Catalá-López, F., Cavalleri, F., Cercy, K., Cerda, J., Chen, W., Chew, A., Chiang, P.P.-C., Chibalabala, M., Chibueze, C.E., Chimed-Ochir, O., Chisumpa, V.H., Choi, J.-Y.J., Chowdhury, R., Christensen, H., Christopher, D.J., Ciobanu, L.G., Cirillo, M., Cohen, A.J., Colistro, V., Colomar, M., Colquhoun, S.M., Cooper, C., Cooper, L.T., Cortinovis, M., Cowie, B.C., Crump, J.A., Damsere-Derry, J., Danawi, H., Dandona, R., Daoud, F., Darby, S.C., Dargan, P.I., das Neves, J., Davey, G., Davis, A.C., Davitoiu, D.V., de Castro, E.F., de Jager, P., Leo, D.D., Degenhardt, L., Dellavalle, R.P., Deribe, K., Deribew, A., Dharmaratne, S.D., Dhillon, P.K., Diaz-Torné, C., Ding, E.L., dos Santos, K.P.B., Dossou, E., Driscoll, T.R., Duan, L., Dubey, M., Duncan, B.B., Ellenbogen, R.G., Ellingsen, C.L., Elyazar, I., Endries, A.Y., Ermakov, S.P., Eshrati, B., Esteghamati, A., Estep, K., Faghmous, I.D.A., Fahimi, S., Faraon, E.J.A., Farid, T.A., Farinha, C.S.e.S., Faro, A., Farvid, M.S., Farzadfar, F., Feigin, V.L., Fereshtehnejad, S.-M., Fernandes, J.G., Fernandes, J.C., Fischer, F., Fitchett, J.R.A., Flaxman, A., Foigt, N., Fowkes, F.G.R., Franca, E.B., Franklin, R.C., Friedman, J., Frostad, J., Fürst, T., Futran, N.D., Gall, S.L., Gambashidze, K., Gamkrelidze, A., Ganguly, P., Gankpé, F.G., Gebre, T., Gebrehiwot, T.T., Gebremedhin, A.T., Gebru, A.A., Geleijnse, J.M., Gessner, B.D., Ghoshal, A.G., Gibney, K.B., Gillum, R.F., Gilmour, S., Giref, A.Z., Giroud, M., Gishu, M.D., Giussani, G., Glaser, E., Godwin, W.W., Gomez-Dantes, H., Gona, P., Goodridge, A., Gopalani, S.V., Gosselin, R.A., Gotay, C.C., Goto, A., Gouda, H.N., Greaves, F., Gugnani, H.C., Gupta, R., Gupta, R., Gupta, V., Gutiérrez, R.A., Hafezi-Nejad, N., Haile, D., Hailu, A.D., Hailu, G.B., Halasa, Y.A., Hamadeh, R.R., Hamidi, S., Hancock, J., Handal, A.J., Hankey, G.J., Hao, Y., Harb, H.L., Harikrishnan, S., Haro, J.M., Havmoeller, R., Heckbert, S.R., Heredia-Pi, I.B., Heydarpour, P., Hilderink, H.B.M., Hoek, H.W., Hogg, R.S., Horino, M., Horita, N., Hosgood, H.D., Hotez, P.J., Hoy, D.G., Hsairi, M., Htet, A.S., Htike, M.M.T., Hu, G., Huang, C., Huang, H., Huiart, L., Husseini, A., Huybrechts, I., Huynh, G., Iburg, K.M., Innos, K., Inoue, M., Iyer, V.J., Jacobs, T.A., Jacobsen, K.H., Jahanmehr, N., Jakovljevic, M.B., James, P., Javanbakht, M., Jayaraman, S.P., Jayatilleke, A.U., Jeemon, P., Jensen, P.N., Jha, V., Jiang, G., Jiang, Y., Jibat, T., Jimenez-Corona, A., Jonas, J.B., Joshi, T.K., Kabir, Z., Kamal, R., Kan, H., Kant, S., Karch, A., Karema, C.K., Karimkhani, C., Karletsos, D., Karthikeyan, G., Kasaeian, A., Katibeh, M., Kaul, A., Kawakami, N., Kayibanda, J.F., Keiyoro, P.N., Kemmer, L., Kemp, A.H., Kengne, A.P., Keren, A., Kereselidze, M., Kesavachandran, C.N., Khader, Y.S., Khalil, I.A., Khan, A.R., Khan, E.A., Khang, Y.-H., Khera, S., Khoja, T.A.M., Kieling, C., Kim, D., Kim, Y.J., Kissela, B.M., Kissoon, N., Knibbs, L.D., Knudsen, A.K., Kokubo, Y., Kolte, D., Kopec, J.A., Kosen, S., Koul, P.A., Koyanagi, A., Krog, N.H., Defo, B.K., Bicer, B.K., Kudom, A.A., Kuipers, E.J., Kulkarni, V.S., Kumar, G.A., Kwan, G.F., Lal, A., Lal, D.K., Lalloo, R., Lallukka, T., Lam, H., Lam, J.O., Langan, S.M., Lansingh, V.C., Larsson, A., Laryea, D.O., Latif, A.A., Lawrynowicz, A.E.B., Leigh, J., Levi, M., Li, Y., Lindsay, M.P., Lipshultz, S.E., Liu, P.Y., Liu, S., Liu, Y., Lo, L.-T., Logroscino, G., Lotufo, P.A., Lucas, R.M., Lunevicius, R., Lyons, R.A., Ma, S., Machado, V.M.P., Mackay, M.T., MacLachlan, J.H., Razek, H.M.A.E., Magdy, M., Razek, A.E., Majdan, M., Majeed, A., Malekzadeh, R., Manamo, W.A.A., Mandisarisa, J., Mangalam, S., Mapoma, C.C., Marcenes, W., Margolis, D.J., Martin, G.R., Martinez-Raga, J., Marzan, M.B., Masiye, F., Mason-Jones, A.J., Massano, J., Matzopoulos, R., Mayosi, B.M., McGarvey, S.T., McGrath, J.J., McKee, M., McMahon, B.J., Meaney, P.A., Mehari, A., Mehndiratta, M.M., Mejia-Rodriguez, F., Mekonnen, A.B., Melaku, Y.A., Memiah, P., Memish,

Z.A., Mendoza, W., Meretoja, A., Meretoja, T.J., Mhimbira, F.A., Micha, R., Millear, A., Miller, T.R., Mirarefin, M., Misganaw, A., Mock, C.N., Mohammad, K.A., Mohammadi, A., Mohammed, S., Mohan, V., Mola, G.L.D., Monasta, L., Hernandez, J.C.M., Montero, P., Montico, M., Montine, T.J., Moradi-Lakeh, M., Morawska, L., Morgan, K., Mori, R., Mozaffarian, D., Mueller, U.O., Murthy, G.V.S., Murthy, S., Musa, K.I., Nachega, J.B., Nagel, G., Naidoo, K.S., Naik, N., Naldi, L., Nangia, V., Nash, D., Nejjari, C., Neupane, S., Newton, C.R., Newton, J.N., Ng, M., Ngalesoni, F.N., de Dieu Ngirabega, J., Nguyen, Q.L., Nisar, M.I., Pete, P.M.N., Nomura, M., Norheim, O.F., Norman, P.E., Norrving, B., Nyakarahuka, L., Ogbo, F.A., Ohkubo, T., Ojelabi, F.A., Olivares, P.R., Olusanya, B.O., Olusanya, J.O., Opio, J.N., Oren, E., Ortiz, A., Osman, M., Ota, E., Ozdemir, R., Pa, M., Pain, A., Pandian, J.D., Pant, P.R., Papachristou, C., Park, E.-K., Park, J.-H., Parry, C.D., Parsaeian, M., Caicedo, A.J.P., Patten, S.B., Patton, G.C., Paul, V.K., Pearce, N., Pedro, J.M., Stokic, L.P., Pereira, D.M., Perico, N., Pesudovs, K., Petzold, M., Phillips, M.R., Piel, F.B., Pillay, J.D., Plass, D., Platts-Mills, J.A., Polinder, S., Pope, C.A., Popova, S., Poulton, R.G., Pourmalek, F., Prabhakaran, D., Qorbani, M., Quame-Amaglo, J., Quistberg, D.A., Rafay, A., Rahimi, K., Rahimi-Movaghar, V., Rahman, M., Rahman, M.H.U., Rahman, S.U., Rai, R.K., Rajavi, Z., Rajsic, S., Raju, M., Rakovac, I., Rana, S.M., Ranabhat, C.L., Rangaswamy, T., Rao, P., Rao, S.R., Refaat, A.H., Rehm, J., Reitsma, M.B., Remuzzi, G., Resnikoff, S., Ribeiro, A.L., Ricci, S., Blancas, M.J.R., Roberts, B., Roca, A., Rojas-Rueda, D., Ronfani, L., Roshandel, G., Rothenbacher, D., Roy, A., Roy, N.K., Ruhago, G.M., Sagar, R., Saha, S., Sahathevan, R., Saleh, M.M., Sanabria, J.R., Sanchez-Niño, M.D., Sanchez-Riera, L., Santos, I.S., Sarmiento-Suarez, R., Sartorius, B., Satpathy, M., Savic, M., Sawhney, M., Schaub, M.P., Schmidt, M.I., Schneider, I.J.C., Schöttker, B., Schutte, A.E., Schwebel, D.C., Seedat, S., Sepanlou, S.G., Servan-Mori, E.E., Shackelford, K.A., Shaddick, G., Shaheen, A., Shahraz, S., Shaikh, M.A., Shakh-Nazarova, M., Sharma, R., She, J., Sheikhbahaei, S., Shen, J., Shen, Z., Shepard, D.S., Sheth, K.N., Shetty, B.P., Shi, P., Shibuya, K., Shin, M.-J., Shiri, R., Shiue, I., Shrime, M.G., Sigfusdottir, I.D., Silberberg, D.H., Silva, D.A.S., Silveira, D.G.A., Silverberg, J.I., Simard, E.P., Singh, A., Singh, G.M., Singh, J.A., Singh, O.P., Singh, P.K., Singh, V., Soneji, S., Søreide, K., Soriano, J.B., Sposato, L.A., Sreeramareddy, C.T., Stathopoulou, V., Stein, D.J., Stein, M.B., Stranges, S., Stroumpoulis, K., Sunguya, B.F., Sur, P., Swaminathan, S., Sykes, B.L., Szoeke, C.E.I., Tabarés-Seisdedos, R., Tabb, K.M., Takahashi, K., Takala, J.S., Talongwa, R.T., Tandon, N., Tavakkoli, M., Taye, B., Taylor, H.R., Ao, B.J.T., Tedla, B.A., Tefera, W.M., Have, M.T., Terkawi, A.S., Tesfay, F.H., Tessema, G.A., Thomson, A.J., Thorne-Lyman, A.L., Thrift, A.G., Thurston, G.D., Tillmann, T., Tirschwell, D.L., Tonelli, M., Topor-Madry, R., Topouzis, F., Towbin, J.A., Traebert, J., Tran, B.X., Truelsen, T., Trujillo, U., Tura, A.K., Tuzcu, E.M., Uchendu, U.S., Ukwaja, K.N., Undurraga, E.A., Uthman, O.A., Dingenen, R.V., van Donkelaar, A., Vasankari, T., Vasconcelos, A.M.N., Venketasubramanian, N., Vidavalur, R., Vijayakumar, L., Villalpando, S., Violante, F.S., Vlassov, V.V., Wagner, J.A., Wagner, G.R., Wallin, M.T., Wang, L., Watkins, D.A., Weichenthal, S., Weiderpass, E., Weintraub, R.G., Werdecker, A., Westerman, R., White, R.A., Wijeratne, T., Wilkinson, J.D., Williams, H.C., Wiysonge, C.S., Woldeyohannes, S.M., Wolfe, C.D.A., Won, S., Wong, J.Q., Woolf, A.D., Xavier, D., Xiao, Q., Xu, G., Yakob, B., Yalew, A.Z., Yan, L.L., Yano, Y., Yaseri, M., Ye, P., Yebyo, H.G., Yip, P., Yirsaw, B.D., Yonemoto, N., Yonga, G., Younis, M.Z., Yu, S., Zaidi, Z., Zaki, M.E.S., Zannad, F., Zavala, D.E., Zeeb, H., Zeleke, B.M., Zhang, H., Zodpey, S., Zonies, D., Zuhlke, L.J., Vos, T., Lopez, A.D. & Murray, C.J.L. 2016. Global, regional, and national life expectancy, all-cause mortality, and cause-specific mortality for 249 causes of death, 1980–2015: a systematic analysis for the global burden of disease study 2015. *The Lancet*, 388(10053):1459-1544.

Workman, P., Aboagye, E., Balkwill, F., Balmain, A., Bruder, G., Chaplin, D., Double, J., Everitt, J., Farningham, D. & Glennie, M. 2010. Guidelines for the welfare and use of animals in cancer research. *British journal of cancer*, 102(11):1555-1577.

CHAPTER 2: LITERATURE REVIEW

1.1 Cancers to be investigated

Cancer incidence and mortality are rapidly increasing worldwide and, as a result, it is predicted to rank as the leading cause of death in the 21st century (Bray *et al.*, 2018). Despite improvements made in cancer diagnostics, early detection of tumours and development of diagnostic agents remains a challenge (Bazak *et al.*, 2015; Frangioni, 2008). Therefore, a large amount of current research is focused on the development of novel imaging agents aimed at improving the detection and imaging of cancer. Consequently, the availability of animal models of cancer is also necessary to allow for *in vivo* preclinical efficacy evaluation. In this chapter, methods for developing tumour-bearing mouse models will be discussed, with the focus being on breast and ovarian malignancies, as well as the application of the models in the screening of a novel radiopharmaceutical agent for tumour diagnostics and imaging.

1.1.1 Breast cancer

Breast cancer is the cause of the majority of cancer-related deaths in the female population, with approximately 2.1 million newly diagnosed cases and 626 679 deaths expected in 2018 worldwide (Bray *et al.*, 2018). In 2015, malignancy of the breast was the third leading cause of mortality in low and middle-income countries (Global Burden of Disease Cancer Collaboration, 2017). Although advancements have been made in treating and diagnosing breast cancer (da Costa Vieira *et al.*, 2017), it is estimated that the number of newly diagnosed cases will increase to about 3.2 million per year worldwide by 2030 (Ginsburg *et al.*, 2017).

1.1.1.1 Breast carcinogenesis

The breast, the most endocrine sensitive organ in women, is composed of the epidermal, dermal, breast stromal and breast glandular tissues. The glandular tissue makes up about 10 to 15 % of the organ by volume and is the area where all breast cancers occur (Schuur & DeAndrade, 2015). The glandular tissue is further constructed from terminal duct lobular units (TDLUs), which are the lactation units of the breast and considered the primary region of breast cancer initiation (Figueroa *et al.*, 2014; Russo & Russo, 2004). The pathological process of breast cancer is not well understood, however, the linear model of breast cancer (Figure 1) is well documented. According to this model, genetic and epigenetic alterations in the epithelial cells lining the TDLUs give rise to atypical ductal hyperplasia (ADH), a premalignant lesion characterised by abnormal cell layers (Vargo-Gogola & Rosen, 2007). Atypical ductal hyperplasia can further develop into ductal carcinoma *in situ* (DCI), which is characterised by uncontrolled proliferation of ductal epithelial cells within the basement membrane (Badruddoja, 2012). Ductal carcinoma *in situ* is

classified as a non-invasive state of breast malignancy and is the precursor of invasive carcinoma although this progression of DCI to invasive breast cancer is not well understood (Pogo & Holland, 2011). At the later stage of breast cancer (invasive carcinoma), tumour cells escape the basement membrane with the potential to enter the vasculature and invade the lymph nodes, which are the primary site for breast cancer metastasis (Vargo-Gogola & Rosen, 2007).

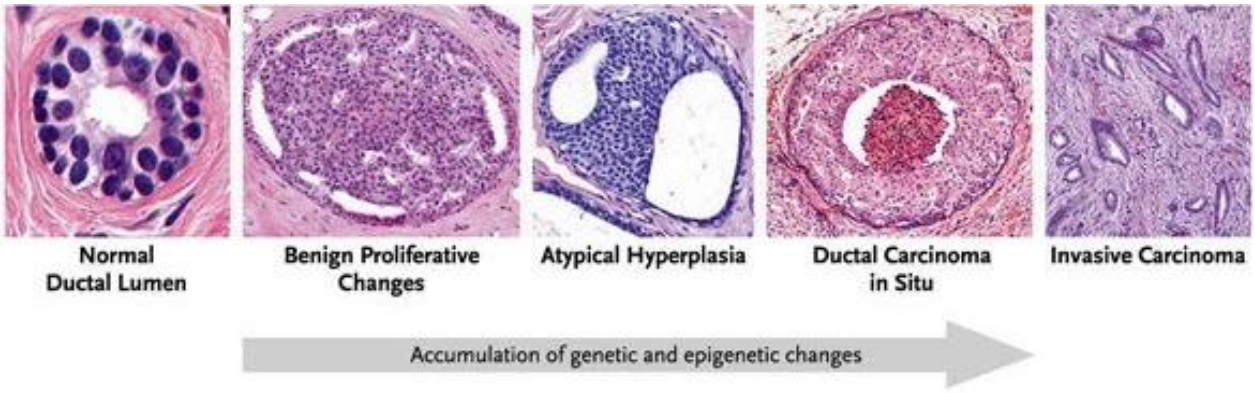

Figure 1: Linear model of breast cancer carcinogenesis. Reproduced from Burstein *et al.* (2004), with permission from copyright Massachusetts Medical Society.

1.1.1.2 Epidemiologic features

The risk of breast cancer increases with age and high incidence rates are observed in older women aged between 25 and 50 years (Mariani-Costantini *et al.*, 2017), with an 85% mortality rate in women aged 50 and older (Angahar, 2017). Interestingly, in Africa, breast malignancy presents at a younger age, with a more advanced stage at diagnosis resulting in a poor prognosis (Mariani-Costantini *et al.*, 2017). Despite improvements in diagnosis and treatment of breast cancer, higher mortality rates are observed in developing countries, including Sub-Saharan Africa, than in developed countries (Akuoko *et al.*, 2017; Pace & Shulman, 2016). The increased death rate in developing countries is mainly due to delayed presentation and late diagnosis, poor health facilities and poor access to treatment (Akuoko *et al.*, 2017; Angahar, 2017; Cumber *et al.*, 2017).

A number of risk factors, mostly hormonal, reproductive and genetic have been implicated in the development and proliferation of breast malignancy. High levels of oestrogen have been strongly proven to induce breast carcinogenesis and as a result, women on oral contraceptives and postmenopausal hormone replacement therapy have a 10% and 23% higher risk, respectively, of developing cancer of the breast than nonusers (Anothaisintawee *et al.*, 2013). Mammary cell

differentiation occurs after pregnancy and during lactation, therefore, women with undifferentiated mammary cells, such as nulliparous women and women who have never breastfed, have a higher incidence of cancer because undifferentiated breast tissues are more susceptible to carcinogens and neoplastic transformation. Furthermore, lactation inhibits ovulation and therefore breast tissue is less exposed to hormones, which may aid in neoplastic transformation during that time (Anothaisintawee *et al.*, 2013; Russo *et al.*, 2005). Women with a family history of breast cancer also have a higher risk of developing breast cancer in their lifetime. In addition, genetic mutations in BRCA 1 and BRCA 2 tumour suppressor genes account for 5 to 10% of hereditary cases of breast cancer (Apostolou & Fostira, 2013; Martin & Weber, 2000). Additional factors such as a high intake of fat and alcohol have also been considered to increase the risk of breast cancer (Angahar, 2017; Persson, 2000).

1.1.1.3 Conventional diagnostic techniques

Physical examination, such as breast cancer self-examination (BSE) and clinical breast cancer examination (CBE), by palpation are simple procedures that are applied for screening of breast cancer. Although BSE and CBE are useful in identifying breast cancer symptoms such as lumps, nipple discharge and skin discolouration, they are mostly recommended for women under 40 years. Unfortunately, BSE and CBE have not proven to reduce mortality rates (Shah & Guraya, 2017; Smith *et al.*, 2003).

Blood-borne tumour markers have the potential to aid in early detection of malignancies, however, at present there are no diagnostic biomarkers for breast cancer (Kazarian *et al.*, 2017). Although several biomarkers such a carcinoembryonic antigen, circulating cytokeratin fragments and epithelial membrane antigen have been recommended, they are limited by poor selectivity and specificity (Kazarian *et al.*, 2017; Loke & Lee, 2018).

Mammography is the gold standard procedure for the screening and diagnosis of breast cancer (Morrow *et al.*, 2011; Nazário *et al.*, 2015; Shah & Guraya, 2017). This technique uses low-dose X-rays for imaging the breast (Badawy *et al.*, 2017) and has reduced breast cancer mortality rates due to early detection (Bleyer & Welch, 2012; Cady *et al.*, 2011; Parris *et al.*, 2013). Despite its ability to detect breast cancer at an early stage, the sensitivity of mammography is compromised in dense breasts and premenopausal women resulting in a high possibility of false-positive and false-negative diagnostic outcomes (Evans, 2012; Wang, 2017).

Ultrasonography is a widely available imaging technique that utilises high-frequency sound waves to detect breast cancer. This procedure is effective in detecting solid tumours and tumours in dense breasts but it is less efficient than mammography due to its inability to detect calcium deposits in breast tumours (Ozmen *et al.*, 2015; Shah & Guraya, 2017; Wang, 2017).

In comparison to ultrasonography and mammography, magnetic resonance imaging is more sensitive in imaging small tumours in women with a high risk of breast cancer by applying magnetic fields and radio waves to produce body images. However, this procedure is less recommended due to high false-positive outcomes and less specificity, which may lead to unnecessary treatment (Roganovic *et al.*, 2015; Shah & Guraya, 2017; Wang, 2017).

1.1.2 Ovarian cancer

Ovarian cancer is the deadliest gynaecological cancer (Mitra, 2016; Webb & Jordan, 2017). Worldwide, ovarian cancer is ranked as the eighth leading cause of cancer-related mortality among women. In 2018, 295 414 newly diagnosed cases are expected, with 184 799 mortality cases(Bray *et al.*, 2018). Due to the asymptomatic presentation, ovarian malignancy is commonly diagnosed at a late stage with poor prognosis (Chornokur *et al.*, 2013; Clarke-Pearson 2009; Tapia *et al.*, 2013). In addition, higher mortality rates have been predicted as a result of late diagnosis, the development of metastases and a lack of effective screening methods for early diagnosis (Doufekas & Olaitan, 2014; Jessmon *et al.*, 2017; Latha *et al.*, 2014).

1.1.2.1 Ovarian carcinogenesis

The ovaries are the female reproductive and endocrine producing organs composed of different cell types, such as germ cells and specialised gonadal stromal cells, and they are covered by a layer of epithelial cells (Kuhn *et al.*, 2012; NASEM, 2016). Ovarian cancer is defined as a heterogeneous disease due to its origin and the progression of ovarian malignancy remains a mystery (NASEM, 2016; Reid *et al.*, 2017). Although the precursor of ovarian cancer is unknown, the current findings suggest that about 90% of ovarian malignancies originate from the epithelial surface of the ovary (Rosen *et al.*, 2009; Zavesky *et al.*, 2011). There are several morphological subtypes of epithelial ovarian cancer, with serous carcinoma being the most common (Russell & McCluggage, 2004; Zavesky *et al.*, 2011). Shih and Kurman (2004) proposed a dualistic model of ovarian carcinogenesis, which suggests two pathways of tumour initiation and progression (Figure 2). Based on the model, Type I pathway is classified as low-grade tumours that develop in a stepwise process from benign serous cystadenoma/adenofibroma, which originate from the ovarian surface epithelium (OSE) or inclusion cysts and ultimately give rise to low-grade serous carcinoma. Based on pathological features, Type I tumours are slow growing and in most cases are restricted to the ovary. Conversely, Type II pathway consists of high-grade tumours that develop *de novo* from ovarian surface epithelium or inclusion cysts (Bell & Scully, 1994; Shih & Kurman, 2004), and are characterised by rapid progression, early metastasis and aggressive behaviour (Shih & Kurman, 2004). Once the ovarian cancer cells have detached from the primary tumour, they form metastatic tumours in the peritoneal cavity, including pelvic and abdominal viscera (Heintz *et al.*, 2006; Mitra, 2016).

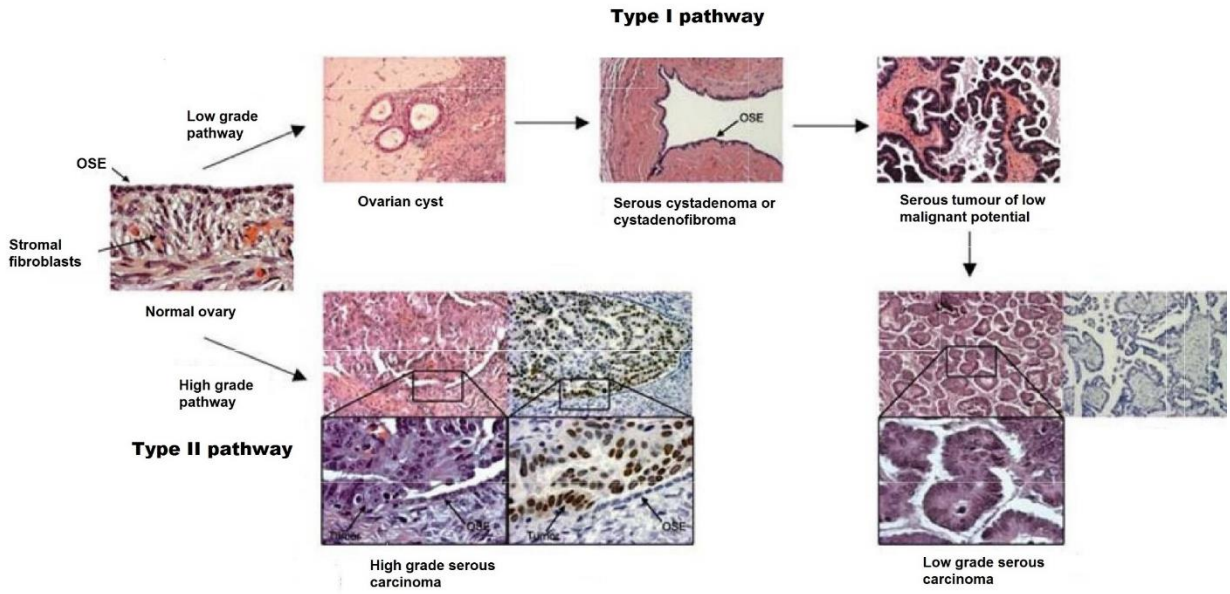

Figure 2: Dualist model for the development of serous ovarian carcinoma. Reproduced from Rosen *et al.* (2009), with permission from Frontiers in Bioscience.

1.1.2.2 Epidemiology features

The incidence of ovarian cancer increases with age, predominately affecting women in their late 70s (Webb & Jordan, 2017). According to epidemiological findings, ovarian cancer incidence is higher in developed countries compared to Sub-Saharan Africa (Ferlay *et al.*, 2015). However, in developing countries, particularly in Africa, high mortality/incidence ratios are observed due to late diagnosis and lack of efficient treatment (Chornokur *et al.*, 2013). Although the aetiology of ovarian cancer is not well established (Permuth-Wey & Sellers, 2009; Zayyan *et al.*, 2017), a number of predisposing factors have been identified. Women with a family history of ovarian cancer have a high incidence of developing the disease and about 7 to 10% of ovarian cancer cases are due to hereditary mutation of BRCA 1 and BRCA 2 suppressor genes (Latha *et al.*, 2014; Webb & Jordan, 2017). Increase in ovulation and circulating gonadotropins, also have a strong correlation with the risk of developing ovarian malignancy (Reid *et al.*, 2017; Riman *et al.*, 2004). Therefore, hormonal and reproductive factors, such as early menstruation, late menopause, infertility and use of menopausal hormone therapy, increase ovarian cancer susceptibility. In addition, gynaecological conditions and procedures such as hysterectomy, pelvic inflammatory diseases and polycystic ovarian syndrome have also been identified as possible risk factors, the findings are however inconclusive (Reid *et al.*, 2017; Riman *et al.*, 2004; Webb & Jordan, 2017).

1.1.2.3 Conventional diagnostic techniques

High levels of cancer antigen 125 (CA-125) is a commonly used biomarker for diagnosis of ovarian cancer (Mitra, 2016) and the marker is detected in 50% of early-stage ovarian tumours (Ueda *et al.*, 2010). Unfortunately, the CA-125 assay is limited by low specificity and sensitivity due to increased levels detected in other malignancies, including endometrial and cervical cancers (Ueda *et al.*, 2010), and non-malignant conditions such as endometriosis and menstruation (Rauh-Hain *et al.*, 2011; Sundar *et al.*, 2015).

Transvaginal ultrasonography (TVUS) is a widely available and first-line imaging technique for the detection of ovarian cancer. Furthermore, the technique has high resolution and does not require ionising radiation (Hebbar & Moideen, 2017; Manegold-Brauer *et al.*, 2014). Although TVUS is the primary imaging technique for diagnosis, it is limited by low specificity, which results in high false-positive diagnostic outcomes (Iyoke *et al.*, 2015). Despite these limitations, CA-125 levels and TVUS are the main diagnostic techniques and contribute to early detection of ovarian cancer (American Cancer Society, 2014; Argento *et al.*, 2008; Kobayashi *et al.*, 2012).

In cases of distant metastases, complementary imaging techniques such as computed tomography (CT) and magnetic resonance imaging (MRI) are considered (Fischerova, 2011). Computed tomography uses ionising radiation or x-rays to create cross-sectional images of the body (Caldemeyer & Buckwalter, 1999). In addition, the use of oral contrast agents allows differentiation of bowel and peritoneal organs, and efficient evaluation of pelvis and abdomen metastases (Jeong *et al.*, 2000). The disadvantages of CT include the application of iodinated contrast agents and exposure to ionising radiation, thus the technique is contraindicated in premenopausal and pregnant women (Lutz *et al.*, 2011). Magnetic resonance imaging (MRI) is considered as a last resort when both CT and TVUS results are inconclusive and is commonly recommended in patients who have contraindications for CT scan (Manegold-Brauer *et al.*, 2014; Park & Lee, 2014). The application of MRI in ovarian cancer diagnosis is however restricted by long examination time, technical difficulties, limited availability and high costs (Fischerova & Burgetova, 2014).

1.2 Animal models in cancer research

1.2.1 Background

Rodents are traditionally utilised to model diseases due to ease of breeding, simple housing requirements, as well as cost-effectiveness. These animals can also be genetically manipulated

with ease and consequently, the induction and transplantation of tumours from various malignant cells have been established for research purposes (Corbett *et al.*, 2004; de Jong & Maina, 2010).

The most commonly used and available rodent tumour models include *in situ* tumour models, such as autochthonous and genetically engineered models as well as transplantable tumour models categorised as allograft and xenograft models. These models have both advantages and disadvantages associated with their experimental application in the assessment of novel anticancer agents as highlighted below.

1.2.2 Types of rodent tumour models

1.2.2.1 Autochthonous model

Autochthonous tumour models include spontaneously occurring and carcinogen-induced (e.g chemical, pathogenic viruses, radiation or microbial flora carcinogens) tumour models (Frese & Tuveson, 2007; Suggitt & Bibby, 2005). These models have been valuable in the identification of oncogenes and tumour suppressor genes, as well as in the mapping of tumour susceptibility traits and preclinical screening of carcinogenic or anticancer compounds (Suggitt & Bibby, 2005).

The advantages of autochthonous tumour models include orthotopic (in the organ of origin) growth, metastatic potential and a tumour histology that lacks changes introduced by transplantation (Suggitt & Bibby, 2005). Despite the advantages mentioned, this model has lost value in drug development research due to the large variability that exists in the tumour take rate and growth and the large number of animals that are required. In addition, it takes several months or years to establish a tumour (Suggitt & Bibby, 2005).

1.2.2.2 Genetically engineered model

Genetically engineered tumour models (GETM) are developed by manipulation of the rodent genome, resulting in inactivation, deletion or overexpression of either one or several genes involved in tumour malignancy (Richmond & Su, 2008). Genetically engineered rodent models of malignant tumours are useful tools for understanding the molecular pathways of tumour initiation and progression, and for selecting anticancer agents targeted to different markers of carcinogenesis *in vivo* (Singh & Johnson, 2006; Suggitt & Bibby, 2005). Despite the advantages, developing GETM is expensive and time-consuming because it takes approximately a year for a tumour to develop (de Jong & Maina, 2010; Richmond & Su, 2008). Additionally, monitoring of the tumours requires imaging techniques such as magnetic resonance imaging (MRI) or micro- computed tomography (Becher & Holland, 2006; Richmond & Su, 2008).

1.2.2.3 Human xenograft model

The human tumour xenograft model, also known as the humanised tumour model, is one of the most utilised models. Establishment of a xenograft model involves transplantation of human tumour cells or patient biopsies under the skin or directly into the organ of tumour origin (Cekanova & Rathore, 2014; Morton & Houghton, 2007; Murphy, 2015). This model requires the use of immune-compromised mice, such as T-cell deficient athymic nude (nu/nu) mice or T-cell and B-cell deficient severe combined immune-deficient (SCID) mice, to prevent rejection of the transplant by the recipient (Shultz *et al.*, 2012; Szadvari *et al.*, 2016).

Human ovarian cancer can be modelled by xenotransplantation of athymic nude (nu/nu) mice with human-derived cancer cell lines (Domcke *et al.*, 2013; Elgqvist *et al.*, 2006; Pourgholami *et al.*, 2006). The human ovarian adenocarcinoma cell line, known as OVCAR-3 is among the most commonly used cell line of ovarian cancer that was derived from malignant ascites of a patient unresponsive to combination chemotherapy (Domcke *et al.*, 2013; Hamilton *et al.*, 1983; Sakhare *et al.*, 2014). *In vitro*, OVCAR-3 grows as a cobblestone, like a monolayer with foci of multi- layering, and has a doubling time of 35 to 48 hours (Hamilton *et al.*, 1983; Hills *et al.*, 1989). Histologically, it represents a high-grade serous ovarian cancer subtype (Domcke *et al.*, 2013). To date, a number of studies have demonstrated the use of OVCAR-3 tumour xenograft for therapeutic evaluation, including photodynamic therapy (Colussi *et al.*, 1999), alpha-radioimmunotherapy (Elgqvist *et al.*, 2006) and chemotherapy (Guichard *et al.*, 2001).

The development of the human tumour xenograft model was a major improvement in moving towards clinically relevant cancer models (Troiani *et al.*, 2008). One major advantage of the human tumour xenograft model is that the tumour is of human origin and therefore, reflects the patient's tumour physiology. In addition, the model can be established with affordability and reproducibility using different types of cancer cells (Murphy, 2015; Teicher, 2006).

However, the predictive power of human tumour xenograft models in terms of clinical efficacy has been questioned due to two limitations. Firstly, the model does not accurately represent disease progression observed in immune-competent patients. Secondly, the genetic characteristics of a human tumour may be compromised due to the tumour microenvironment being that of mouse origin (Murphy, 2015; Neale *et al.*, 2008). This model, despite its limitations, remains the gold standard in evaluating new anticancer drugs, and is successful in predicting the therapeutic response of patients in numerous clinical trials (Chen *et al.*, 2014; Pierrillas *et al.*, 2016; Voskoglou-Nomikos *et al.*, 2003).

1.2.2.4 Allograft model

The allograft tumour model, also known as syngeneic, is developed by growing rodent tumour tissue or cells in the same strain of immune-competent host in which the tumour originated (Murphy, 2015). For example, murine mammary adenocarcinoma cell line, denoted as E0771, is commonly used for developing an allograft model of breast cancer by implantation into a C57BL/6 mouse (Ewens *et al.*, 2006; Ewens *et al.*, 2005; Johnstone *et al.*, 2015; Stagg *et al.*, 2010).

E0771 was derived spontaneously from a C57BL/6 mouse (Sugiura & Stock, 1952) and when cultured *in vitro,* it forms a monolayer of fibroblast-like cells having an elongated shape (Thomas, 2012); in addition, histologic representation resembles undifferentiated high-grade phenotype (Johnstone *et al.*, 2015). The E0771 tumour-bearing model has been previously used for efficacy testing of immunotherapy and chemoimmunotherapy for inhibition of metastasis (Blake *et al.*, 2016; Ewens *et al.*, 2006) and to further understand the role of the immune system in tumourigenesis (Huang *et al.*, 2015).

The advantages of using syngeneic tumour models in drug development research include cost- effectiveness, effortless implantation, reproducible experimental tumour histology and growth rate, successful establishment of a wide variety of tumour types, and availability of a strong baseline of drug response data from decades of use (de Jong & Maina, 2010; Murphy, 2015). Studies are easily conducted with statistically meaningful numbers of mice per group because the hosts are readily available (de Jong & Maina, 2010; Murphy, 2015). In contrast to xenograft models, this model has an intact immune system and is, therefore, suitable to study anti-tumour immune response (House *et al.*, 2014).

However, as therapeutic research is being directed to specific cancer molecular targets, syngeneic cancer models have lost their reputation in drug development research, due to differences in homology between rodents and human that results in failure to correlate preclinical activity and efficacy in clinical trials (Cook *et al.*, 2012; de Jong & Maina, 2010). Despite the failure of the syngeneic models to predict patient outcome, this model remains valuable in the evaluation of therapies that utilise the immune system's ability to target and destroy cancer cells (Murphy, 2015).

1.3 Establishing allograft and xenograft mouse models

The most promising route with which to establish a transplantable tumour-bearing mouse model is that of the syngeneic and xenograft models. In general, a number of variables, such as the origin of a tumour, site of implantation, number of inoculation cells, sex of the host, tumour growth

characteristics and histology, should be considered when establishing these models (Workman *et al.*, 2010).

1.3.1 The origin of a tumour

Tumour-bearing mouse models can be established from tumour cell culture, initiated cell lines or patient biopsies (Schuh, 2004). Most researchers commonly use cell lines due to their higher take rate (Troiani *et al.*, 2008), ease of accessibility and maintenance, possible selection of unique mutations *in vitro* and availability of numerous publications on *in vivo* behaviour in immune- deficient, immune-suppressed and immune-competent strains of mice (Schuh, 2004). Contamination, particularly mycoplasma contamination, is one of the main challenges of using cultured cells as this may alter cell proliferation and gene expression (DesRochers *et al.*, 2015). Another drawback of using cell lines is that the sub-culturing (> 100 passages) (Fiebig & Burger, 2002; Sausville & Burger, 2006) results in undifferentiated tumours without resemblance to the original tumour (Becher & Holland, 2006; Sausville & Burger, 2006). Therefore, to maintain the tumour integrity, it is important the cell lines are monitored for microbial contamination and detailed characterisation of a tumour should be done to ensure the molecular pathology resembles the original tumour (Santarius *et al.*, 2010; Workman *et al.*, 2010).

1.3.2 Site of transplantation

The transplantation site is critical because it may have an influence on the tumour growth and efficacy outcome (Schuh, 2004). The most commonly used site for tumour implantation is subcutaneous. In this technique, the site of transplantation differs from the origin of the tumour and the major limitation is a failure of the tumour to metastasise (Workman *et al.*, 2010). For metastatic modelling, direct implantation of a tumour in the site of tumour origin (orthotopic) should be employed (Jung, 2014). Despite the limitations, there is a high preference for the subcutaneous route in efficacy studies because tumour growth can be easily assessed and treatment can begin when a tumour has reached the desirable size (Becher & Holland, 2006; Jung, 2014).

1.3.3 Number of inoculation cells

To minimise tumour burden, the number of cells to be transplanted should be taken into account. Furthermore, the number of cells is dependent on the site of transplantation. Ideally, about 1 to 5 million cells in 100 µl should be used for subcutaneous inoculation. For orthotopic transplantation in more sensitive sites, such as intracranial implantation, about 10-50 000 cells in 5 µl is recommended to prevent tissue damage and leakage of cells (Workman *et al.*, 2010).

1.3.4 The sex of the host

Hormones play a critical role in cancer initiation and progression. In breast and ovarian cancer particularly, the female sex hormone known as oestrogen has been identified as a major carcinogen. According to literature, oestrogen induces carcinogenesis by either DNA damage or altering expression of genes responsible for cell growth and proliferation, consequently triggering uncontrolled multiplication of epithelial cells of the breast and ovary (Ptak & Gregoraszczuk, 2013). Therefore, to ensure the successful establishment of hormone-dependent tumours such as breast and ovarian cancer, the gender of the animals should be taken into consideration.

1.3.5 Tumour growth characteristics

Transplanted tumours may develop at a slow or inconsistent incidence and growth rate (Workman *et al.*, 2010). One method to optimise tumour growth is by the selection of cell variants with enhanced tumorigenic potential (Workman *et al.*, 2010). Another commonly used method is the co-injection of cells with murine tumour-derived basement membrane extract, rich in extracellular matrix proteins (growth factors, laminin, collagen IV and entactin) such as Matrigel. Co-injection with Matrigel results in enhanced tumour growth and take rate, promotion of angiogenesis and prevention of tumour cell apoptosis by providing a growth-enhancing environment that resembles the tumour microenvironment (Benton *et al.*, 2014; Workman *et al.*, 2010; Xu & Prestwich, 2010).

1.3.6 Histology

According to Schuh (2004), the histological investigation should be included in tumour modelling studies to confirm and identify the degree of differentiation of the malignant tissues. In addition, histological characterisation should also examine histological features such as necrosis, angiogenesis and haemorrhage (Schuh, 2004). The haematoxylin and eosin (H& E) stain is the most routinely used staining technique for tumour histological diagnoses because it can be used to analyse different tissues with ease of application (Wittekind, 2003).

1.4 Use of radiopharmaceuticals for imaging of cancer with PET/CT

Radiopharmaceuticals are radioactive compounds used mainly for therapy or diagnosis of various diseases, including cancer (Dar *et al.*, 2015; Vallabhajosula, 2009). In the area of diagnostics, radiopharmaceuticals are readily applied for non-invasive imaging of cancer using techniques such as single photon emission computed tomography (SPECT) and positron-emission tomography (PET). In general, imaging radiopharmaceuticals are administered at very low concentrations (10^{-6} – 10^{-8} M) without any physiological response and pharmacological effects

(Bhattacharyya & Dixit, 2011; Chen *et al.*, 2010; Liu, 2004; Vallabhajosula, 2009). The current focus of much research is to make improvements in radionuclide imaging by investigating the development of target-specific radiopharmaceuticals for non-invasive imaging (Bhattacharyya & Dixit, 2011; Chen *et al.*, 2010).

Positron emission tomography (PET) is a popular nuclear imaging technique that depends on the use of positron-emitting radiopharmaceuticals for non-invasive imaging of cancer and other diseases (Cherry & Gambhir, 2001). Unlike anatomical imaging techniques, such as ultrasonography and CT, PET evaluates the biological and physiological changes at a cellular level (Chen & Chen, 2011) and its use in oncology allows precise staging and early diagnosis, which in turn, may result in earlier treatment and therefore a better prognosis (Townsend, 2004). Another advantage of PET is that it can also distinguish between malignant and non-cancerous tumours (Kapoor *et al.*, 2004), but is unfortunately limited by prolonged scans and poor anatomical localisation and visualisation of soft tissues due to low spatial resolution. To overcome these limitations and instead of using PET and CT scans alone, a combination of the two has been a major advancement in nuclear medicine. Consequently, PET/CT scans allow simultaneous imagining of physiological and anatomical changes with high-resolution and minimising the scan time required (Townsend, 2004). In this study, PET/CT scan was used for imaging purposes.

1.4.1 Design of a diagnostic radiopharmaceutical for imaging

In general, to achieve tumour targeted imaging or therapy, a radiopharmaceutical should consist of a radionuclide, targeting molecule, bifunctional chelating agent (BFCA) and a linker (Figure 3) (Liu, 2008; Sarko *et al.*, 2012; Tornesello *et al.*, 2017).

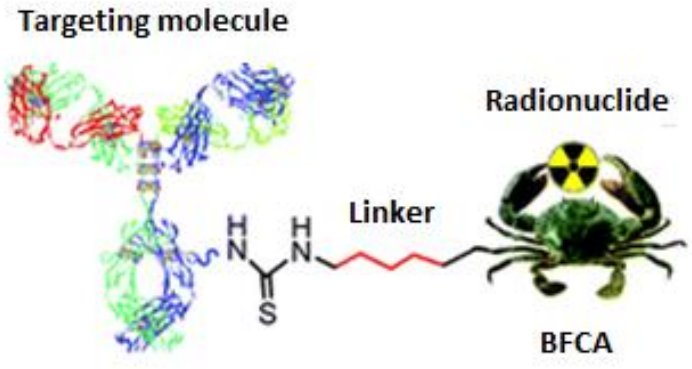

Figure 3: Structural properties of the target-specific radiopharmaceutical. Adapted from Bhattacharyya and Dixit (2011), with permission from The Royal Society of Chemistry.

1.4.2 Radionuclide

When designing a radiopharmaceutical, the choice of a radionuclide depends on the half-life ($t_{1/2}$), availability and decay mode, and the emission properties of the radionuclide (Ting *et al.*, 2009; Wadsak & Mitterhauser, 2010). There are a number of positron-emitting radionuclides available for PET (Table 1), but the most commonly used in diagnostic imaging is Fluorine-18 (^{18}F) due to its favourable decay properties (97% β^+ decay, 635 keV positron energy and $t_{1/2}$= 110 min) (Bhattacharyya & Dixit, 2011; Elsinga, 2012; Jacobson *et al.*, 2015). Recently, Copper-64 (^{64}Cu) has gained more recognition as a potential imaging radionuclide for PET because of its longer half-life (12.7 hours) and availability in high specific activity (activity per quantity of a radionuclide). In comparison to ^{18}F, the use of ^{64}Cu enables imaging at delayed time points because of its longer half-life, thereby allowing enough time for clearance of the radiopharmaceutical from background tissues to increase the image contrast (Gutfilen & Valentini, 2014).

Table 1: PET radionuclides, adapted from Elsinga (2012).

Radionuclide	Half-life
Carbon-11	20 min
Fluorine-18	110 min
Copper-64	12.7 h
Gallium-68	68 min
Zarconium-89	78 h
Iodine-124	100 h

1.4.3 Targeting molecule

The targeting molecule is the integral part of the radiopharmaceutical for selective delivery of the radionuclide to the tumour site by either active or passive targeting (Kue *et al.*, 2016; Yin *et al*., 2014).

1.4.3.1 Active targeting agent

Active targeting facilitates the uptake of the radionuclide by the tumour cells via ligand-receptor binding (Bazak *et al.*, 2015; Danhier *et al.*, 2010). This phenomenon is extensively investigated in therapeutic targeting of cancer and to date, a number of monoclonal antibodies including Cetuximab (Erbitux) targeting epidermal growth factor receptor (EGFR) and Rituximab (Tituxan) targeting CD-20 receptor, have been clinically approved (Yan *et al.*, 2011).

According to the Warburg effect, cancer cells metabolise more glucose to lactate compared to normal cells (cited by Bensinger & Christofk, 2012). This demand for glucose is maintained by a high expression of glucose receptors (GLUT), mainly GLUT-1 (Hamanaka & Chandel, 2012; Hanahan & Weinberg, 2011). The high uptake of glucose by cancerous cells has been exploited for target-specific imaging of cancer. The most documented application of this is the use of a glucose analogue, fluoro-2-deoxy-D-glucose radiolabelled with ^{18}F (^{18}F-FDG) for PET imaging (Hanahan & Weinberg, 2011; Kumar & Dadparvar, 2007; Schroeder *et al.*, 2011).

1.4.3.2 Passive targeting agent

A second means of potentially accumulating the radionuclide at the site of the tumour is through passive targeting by means of the enhanced permeability and retention (EPR) effect. The EPR effect is due to the rapid growth and high demand for nutrients and oxygen by the tumour, which increases the vascularisation of the tumour but with poorly laid down, 'leaky' blood vessels (enhanced permeability) and minimal lymph ducts (retention) (Bertrand *et al.*, 2014; Danhier *et al.*, 2010). In principle, to enhance the retention of a molecule at the site of a tumour by the EPR effect, the size of the molecule should be more than 40 kDa (Fang *et al.*, 2011; Li *et al.*, 2017; Vasir & Labhasetwar, 2005). Albumin, a plasma protein with a molecular weight of 66.5 kDa (Kratz, 2008; Park, 2012) has been employed for delivery of compounds via the EPR effect and targeted imaging and therapy (Meng *et al.*, 2012). The advantages of using albumin as a drug carrier include: 1) high stability and solubility in various buffers with a wide range of pH and temperatures; 2) ligand binding capacity of various compounds including heavy metals; 3) lack of toxicity and immunogenicity; 4) availability and biodegradability; 5) preferential uptake in tumour and inflamed tissue (Kratz, 2008; Meng *et al.*, 2012). For diagnostic applications, Technetium-99m (^{99m}Tc) radiolabelled albumin is commonly used for the diagnosis of pulmonary embolism and some cancers using SPECT imaging (Bairagi *et al.*, 2015; Gandhi *et al.*, 2013).

1.4.4 Bifunctional chelating agent

The purpose of a bifunctional chelating agent (BFCA) in a target-specific radiopharmaceutical is to conjugate the radionuclide and targeting molecule. The choice of a BFCA depends on the oxidation state of the radionuclide and its affinity for the donor atoms of the chelator in order to

form a kinetically inert and thermodynamically stable complex (Bhattacharyya & Dixit, 2011). Cyclam is one of the most utilised BFCA due to its ability to form highly stable complexes with radionuclides, especially ^{64}Cu (Liang & Sadler, 2004).

1.4.5 Linker

The targeting molecules and BFCA are separated by a linker to prevent a possible disruption of receptor-ligand binding by the radionuclide chelate complex (Bhattacharyya & Dixit, 2011). The stability of the linker within the bloodstream has influence on the pharmacokinetic profile of the radiopharmaceutical by preventing early release of the radionuclide and consequently allowing imaging of the tumour (Chen & Chen, 2010; Lu *et al.*, 2016; Parslow *et al.*, 2016; Quadri & Vriesendorp, 1998; Sarko *et al.*, 2012).

1.5 Combination of active and passive targeting

In order to benefit from active targeting, the ligand should be in close proximity to the target receptor (Bertrand *et al.*, 2014). Consequently, active targeting depends on passive targeting since the ligand-receptor binding occurs only after accumulation and retention in a tumour by vascular delivery (Upponi & Torchilin, 2014). To maximise the advantages of active and passive targeting pathways and to minimise their shortcomings, a better approach would be to combine both active and passive targeting agents. This will increase the circulation and retention in the tumour and provide enough time for the targeting agent to interact with its respective receptor (Kudgus *et al.*, 2014). The approach of dual targeting by both active and passive targeting has been explored in targeted therapy to decrease cytotoxicity and increase efficacy (Zheng *et al.*, 2015). In this study, a dual targeting radiopharmaceutical was investigated for tumour localisation and imaging.

1.6 Targeted diagnostic radiopharmaceutical: ^{64}Cu-GluCAB

1.6.1 Structure

^{64}Cu-GluCAB (Figure 4) is a dual target imaging radiopharmaceutical, designed and synthesised by the Nuclear Energy Corporation of South Africa (Necsa). Cyclam (BFCA) is linked to a glucose moiety and to albumin to form a bio-conjugate (GluCAB), which is radiolabelled with the ^{64}Cu isotope.

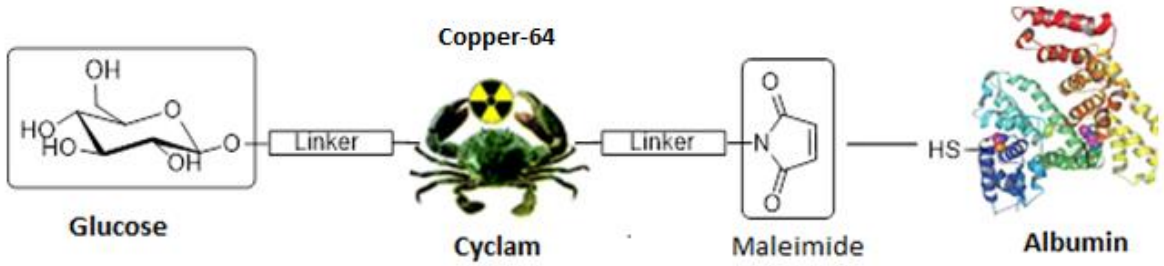

Figure 4: Basic structure of ^{64}Cu-GluCAB

1.6.2 Proposed mechanism of action

After administration of the ^{64}Cu-GluCAB precursor (without albumin), the maleimide moiety in the linker will bind *in vivo* to free thiol groups of albumin to form the full ^{64}Cu-GluCAB bioconjugate. Thereafter, albumin as a drug carrier will deliver and accumulate ^{64}Cu-GluCAB at the tumour site through the enhanced permeability and retention (EPR) effect. The glucose will then selectively bind to overexpressed glucose receptor (GLUT-1) on tumour cells (Calvo *et al.*, 2010) and after tumour localisation, the tumour can be imaged using ^{64}Cu.

1.6.3 Application of transplantable tumour-bearing mouse models in imaging radiopharmaceuticals

The design and application of preclinical cancer models depends on the therapeutic or diagnostic agent under investigation (Killion *et al.*, 1998). Therefore, in order to design an appropriate tumour model for screening of molecular targeting agents, histopathological endpoints should be incorporated into studies to confirm the presence of targeted molecular markers (Kelland, 2004; Schuh, 2004).

Several studies have been successful in demonstrating the use of cancer-bearing models in efficacy screening of target-specific imaging radiopharmaceuticals. For example, a study by Ping Li *et al.* (2008) used cancer-bearing mice for the screening of a ^{64}Cu labelled monoclonal antibody (cetuximab) with high affinity to epidermal growth factor receptor (EGFR) for target-specific imaging. In this study, ^{64}Cu-DOTA-cetuximab was screened against A431 (human epithelial carcinoma, EGFR+) and MDA-MB-434 (human melanoma, EGFR-) tumour-bearing mice and based on microPET imaging, higher uptake was observed in A431 than MDA-MB-434 tumours. In another study, prostate cancer with ^{18}F labelled prostate-specific membrane antigen (^{18}F- PSMA-1007) was successfully visualised in mice-bearing LNCaP (lymph node carcinoma of the prostate, PSMA+) tumours (Cardinale *et al.*, 2017). In the current study, a tumour-bearing

mouse model was used for evaluation of dual targeting ^{64}Cu-GluCAB by micro-PET/CT scan. Based on the proposed targeting approach of ^{64}Cu-GluCAB, the study hypothesised that higher uptake of the agent by the tumour would be observed.

1.7 Conclusion

To evaluate the application of novel dual targeting agents like ^{64}Cu-GluCAB in cancer imaging successfully, the use of tumour-bearing mouse models is required. Two different cancer animal models, ovarian OVCAR-3 xenograft and breast E0771 allograft models were therefore developed and investigated. The model that illustrated the most potential as an effective tool for application in testing new radiopharmaceuticals was used in the evaluation of ^{64}Cu-GluCAB as a potential imaging agent for cancer.

REFERENCES

Akuoko, C.P., Armah, E., Sarpong, T., Quansah, D.Y., Amankwaa, I. & Boateng, D. 2017. Barriers to early presentation and diagnosis of breast cancer among African women living in sub-Saharan Africa. *PloS one*, 12(2):e0171024.

American Cancer Society. 2014. Can ovarian cancer be found early? https://www.cancer.org/cancer/ovarian-cancer/detection-diagnosis-staging/detection.html Date of access: 09-04-2018.

Angahar, L.T. 2017. An overview of breast cancer epidemiology, risk factors, pathophysiology, and cancer risks reduction. *MOJ biology & medicie*, 1(4): 92-96.

Anothaisintawee, T., Wiratkapun, C., Lerdsitthichai, P., Kasamesup, V., Wongwaisayawan, S., Srinakarin, J., Hirunpat, S., Woodtichartpreecha, P., Boonlikit, S. & Teerawattananon, Y. 2013. Risk factors of breast cancer: a systematic review and meta-analysis. *Asia Pacific journal of public health*, 25(5):368-387.

Apostolou, P. & Fostira, F. 2013. Hereditary breast cancer: the era of new susceptibility genes. *BioMed research international*, 2013:11.

Argento, M., Hoffman, P. & Gauchez, A.-S. 2008. Ovarian cancer detection and treatment: current situation and future prospects. *Anticancer research*, 28(5B):3135-3138.

Badawy, S.M., Hefnawy, A.A., Zidan, H.E. & GadAllah, M.T. 2017. Breast cancer detection with mammogram segmentation: A qualitative study. *Breast cancer*, 8(10): 177-120.

Badruddoja, M. 2012. Ductal carcinoma *in situ* of the breast: a surgical perspective. *International journal of surgical oncology*, 2012:12.

Bairagi, U., Mittal, P. & Mishra, B. 2015. Albumin: a versatile drug carrier. *Austin therapeutics*, 2(2):1021.

Bazak, R., Houri, M., El Achy, S., Kamel, S. & Refaat, T. 2015. Cancer active targeting by nanoparticles: a comprehensive review of literature. *Journal of cancer research and clinical oncology*, 141(5):769-784.

Becher, O.J. & Holland, E.C. 2006. Genetically engineered models have advantages over xenografts for preclinical studies. *Cancer research*, 66(7):3355-3359.

Bell, D.A. & Scully, R.E. 1994. Early de novo ovarian carcinoma. A study of fourteen cases. *Cancer*, 73(7):1859-1864.

Bensinger, S.J. & Christofk, H.R. 2012. New aspects of the Warburg effect in cancer cell biology. *Seminars in cell & developmental biology*, 23(4):352-361.

Benton, G., Arnaoutova, I., George, J., Kleinman, H.K. & Koblinski, J. 2014. Matrigel: From discovery and ECM mimicry to assays and models for cancer research. *Advanced drug delivery reviews*, 79–80:3-18.

Bertrand, N., Wu, J., Xu, X., Kamaly, N. & Farokhzad, O.C. 2014. Cancer nanotechnology: The impact of passive and active targeting in the era of modern cancer biology. *Advanced drug delivery reviews*, 66:2-25.

Bhattacharyya, S. & Dixit, M. 2011. Metallic radionuclides in the development of diagnostic and therapeutic radiopharmaceuticals. *Dalton transactions (Cambridge, England : 2003)*, 40(23):6112-6128.

Blake, S.J., Stannard, K., Liu, J., Allen, S., Yong, M.C.R., Mittal, D., Roman Aguilera, A., Miles, J.J., Lutzky, V.P., Ferrari de Andrade, L., Martinet, L., Colonna, M., Takeda, K., Kuhnel, F., Gurlevik, E., Bernhardt, G., Teng, M.W.L. & Smyth, M.J. 2016. Suppression of metastases using a new lymphocyte checkpoint target for cancer immunotherapy. *Cancer discovery*, 06:41.

Bleyer, A. & Welch, H.G. 2012. Effect of three decades of screening mammography on breast-cancer incidence. *New England journal of medicine*, 367(21):1998-2005.

Bray, F., Ferlay, J., Soerjomataram, I., Siegel, R.L., Torre, L.A. & Jemal, A. 2018. Global cancer statistics 2018: GLOBOCAN estimates of incidence and mortality worldwide for 36 cancers in 185 countries. *CA: A cancer journal for clinicians*, 0(0):3-31.

Burstein, H.J., Polyak, K., Wong, J.S., Lester, S.C. & Kaelin, C.M. 2004. Ductal carcinoma *in situ* of the breast. *New England journal of medicine*, 350(14):1430-1441.

Cady, B., Michaelson, J.S. & Chung, M.A. 2011. The “tipping point” for breast cancer mortality decline has resulted from size reductions due to mammographic screening. *Annals of surgical oncology*, 18(4):903-906.

Caldemeyer, K.S. & Buckwalter, K.A. 1999. The basic principles of computed tomography and magnetic resonance imaging. *Journal of the American Academy of Dermatology*, 41(5):768-771.

Calvo, M.B., Figueroa, A., Pulido, E.G., Campelo, R.G. & Aparicio, L.A. 2010. Potential role of sugar transporters in cancer and their relationship with anticancer therapy. *International journal of endocrinology*, 2010:14.

Cardinale, J., Schäfer, M., Benešová, M., Bauder-Wüst, U., Leotta, K., Eder, M., Neels, O.C., Haberkorn, U., Giesel, F.L. & Kopka, K. 2017. Preclinical evaluation of 18F-PSMA-1007, a new prostate-specific membrane antigen ligand for prostate cancer imaging. *Journal of nuclear medicine*, 58(3):425-431.

Cekanova, M. & Rathore, K. 2014. Animal models and therapeutic molecular targets of cancer: utility and limitations. *Drug design development therapy*, 8:1911-1921.

Chen, K. & Chen, X. 2010. Design and development of molecular imaging probes. *Current topics in medicinal chemistry*, 10(12):1227-1236.

Chen, K. & Chen, X. 2011. Positron emission tomography imaging of cancer biology: Current status and future prospects. *Seminars in oncology*, 38(1):70-86. (Abstract).

Chen, Y., Williams, V., Filippova, M., Filippov, V. & Duerksen-Hughes, P. 2014. Viral carcinogenesis: Factors inducing DNA damage and virus integration. *Cancers*, 6(4):2155.

Chen, Y., Xiong, Q.-F., Yang, X.-Q., He, L. & Huang, Z.-W. 2010. Evaluation of ^{188}Re-DTPA-Deoxyglucose as a potential cancer radiopharmaceutical. *American journal of roentgenology*, 194(3):761-765.

Cherry, S.R. & Gambhir, S.S. 2001. Use of positron emission tomography in animal research. *ILAR journal*, 42(3):219-232.

Chornokur, G., Amankwah, E.K., Schildkraut, J.M. & Phelan, C.M. 2013. Global ovarian cancer health disparities. *Gynecologic oncology*, 129(1):258-264.

Clarke-Pearson , D.L. 2009. Screening for ovarian cancer. *New England journal of medicine*, 361(2):170-177.

Colussi, V.C., Feyes, D.K., Mulvihill, J.W., Li, Y.-S., Kenney, M.E., Elmets, C.A., Oleinick, N.L. & Mukhtar, H. 1999. Phthalocyanine 4 (Pc 4) photodynamic therapy of human OVCAR-3 tumor xenografts. *Photochemistry and photobiology*, 69(2):236-241.

Cook, N., Jodrell, D.I. & Tuveson, D.A. 2012. Predictive *in vivo* animal models and translation to clinical trials. *Drug discovery today*, 17(5–6):253-260.

Corbett, T., Polin, L., LoRusso, P., Valeriote, F., Panchapor, C., Pugh, S., Wite, K., Knight, J., Lisa, D., Jones, J., Jones, L. & Lisow, L. 2004. *In vivo* methods for screening and preclinical testing. In Teicher, B.A. & Andrews, P.A. (Eds.). *Anticancer drug development guide: preclinical screening, clinical trial and approval* (2.). Totowa, N.J.: Humana Press. http://nwulib.nwu.ac.za/login?url=http://search.ebscohost.com/login.aspx?direct=true&db=nlebk&AN=106701 Date of access 16 Apr. 2017.

Cumber, S.N., Nchanji, K.N. & Tsoka-Gwegweni, J.M. 2017. Breast cancer among women in sub-Saharan Africa: prevalence and a situational analysis. *Southern African journal of gynaecological oncology*, 9(2):35-37.

da Costa Vieira, R.A., Biller, G., Uemura, G., Ruiz, C.A. & Curado, M.P. 2017. Breast cancer screening in developing countries. *Clinics*, 72(4):244-253.

Danhier, F., Feron, O. & Préat, V. 2010. To exploit the tumor microenvironment: passive and active tumor targeting of nanocarriers for anti-cancer drug delivery. *Journal of controlled release*, 148(2):135-146.

Dar, M., Masoodi, M.H. & Farooq, S. 2015. Medical uses of radiopharmaceuticals. *PharmaTutor*, 3(8):24-29.

de Jong, M. & Maina, T. 2010. Of mice and humans: are they the same?-implications in cancer translational research. *The journal of nuclear medicine*, 51(4):501-504.

DesRochers, T.M., Kuo, I.Y., Kimmerling, E.P., Ehrlich, B.E. & Kaplan, D.L. 2015. The effects of Mycoplasma contamination upon the ability to form bioengineered 3D kidney cysts. *PLoS ONE*, 10(3):e0120097.

Domcke, S., Sinha, R., Levine, D.A., Sander, C. & Schultz, N. 2013. Evaluating cell lines as tumour models by comparison of genomic profiles. *Nature communications*, 4:2126.

Doufekas, K. & Olaitan, A. 2014. Clinical epidemiology of epithelial ovarian cancer in the UK. *International journal of women's wealth*, 6:537-545.

Elgqvist, J., Andersson, H., Back, T., Claesson, I., Hultborn, R., Jensen, H., Johansson, B.R., Lindegren, S., Olsson, M. & Palm, S. 2006. α-radioimmunotherapy of intraperitoneally growing OVCAR-3 tumors of variable dimensions: outcome related to measured tumor size and mean absorbed dose. *Journal of nuclear medicine*, 47:1342-1350.

Elsinga, P.H. 2012. Present and future of PET-radiopharmaceuticals. *Nuclear medicine review*, 15(C):13-16.

Evans, W. 2012. Breast cancer screening: successes and challenges. *CA: A cancer journal for clinicians*, 62(1):5-9.

Ewens, A., Luo, L., Berleth, E., Alderfer, J., Wollman, R., Hafeez, B.B., Kanter, P., Mihich, E. & Ehrke, M.J. 2006. Doxorubicin plus interleukin-2 chemoimmunotherapy against breast cancer in mice. *Cancer research*, 66(10):5419-5426.

Ewens, A., Mihich, E. & Ehrke, M.J. 2005. Distant metastasis from subcutaneously grown E0771 medullary breast adenocarcinoma. *Anticancer research*, 25(6B):3905-3915.

Fang, J., Nakamura, H. & Maeda, H. 2011. The EPR effect: unique features of tumor blood vessels for drug delivery, factors involved, and limitations and augmentation of the effect. *Advanced drug delivery reviews*, 63(3):136-151.

Ferlay, J., Soerjomataram, I., Dikshit, R., Eser, S., Mathers, C., Rebelo, M., Parkin, D.M., Forman, D. & Bray, F. 2015. Cancer incidence and mortality worldwide: sources, methods and major patterns in GLOBOCAN 2012. *International journal of cancer*, 136(5):E359-E386.

Fiebig, H.-H. & Burger, A.M. 2002. Human tumor xenografts and explants. *(In* Teicher, B.A., *ed.* Tumor models in cancer research. Totowa, NJ: Humana Press. p. 113-137).

Figueroa, J.D., Pfeiffer, R.M., Patel, D.A., Linville, L., Brinton, L.A., Gierach, G.L., Yang, X.R., Papathomas, D., Visscher, D. & Mies, C. 2014. Terminal duct lobular unit involution of the normal breast: implications for breast cancer etiology. *JNCI: Journal of the National Cancer Institute*, 106(10):1-11.

Fischerova, D. 2011. Ultrasound scanning of the pelvis and abdomen for staging of gynecological tumors: a review. *Ultrasound in obstetrics & gynecology*, 38(3):246-266.

Fischerova, D. & Burgetova, A. 2014. Imaging techniques for the evaluation of ovarian cancer. *Best practice & research clinical obstetrics & gynaecology*, 28(5):697-720.

Frangioni, J.V. 2008. New technologies for human cancer imaging. *Journal of Clinical Oncology*, 26(24):4012-4021.

Frese, K.K. & Tuveson, D.A. 2007. Maximizing mouse cancer models. *Nature reviews cancer*, 7(9):654-658.

Gandhi, S.J., Babu, S., Subramanyam, P. & Shanmuga Sundaram, P. 2013. Tc-99m macro aggregated albumin scintigraphy – indications other than pulmonary embolism: a pictorial essay. *Indian journal of nuclear medicine : IJNM : The Official Journal of the Society of Nuclear Medicine, India*, 28(3):152-162.

Ginsburg, O., Bray, F., Coleman, M.P., Vanderpuye, V., Eniu, A., Kotha, S.R., Sarker, M., Huong, T.T., Allemani, C. & Dvaladze, A. 2017. The global burden of women's cancers: a grand challenge in global health. *The Lancet*, 389(10071):847-860.

Global Burden of Disease Cancer Collaboration. 2017. Global, regional, and national cancer incidence, mortality, years of life lost, years lived with disability, and disability-adjusted life-years for 32 cancer groups, 1990 to 2015: A systematic analysis for the global burden of disease study. *JAMA oncology*, 3(4):524-548.

Guichard, S., Montazeri, A., Chatelut, E., Hennebelle, I., Bugat, R. & Canal, P. 2001. Schedule-dependent activity of topotecan in OVCAR-3 ovarian carcinoma xenograft. *Pharmacokinetic and pharmacodynamic evaluation*, 7(10):3222-3228.

Gutfilen, B. & Valentini, G. 2014. Radiopharmaceuticals in nuclear medicine: recent developments for SPECT and PET studies. *BioMed research international*, 2014:426892.

Hamanaka, R.B. & Chandel, N.S. 2012. Targeting glucose metabolism for cancer therapy. *The journal of experimental medicine*, 209(2):211-215.

Hamilton, T.C., Young, R.C., McKoy, W.M., Grotzinger, K.R., Green, J.A., Chu, E.W., Whang-Peng, J., Rogan, A.M., Green, W.R. & Ozols, R.F. 1983. Characterization of a human ovarian carcinoma cell line (NIH:OVCAR-3) with androgen and estrogen receptors. *Cancer research*, 43(11):5379-5389.

Hanahan, D. & Weinberg, Robert A. 2011. Hallmarks of cancer: the next generation. *Cell*, 144(5):646-674.

Hebbar, S.S. & Moideen, N. 2017. Imaging in ovarian cancer. *International journal of reproduction, contraception, obstetrics and gynecology*, 4(1):1-8.

Heintz, A., Odicino, F., Maisonneuve, P., Quinn, M., Benedet, J., Creasman, W., Ngan, H., Pecorelli, S. & Beller, U. 2006. Carcinoma of the ovary. *International journal of gynecology & obstetrics*, 95:S161-S192.

Hills, C.A., Kelland, L.R., Abel, G., Siracky, J., Wilson, A.P. & Harrap, K.R. 1989. Biological properties of ten human ovarian carcinoma cell lines: calibration in vitro against four platinum complexes. *British journal of cancer*, 59:527.

House, C., Hernandez, L. & Annunziata, C. 2014. Recent technological advances in using mouse models to study ovarian cancer. *Frontiers in oncology*, 4:26.

Huang, Y., Ma, C., Zhang, Q., Ye, J., Wang, F., Zhang, Y., Hunborg, P., Varvares, M.A., Hoft, D.F., Hsueh, E.C. & Peng, G. 2015. CD4(+) and CD8(+) T cells have opposing roles in breast cancer progression and outcome. *Oncotarget*, 6(19):17462-17478.

Iyoke, C.A., LuckyLawani, O., Ugwu, G.O., Ezugwu, E.C., Ajah, L.O. & Onoh, R.C. 2015. Ovarian cancer screening: the role and drawbacks of lltrasonography and feasibility in low resource settings. *American journal of clinical medicine research*, 3(1):1-8.

Jacobson, O., Kiesewetter, D.O. & Chen, X. 2015. Fluorine-18 radiochemistry, labeling strategies and synthetic routes. *Bioconjugate chemistry*, 26(1):1-18.

Jeong, Y.-Y., Outwater, E.K. & Kang, H.K. 2000. Imaging evaluation of ovarian masses. *Radiographics*, 20(5):1445-1470.

Jessmon, P., Boulanger, T., Zhou, W. & Patwardhan, P. 2017. Epidemiology and treatment patterns of epithelial ovarian cancer. *Expert review of anticancer therapy*, 17(5):427-437. (Abstract).

Johnstone, C.N., Smith, Y.E., Cao, Y., Burrows, A.D., Cross, R.S., Ling, X., Redvers, R.P., Doherty, J.P., Eckhardt, B.L. & Natoli, A.L. 2015. Functional and molecular characterisation of EO771. LMB tumours, a new C57BL/6-mouse-derived model of spontaneously metastatic mammary cancer. *Disease models & mechanisms*, 8:1-15.

Jung, J. 2014. Human tumor xenograft models for preclinical assessment of anticancer drug development. *Toxicological research*, 30(1):1-5.

Kapoor, V., McCook, B.M. & Torok, F.S. 2004. An introduction to PET-CT imaging. *Radiographics*, 24(2):523-543.

Kazarian, A., Blyuss, O., Metodieva, G., Gentry-Maharaj, A., Ryan, A., Kiseleva, E.M., Prytomanova, O.M., Jacobs, I.J., Widschwendter, M., Menon, U. & Timms, J.F. 2017. Testing breast cancer serum biomarkers for early detection and prognosis in pre-diagnosis samples. British journal of cancer, 116(4):501-508.

Kelland, L.R. 2004. Of mice and men: values and liabilities of the athymic nude mouse model in anticancer drug development. *European journal of cancer*, 40(6):827-836.

Killion, J.J., Radinsky, R. & Fidler, I.J. 1998. Orthotopic models are necessary to predict therapy of transplantable tumors in mice. *Cancer and metastasis reviews*, 17(3):279-284.

Kobayashi, E., Ueda, Y., Matsuzaki, S., Yokoyama, T., Kimura, T., Yoshino, K., Fujita, M., Kimura, T. & Enomoto, T. 2012. Biomarkers for screening, diagnosis, and monitoring of ovarian cancer. *Cancer epidemiology and prevention biomarkers*, 21(11):1902-1912.

Kratz, F. 2008. Albumin as a drug carrier: design of prodrugs, drug conjugates and nanoparticles. *Journal of controlled release*, 132(3):171-183.

Kudgus, R.A., Walden, C.A., McGovern, R.M., Reid, J.M., Robertson, J.D. & Mukherjee, P. 2014. Tuning pharmacokinetics and biodistribution of a targeted drug delivery system through incorporation of a passive targeting component. *Scientific reports*, 4:5669.

Kue, C.S., Kamkaew, A., Burgess, K., Kiew, L.V., Chung, L.Y. & Lee, H.B. 2016. Small molecules for active targeting in cancer. *Medicinal research reviews*, 36(3):494-575.

Kuhn, E., Kurman, R.J. & Shih, I.-M. 2012. Ovarian cancer is an imported disease: fact or fiction? *Current obstetrics and gynecology reports*, 1(1):1-9.

Kumar, R. & Dadparvar, S. 2007. 18F-fluoro-2-deoxy-D-glucose–positron emission tomography (PET)/PET-computed tomography in carcinoma of the cervix. *Cancer*, 110(8):1650-1653.

Latha, T.S., Panati, K., Gowd, D.S.K., Reddy, M.C. & Lomada, D. 2014. Ovarian cancer biology and immunotherapy. *International reviews of immunology*, 33(5):428-440. (Abstract).

Li, R., Zheng, K., Yuan, C., Chen, Z. & Huang, M. 2017. Be active or not: the relative contribution of cctive and passive tumor targeting of nanomaterials. *Nanotheranostics*, 1(4):346-357.

Liang, X. & Sadler, P.J. 2004. Cyclam complexes and their applications in medicine. *Chemical Society Reviews*, 33(4):246-266.

Liu, S. 2004. The role of coordination chemistry in the development of target-specific radiopharmaceuticals. *Chemical Society Reviews*, 33(7):445-461.

Liu, S. 2008. Bifunctional coupling agents for radiolabeling of biomolecules and target-specific delivery of metallic radionuclides. *Advanced drug delivery reviews*, 60(12):1347-1370.

Loke, S.Y. & Lee, A.S.G. 2018. The future of blood-based biomarkers for the early detection of breast cancer. *European journal of cance*r, 92:54-68.

Lu, J., Jiang, F., Lu, A. & Zhang, G. 2016. Linkers having a crucial role in antibody–drug conjugates. *International journal of molecular sciences*, 17(4):561.

Lutz, A.M., Willmann, J.K., Drescher, C.W., Ray, P., Cochran, F.V., Urban, N. & Gambhir, S.S. 2011. Early diagnosis of ovarian carcinoma: is a solution in sight? *Radiology*, 259(2):329-345.

Manegold-Brauer, G., Bellin, A.K., Tercanli, S., Lapaire, O. & Heinzelmann-Schwarz, V. 2014. The special role of ultrasound for screening, staging and surveillance of malignant ovarian tumors:

distinction from other methods of diagnostic imaging. *Archives of gynecology and obstetrics*, 289(3):491-498.

Mariani-Costantini, R., Elhassan, M.M.A., Aceto, G.M., Mohamedani, A.A. & Awadelkarim, K.D. 2017. Epidemiology, pathology, management and open challenges of breast cancer in central Sudan: a prototypical limited resource African setting. In Pham, P.V. (Ed.). *Breast cancer - from biology to medicine* (pp. Ch. 01). Rijeka: InTech. http://dx.doi.org/10.5772/67175 Date of access 12 Mar.2018.

Martin, A.-M. & Weber, B.L. 2000. Genetic and hormonal risk factors in breast cancer. *JNCI: Journal of the National Cancer Institute*, 92(14):1126-1135.

Meng, Y., Susan, H., Luxi, C. & Zhen, C. 2012. Human serum albumin conjugated biomolecules for cancer molecular imaging. *Current pharmaceutical design*, 18(8):1023-1031.

Mitra, A.K. 2016. Ovarian cancer metastasis: a unique mechanism of dissemination. In Xu, K. (Ed.). *Tumor metastasis*. Rijeka: InTech. http://dx.doi.org/10.5772/64700 Date of access 27 Mar.2018.

Morrow, M., Waters, J. & Morris, E. 2011. MRI for breast cancer screening, diagnosis, and treatment. *The Lancet*, 378(9805):1804-1811.

Morton, C.L. & Houghton, P.J. 2007. Establishment of human tumor xenografts in immunodeficient mice. *Nature protocols*, 2(2):247.

Murphy, J.F. 2015. Pre-clinical murine models: syngeneic models for immuno-oncology. *MOJ Immunonology*, 2(4):00052.

NASEM (National Academies of Sciences, Engineering & Medicine). 2016. Ovarian cancers: evolving paradigms in research and care. Washington, DC: National Academies Press. Available: https://www.nap.edu/read/21841/chapter/4 Date of access 27 Mar.2018.

Nazário, A.C.P., Facina, G. & Filassi, J.R. 2015. Breast cancer: news in diagnosis and treatment. *Revista da Associação Médica Brasileira*, 61(6):543-552.

Neale, G., Su, X., Morton, C.L., Phelps, D., Gorlick, R., Lock, R.B., Reynolds, C.P., Maris, J.M., Friedman, H.S., Dome, J., Khoury, J., Triche, T.J., Seeger, R.C., Gilbertson, R., Khan, J., Smith, M.A. & Houghton, P.J. 2008. Molecular characterization of the pediatric preclinical testing panel. *Clinical cancer research*, 14(14):4572-4583.

Ozmen, N., Dapp, R., Zapf, M., Gemmeke, H., Ruiter, N.V. & van Dongen, K.W. 2015. Comparing different ultrasound imaging methods for breast cancer detection. *IEEE transactions on ultrasonics, ferroelectrics, and frequency control*, 62(4):637-646.

Pace, L.E. & Shulman, L.N. 2016. Breast cancer in sub-Saharan Africa: challenges and opportunities to reduce mortality. *The oncologist*, 21(6):739-744.

Park, K. 2012. Albumin: a versatile carrier for drug delivery. *Journal of controlled release*, 157(1):3.

Park, S.B. & Lee, J.B. 2014. MRI features of ovarian cystic lesions. *Journal of magnetic resonance imaging*, 40(3):503-515.

Parris, T., Wakefield, D. & Frimmer, H. 2013. Real world performance of screening breast ultrasound following enactment of Connecticut Bill 458. *The breast journal*, 19(1):64-70.

Parslow, A.C., Parakh, S., Lee, F.-T., Gan, H.K. & Scott, A.M. 2016. Antibody–drug conjugates for cancer therapy. *Biomedicines*, 4(3):14.

Permuth-Wey, J. & Sellers, T.A. 2009. Epidemiology of ovarian cancer. In Verma, M. (Ed.). *Cancer Epidemiology: modifiable factors* (Vol. 472. pp. 413-437). Totowa, NJ: Humana Press. (Abstract). https://doi.org/10.1007/978-1-60327-492-0_20 Date of access 28 Mar.2018.

Persson, I. 2000. Estrogens in the causation of breast, endometrial and ovarian cancers — evidence and hypotheses from epidemiological findings. *The Journal of steroid biochemistry and molecular biology*, 74(5):357-364.

Pierrillas, P.B., Tod, M., Amiel, M., Chenel, M. & Henin, E. 2016. Improvement of parameter estimations in tumor growth inhibition models on xenografted animals: a novel method to handle the interval censoring caused by measurement of smaller tumors. *The AAPS Journal*, 18(2):404-415.

Ping Li, W., Meyer, L.A., Capretto, D.A., Sherman, C.D. & Anderson, C.J. 2008. Receptor-binding, biodistribution, and metabolism studies of ^{64}Cu-DOTA-cetuximab, a PET-imaging agent for epidermal growth-factor receptor-positive tumors. *Cancer biotherapy & radiopharmaceuticals*, 23(2):158-171. (Abstract).

Pogo, B. & Holland, J.F. 2011. Breast cancer carcinogenesis. In Schwab, M. (Ed.). *Encyclopedia of cancer* (pp. 493-496). Berlin, Heidelberg: Springer Berlin Heidelberg. https://doi.org/10.1007/978-3-642-16483-5_6665 Date of access 22 Mar.2018.

Pourgholami, M.H., Cai, Z.Y., Lu, Y., Wang, L. & Morris, D.L. 2006. Albendazole: a potent inhibitor of vascular endothelial growth factor and malignant ascites formation in OVCAR-3 tumor-bearing nude mice. *Clinical cancer research*, 12(6):1928-1935.

Ptak, A. & Gregoraszczuk, E.L. 2013. Oestrogens, xenoestrogens and hormone-dependent cancers. *Carcinogenesis*: InTech. https://www.intechopen.com/books/carcinogenesis/oestrogens-xenoestrogens-and-hormone-dependent-cancers Date of access 27 Jun.2018.

Quadri, S. & Vriesendorp, H. 1998. Effects of linker chemistry on the pharmacokinetics of radioimmunoconjugates. *The quarterly journal of nuclear medicine and molecular imaging*, 42(4):250. (Abstract).

Rauh-Hain, J.A., Krivak, T.C., del Carmen, M.G. & Olawaiye, A.B. 2011. Ovarian cancer screening and early detection in the general population. *Reviews in obstetrics and gynecology*, 4(1):15.

Reid, B.M., Permuth, J.B. & Sellers, T.A. 2017. Epidemiology of ovarian cancer: a review. *Cancer biology & medicine*, 14(1):9-32.

Richmond, A. & Su, Y. 2008. Mouse xenograft models vs GEM models for human cancer therapeutics. *Disease models & mechanisms*, 1(2-3):78-82.

Riman, T., Nilsson, S. & Persson, I.R. 2004. Review of epidemiological evidence for reproductive and hormonal factors in relation to the risk of epithelial ovarian malignancies. *Acta obstetricia et gynecologica Scandinavica*, 83(9):783-795.

Roganovic, D., Djilas, D., Vujnovic, S., Pavic, D. & Stojanov, D. 2015. Breast MRI, digital mammography and breast tomosynthesis: comparison of three methods for early detection of breast cancer. *Bosnian journal of basic medical sciences*, 15(4):64-68.

Rosen, D.G., Yang, G., Liu, G., Mercado-Uribe, I., Chang, B., Xiao, X., Zheng, J., Xue, F.-X. & Liu, J. 2009. Ovarian cancer: pathology, biology, and disease models. *Frontiers in bioscience : a journal and virtual library*, 14:2089-2102.

Russell, S.E. & McCluggage, W.G. 2004. A multistep model for ovarian tumorigenesis: the value of mutation analysis in the KRAS and BRAF genes. *The Journal of pathology*, 203(2):617-619.

Russo, J., Mailo, D., Hu, Y.-F., Balogh, G., Sheriff, F. & Russo, I.H. 2005. Breast differentiation and its implication in cancer prevention. *Clinical cancer research*, 11(2):931s-936s.

Russo, J. & Russo, I.H. 2004. Development of the human breast. *Maturitas*, 49(1):2-15.

Sakhare, S.S., Rao, G.G., Mandape, S.N. & Pratap, S. 2014. Transcriptome profile of OVCAR3 cisplatin-resistant ovarian cancer cell line. *BMC Bioinformatics*, 15(Suppl 10):P21-P21.

Santarius, T., Shipley, J., Brewer, D., Stratton, M.R. & Cooper, C.S. 2010. A census of amplified and overexpressed human cancer genes. *Nature reviews of cancer*, 10(1):59-64.

Sarko, D., Eisenhut, M., Haberkorn, U. & Mier, W. 2012. Bifunctional chelators in the design and application of radiopharmaceuticals for oncological diseases. *Current medicinal chemistry*, 19(17):2667-2688.

Sausville, E.A. & Burger, A.M. 2006. Contributions of human tumor xenografts to anticancer drug development. *Cancer research*, 66(7):3351-3354.

Schroeder, T., Vidal Melo, M.F. & Venegas, J.G. 2011. Analysis of 2-[Fluorine-18]-Fluoro-2-deoxy-D-glucose uptake kinetics-in PET studies of pulmonary inflammation. *Academic radiology*, 18(4):418-423.

Schuh, J.C.L. 2004. Trials, tribulations, and trends in tumor modeling in mice. *Toxicologic pathology*, 32(1_suppl):53-66.

Schuur, E.R. & DeAndrade, J.P. 2015. Breast cancer: Molecular mechanisms, diagnosis, and treatment. In De Mello, R.A., Tavares, Á. & Mountzios, G. (Eds.). *International manual of oncology practice: (iMOP) - Principles of medical oncology* (pp. 155-200). Cham: Springer international publishing. https://doi.org/10.1007/978-3-319-21683-6_9 Date of access 23 Aprl.2018.

Shah, T.A. & Guraya, S.S. 2017. Breast cancer screening programs: review of merits, demerits, and recent recommendations practiced across the world. *Journal of microscopy and ultrastructure*, 5(2):59-69.

Shih, I.-M. & Kurman, R.J. 2004. Ovarian tumorigenesis: a proposed model based on morphological and molecular genetic analysis. *The American journal of pathology*, 164(5):1511-1518.

Shultz, L.D., Brehm, M.A., Garcia, J.V. & Greiner, D.L. 2012. Humanized mice for immune system investigation: progress, promise and challenges. *Nature reviews. Immunology*, 12(11):786-798.

Singh, M. & Johnson, L. 2006. Using genetically engineered mouse models of cancer to aid drug development: an industry perspective. *Clinical cancer research*, 12(18):5312-5328.

Smith, R.A., Saslow, D., Sawyer, K.A., Burke, W., Costanza, M.E., Evans, W.P., Foster, R.S., Hendrick, E., Eyre, H.J. & Sener, S. 2003. American Cancer Society Guidelines for breast cancer screening: Update 2003. *CA: A cancer journal for clinicians*, 53(3):141-169.

Stagg, J., Divisekera, U., McLaughlin, N., Sharkey, J., Pommey, S., Denoyer, D., Dwyer, K.M. & Smyth, M.J. 2010. Anti-CD73 antibody therapy inhibits breast tumor growth and metastasis. *Proceedings of the National Academy of Sciences*, 107(4):1547-1552.

Suggitt, M. & Bibby, M.C. 2005. 50 Years of preclinical anticancer drug screening: empirical to target-driven approaches. *Clinical cancer research*, 11(3):971-981.

Sugiura, K. & Stock, C.C. 1952. Studies in a tumor spectrum. I. Comparison of the action of methylbis (2-chloroethyl) amine and 3-bis (2-chloroethyl) aminomethyl-4-methoxymethyl-5-hydroxy-6-methylpyridine on the growth of a variety of mouse and rat tumors. *Cancer*, 5(2):382-402.

Sundar, S., Neal, R.D. & Kehoe, S. 2015. Diagnosis of ovarian cancer. *BMJ*, 351:h4443.

Szadvari, I., Krizanova, O. & Babula, P. 2016. Athymic nude mice as an experimental model for cancer treatment. *Physiological research*, 65(Supplementum 4):S441.

Tapia, J., Alvarado, M.d., Bustos, B.n., Lukoviek, V. & Rice, G.E. 2013. Ovarian cancer in vitro diagnostics: new approaches to earlier detection. In DíAz-Padilla, I.N. (Ed.). *Ovarian cancer - a clinical and translational update*. Rijeka: InTechOpen. https://www.intechopen.com/books/ovarian-cancer-a-clinical-and-translational-update/ovarian-cancer-in-vitro-diagnostics-new-approaches-to-earlier-detection Date of access 03 Aprl.2018.

Teicher, B.A. 2006. Tumor models for efficacy determination. *Molecular cancer therapeutics*, 5(10):2435-2443.

Thomas, M.P. 2012. Differential tolerance of a cancer and non-cancer cell line to amino acid depriviation: mechanistic insight and clinical potential. Stellenbosch: SUN.(Dissetation-PhD).

Ting, G., Chang, C.-H. & Wang, H.-E. 2009. Cancer nanotargeted radiopharmaceuticals for tumor imaging and therapy. *Anticancer research*, 29(10):4107-4118.

Tornesello, A., Buonaguro, L., Tornesello, M. & Buonaguro, F. 2017. New insights in the design of bioactive peptides and chelating agents for imaging and therapy in oncology. *Molecules*, 22(8):1282.

Townsend, D. 2004. Physical principles and technology of clinical PET imaging. *Annals-Academy of Medicine Singapore*, 33(2):133-145.

Troiani, T., Schettino, C., Martinelli, E., Morgillo, F., Tortora, G. & Ciardiello, F. 2008. The use of xenograft models for the selection of cancer treatments with the EGFR as an example. *Critical reviews in oncology / hematology*, 65(3):200-211.

Ueda, Y., Enomoto, T., Kimura, T., Miyatake, T., Yoshino, K., Fujita, M. & Kimura, T. 2010. Serum biomarkers for early detection of gynecologic cancers. *Cancers*, 2(2):1312-1327.

Upponi, J.R. & Torchilin, V.P. 2014. Passive vs. active targeting: an update of the EPR role in drug delivery to tumors. In Alonso, M.J. & Garcia-Fuentes, M. (Eds.). *Nano-oncologicals: new targeting and delivery approaches* (pp. 3-45). Cham: Springer International Publishing. https://doi.org/10.1007/978-3-319-08084-0_1 Date of access 27 Jun.2018.

Vallabhajosula, S. 2009. Molecular imaging: radiopharmaceuticals for PET and SPECT: Springer Science & Business Media. https://books.google.co.za/books?hl=en&lr=&id=bUmcxfnlkt8C Date of access 06 Apr 2017.

Vargo-Gogola, T. & Rosen, J.M. 2007. Modelling breast cancer: one size does not fit all. *Nature reviews cancer*, 7(9):659-672.

Vasir, J.K. & Labhasetwar, V. 2005. Targeted drug delivery in cancer therapy. *Technology in cancer research & treatment*, 4(4):363-374.

Voskoglou-Nomikos, T., Pater, J.L. & Seymour, L. 2003. Clinical predictive value of the in vitro cell Line, human xenograft, and mouse allograft preclinical cancer models. *Clinical cancer research*, 9(11):4227-4239.

Wadsak, W. & Mitterhauser, M. 2010. Basics and principles of radiopharmaceuticals for PET/CT. *European journal of radiology*, 73(3):461-469.

Wang, L. 2017. Early diagnosis of breast cancer. *Sensors*, 17(7):1572.

Webb, P.M. & Jordan, S.J. 2017. Epidemiology of epithelial ovarian cancer. *Best practice & research clinical obstetrics & gynaecology*, 41:3-14.

Wittekind, D. 2003. Traditional staining for routine diagnostic pathology including the role of tannic acid. 1. Value and limitations of the hematoxylin-eosin stain. *Biotechnic & histochemistry*, 78(5):261-270.

Workman, P., Aboagye, E., Balkwill, F., Balmain, A., Bruder, G., Chaplin, D., Double, J., Everitt, J., Farningham, D. & Glennie, M. 2010. Guidelines for the welfare and use of animals in cancer research. *British journal of cancer*, 102(11):1555.

Xu, X. & Prestwich, G.D. 2010. Inhibition of tumor growth and angiogenesis by a lysophosphatidic acid antagonist in an engineered three-dimensional lung cancer xenograft model. *Cancer*, 116(7):1739-1750.

Yan, L., Rosen, N. & Arteaga, C. 2011. Targeted cancer therapies. *Chinese journal of cancer*, 30(1):1-4.

Yin, H., Liao, L. & Fang, J. 2014. Enhanced permeability and retention (EPR) effect based tumor targeting: the concept, application and prospect. *JSM Clinical oncolology and research*, 2(1):1010.

Zavesky, L., Jancarkova, N. & Kohoutova, M. 2011. Ovarian cancer: origin and factors involved in carcinogenesis with potential use in diagnosis, treatment and prognosis of the disease. *Neoplasma*, 58(6):457.

Zayyan, M.S., Ahmed, S.A., Oguntayo, A.O., Kolawole, A.O. & Olasinde, T.A. 2017. Epidemiology of ovarian cancers in Zaria, Northern Nigeria: a 10-year study. *International journal of women's health*, 9:855-860.

Zheng, K., Li, R., Zhou, X., Hu, P., Zhang, Y., Huang, Y., Chen, Z. & Huang, M. 2015. Dual actions of albumin packaging and tumor targeting enhance the antitumor efficacy and reduce the cardiotoxicity of doxorubicin *in vivo*. *International journal of nanomedicine*, 10:5327-5342.

CHAPTER 3: ESTABLISHMENT AND CHARACTERISATION OF BREAST AND OVARIAN TUMOUR-BEARING MOUSE MODELS

Abstract

Aim: The purpose of this study was to develop an immune-competent allograft mouse model of rodent breast cancer and an immune-compromised xenograft mouse model of human ovarian cancer which will be used to evaluate the efficacy of novel therapeutic and diagnostic agents.

Methods: The breast tumour model was established by co-injection of E0771 cells with Matrigel subcutaneously into the mammary fat pad of C57BL/6 (immune-competent) female mice post anaesthetisation. The human ovarian tumour model had OVCAR-3 cells inoculated, combined with either PBS or Matrigel subcutaneously, above the proximal tibia of athymic nude (nu/nu) (immune-deficient) female mice. Once a tumour was palpable, tumour progression was monitored two to three times a week by measuring tumour size using a digital calliper and the tumour volume was determined. The animals were humanely euthanised once tumour volumes of ≥300 mm^3 were attained. The tumours were then harvested to determine the tumour growth rate and histological characterisation was done using haematoxylin and eosin (H & E) staining.

Results: A tumour take rate of 100% (26/26) was obtained for the E0771 breast allograft mouse model with tumour onset detected within 7 days post inoculation. The OVACAR-3 cell line grew subcutaneously, with or without the use of Matrigel, however faster tumour growth was achieved by co-inoculation with Matrigel. Both E0771 and OVCAR-3 tumours were actively proliferating, as demonstrated by the presence of mitotic figures. Furthermore, inoculum of OVCAR-3 cells with Matrigel resulted in enhanced tumour vascularisation compared to PBS inoculum.

Conclusion: The E0771 breast tumour model was successfully established with reproducibility. The OVCAR-3 cell line grew slowly subcutaneously, however, earlier tumour onset and enhanced tumour growth can be obtained by the use of an extracellular matrix.

***Key words*:** Breast cancer, ovarian cancer, tumour-bearing mouse model, allograft, xenograft

1.1 Introduction

Breast and ovarian malignancies are among the cancers affecting the female population with 2.1 million and 295 414 newly diagnosed cases expected in 2018 worldwide, respectively (Bray et al., 2018). Although ovarian cancer is less common than breast cancer, it is the most lethal gynaecological cancer (Nezhat et al., 2015; Taylor, 2001). Much research is being directed towards finding effective ways to treat and diagnose breast and ovarian cancers and as a result representative and reliable animal models are required for the successful translation of preclinical data into clinical outcome.

One of the most effective and preferable methods to model cancer includes the transplantation of murine cancer cells into immune-competent mice (termed allograft model) or transplantation of human originating cancer cells into immune-deficient mice (termed xenograft model) (Navale, 2013; Schuh, 2004; Workman *et al.*, 2010). To successfully develop an allograft or xenograft model, a number of factors such as the site of transplantation, number of cells and host animal should be considered, as these may influence the tumour take rate and growth (Benton *et al.*, 2014). In addition, the type of cells should also be considered as some cells that exhibit good growth *in vitro*, grow poorly *in vivo* (Benton *et al.*, 2011; Workman *et al.*, 2010). Furthermore, co- injection of tumour cells with extracellular matrix proteins, such as the soluble basement membrane proteins extracted from a mouse sarcoma known as Matrigel (Kleinman & Martin, 2005; Workman *et al.*, 2010) has shown to enhance *in vivo* tumour growth of different types of cells (Fridman *et al.*, 1991). Moreover, the advantage of using Matrigel to induce tumour growth includes the reduction of study duration and therefore, the cost of animal care (Benton *et al.*, 2011).

According to Schuh (2004), the design of preclinical studies involving the use of tumour-bearing mouse models requires knowledge of the tumour behaviour *in vivo*. This can be done by setting up pilot tumour growth studies consisting of 5 to10 animals which could help define tumour growth patterns, adverse effects related to tumour growth, humane end points and determine whether the model is reproducible (Workman *et al.*, 2010). This data can also be valuable in determining the number of animals required, the study time frame and statistically significant endpoints for the main study (Workman *et al.*, 2010). The implantation technique should also be refined to prevent accidental implantation into the muscle mass or visceral cavities which may then delay tumour onset or cause failure of tumour engraftment and affect the reproducibility of the study (Schuh, 2004).

The main interest of the current study was to establish murine breast and human ovarian tumour-bearing models by subcutaneous implantation of E0771 and OVCAR-3 cells into immune-competent and immune-deficient mice, respectively and to define the *in vivo* growth

characteristics of each model. In addition, the histological characteristics of the tumours derived from each cell line post-inoculation were also determined.

1.2 Materials and Methods

1.2.1 Materials

The human ovarian cancer cell line, OVCAR-3 was purchased from American Type Culture Collection (ATCC) (Manassas, Virginia, US) and the murine breast cancer cell line, E0771 was donated by Stellenbosch University (Western Cape, SA). Trypsin/EDTA, trypan blue, penicillin/streptomycin (PenStrep) a broad spectrum antibiotic cocktail, Dulbecco's Modified Eagle's Medium (DMEM) with glutamine and Roswell Park Memorial Institute (RPMI) 1640 with HEPES (4-(2-hydroxyethyl)-1-piperazineethanesulfonic acid) culture medium were purchased from Lonza (Basel, Switzerland). Matrigel basement membrane matrix was purchased from Corning (New York, US). Bovine insulin, phosphate-buffered saline (PBS) tablets and histological grade xylene were bought from Sigma-Aldrich (St.Louis, MO, USA). Absolute ethanol and Entellan® mounting media were purchased from Merck (Darmstadt, Germany). Foetal bovine serum (FBS) was obtained from GE Healthcare HyClone (Chicago, IIIinois, US). Formalin was supplied by Pathcare (Goodwood, SA). The histoplast wax was obtained from ThermoFisher Scientific (Waltham, Massachusetts, US).

1.2.2 Methods

1.2.2.1 Cell culture

The mouse mammary adenocarcinoma cells, E0771, were cultured in DMEM supplemented with 20% FBS and 1% PenStrep. The human ovarian cancer cells, OVCAR-3, were cultured in RPMI media supplemented with 10% FBS, 0.01 mg/ml bovine insulin and 1% PenStrep. Both cell lines were maintained at 37°C in a humidified incubator containing 5% CO_2.

The cells were routinely passaged at 70-80% confluency. Detachment of the cells from the plate was done by trypsinisation for 4 min and the digestion reaction was deactivated by addition of complete medium. Subsequently, the cells were pelleted using a PLC-012 universal centrifuge (GEMMY Industrial Corporation, Taipei, Taiwan) at 1000 rpm for 4 min and re-suspended in complete medium. To determine cell viability, 40 µl of cell suspension was mixed with 40 µl trypan blue followed by manual counting of the viable cells using a haemocytometer. The cell density (cells/ml) was calculated using the following equation:

$$\text{Cell density} = \text{Total average of viable cells} \times 2 \times 10^4 \qquad \textbf{(Equation 1)}$$

1.2.2.2 Animal husbandry

Female C57BL/6 and athymic nude (nu/nu) mice aged 6-8 weeks old were bred in house. The animals were housed at the PCDDP Vivarium at the North-West University where they were looked after by qualified care givers. The animals were group-caged (3-6 mice/cage) in individually ventilated cages (IVC) under normal conditions (22 ± 2˚C, 55± 10% humidity, 15 ± 5 Pa and 12 h light/dark cycles). Sterile standard rodent chow and water were provided *ad libitum* and; the sterile corncob bedding was changed regularly. Prior to inoculation, a preliminary health check and enrolment of the animals in the study was done by a qualified laboratory animal technician. The procedures involving the animals were approved by the NWU-AnimCare REC committee (Ethics approval number: NWU-00254-17-A5).

1.2.2.3 Establishing allograft and xenograft tumour-bearing mouse models

An allograft model of E0771 breast tumour was established in C57BL/6 mice and a xenograft model of OVCAR-3 ovarian tumour was established in athymic nude (nu/nu) mice. Both models were characterised with respect to their tumour growth patterns, gross pathology and histology to confirm malignancy.

1.2.2.3.1 E0771 derived allograft model

For establishment of the breast tumour model, E0771 cells were harvested by trypsinisation once they reached 70-80 % confluency and cell viability was determined as described above. The cells were then pelleted by centrifugation at 1000 rpm for 4 min and re-suspended in DMEM (without FBS and PenStrep) to obtain a concentration of 2.5 x 10^6 cells/ml. Subsequently, the cell suspension was mixed with ice cold Matrigel (1:1). The cell suspension and any tool used for cell preparation was kept on ice until injection to prevent Matrigel from solidifying.

Prior to inoculation, each C57BL/6 mouse was anaesthetised using 4% isoflurane in oxygen and then 2% for maintenance. Following anaesthesia, 0.1 ml of the cell suspension in Matrigel (2.5 x 10^5 cells/ mouse) was subcutaneously inoculated into the left thoracic mammary fat pad using an ice cold 23 gauge (G) needle as previously described by Davis (2016).

A pilot study consisting of two groups of six animals each (12 animals) was carried out with inoculation of the two groups on two separate occasions as part of the establishment of the tumour model. Upon completion of the pilot study, an additional group with 14 animals (BC-G3) was inoculated for a separate study and the data was included in the current study. The details of the cell suspension and dates of inoculation for each group are given in Table 1.

Table 1: Details of E0771 cell suspension for inoculation into female C57BL/6 mice

Inoculation date	BC-G	#Animals	Cell Passage	Cell viability (%)	Matrigel concentration (mg/ml)
06-04-2017	1	6	33	100	19.90
11-05-2017	2	6	28	94	19.90
23-06-2017	3	14	32	84	9.20

BC-G: Breast cancer group

The growth of E0771 tumours was monitored (described in section 2.2.4) and the following parameters were evaluated: tumour take and growth rate and; the influence of Matrigel concentration on tumour onset and tumour take rate.

1.2.2.3.2 OVCAR-3 derived xenograft model

For the establishment of the ovarian tumour model, OVCAR-3 cells were harvested at 70-80% confluency by trypsinisation and the number of viable cells were determined as described above. For inoculation using PBS, the cells were pelleted by centrifugation (1000 rpm for 4 min) and re- suspended to 10 x 10^6 cells/ml in PBS. Thereafter, six athymic nude (nu/nu) mice (3 animals/group) were inoculated with 0.1 ml of cell suspension (1× 10^6 cells/mouse) subcutaneously above the proximal tibia using a 25 G needle.

For inoculation using Matrigel, the cells were re-suspended in ice cold RPMI medium (without FBS, PenStrep and insulin bovine) and 9.20 mg/ml Matrigel (1:1) to obtain 10 x 10^6 cells/ml. Thereafter, four athymic nude (nu/nu) mice were inoculated with 0.1 ml of cell suspension/Matrigel (1×10^6 cells/mouse) subcutaneously above the proximal tibia using a 25 G needle. The cell suspension and any tool used for cell preparation was kept on ice until injection to prevent Matrigel from solidifying.

Initially, 12 animals were selected to establish the experimental protocol, however, due to a shortage of animals the number was reduced. Two groups of three animals per group were inoculated on separate dates with the PBS inoculum, while four animals were inoculated with the Matrigel inoculum. The details of cell suspension and dates of inoculation for each group are given in Table 2. The growth of the OVCAR-3 tumours was monitored (described in section 2.2.4) and the following parameters were evaluated: tumour take rate, tumour onset and the influence of Matrigel on tumour growth.

Table 2: Details of OVCAR-3 cell suspension for inoculation into female athymic nude (nu/nu) mice.

Inoculation date	OV-G	#Animals	Cell Passage	Cell viability (%)	Suspension medium
13-07-2017	1	3	3	87	PBS
28-07-2017	2	3	4	100	PBS
15-08-2017	3	4	7	93	Matrigel (9.20 mg/ml)

OV-G: Ovarian cancer group

1.2.2.4 Monitoring tumour growth post inoculation

The dimensions of the tumours were measured with a digital calliper (Toolquip & Allied, South Africa) two to three times a week, where the length was the longest dimension and the width was the shortest dimension. The measurements were then used to determine tumour volume using the following equation:

$$\text{Tumour volume } (mm^3) = \tfrac{1}{2} (\text{length (mm)} \times [\text{width (mm)}]^2) \quad \textbf{(Equation 2)}$$

Health assessments were carried out throughout the duration of the study prior to measuring the tumours by monitoring the following clinical signs: weight loss, tumour ulceration and any abnormal behaviour indicating pain. The animals were euthanised by cervical dislocation once the tumours reached a volume of ≥ 300 mm^3. This study end point was based on a previous study (Davis, 2016). After euthanasia, the tumour tissue was harvested for gross pathology analysis and immediately fixed in formalin.

1.2.2.5 Gross pathology

The tumour tissues were examined for the presence or absence of ulceration. The length (mm) and the width (mm) of the tumours were measured using digital callipers and tumour volume (mm^3) was determined using Equation 2. The tumours were also weighed (g) using a Sartorius Entris 2202-1s balance (Sartorius Lab instruments GmbH &Co. KG, Germany) and the tumour growth rate was determined using the following equation:

$$\text{Growth rate (g/day)} = \text{Final } \textit{ex vivo} \text{ tumour weight (g)/days from tumour onset till euthanasia} \quad \textbf{(Equation 3)}$$

1.2.2.6 Histological characterisation

Formalin fixed E0771 and OVCAR-3 derived tumour tissues were rinsed under running tap water and dehydrated in a series of increasing percentages of alcohol (Figure 1). Thereafter, the tissues were elucidated with xylene and infiltrated with paraffin wax at 60°C under vacuum (Figure 1). Following wax infiltration, the tissues were embedded in paraffin wax blocks using a SLEE MPS/P2 embedding centre (SLEE medical GmbH, Germany) and left overnight to harden.

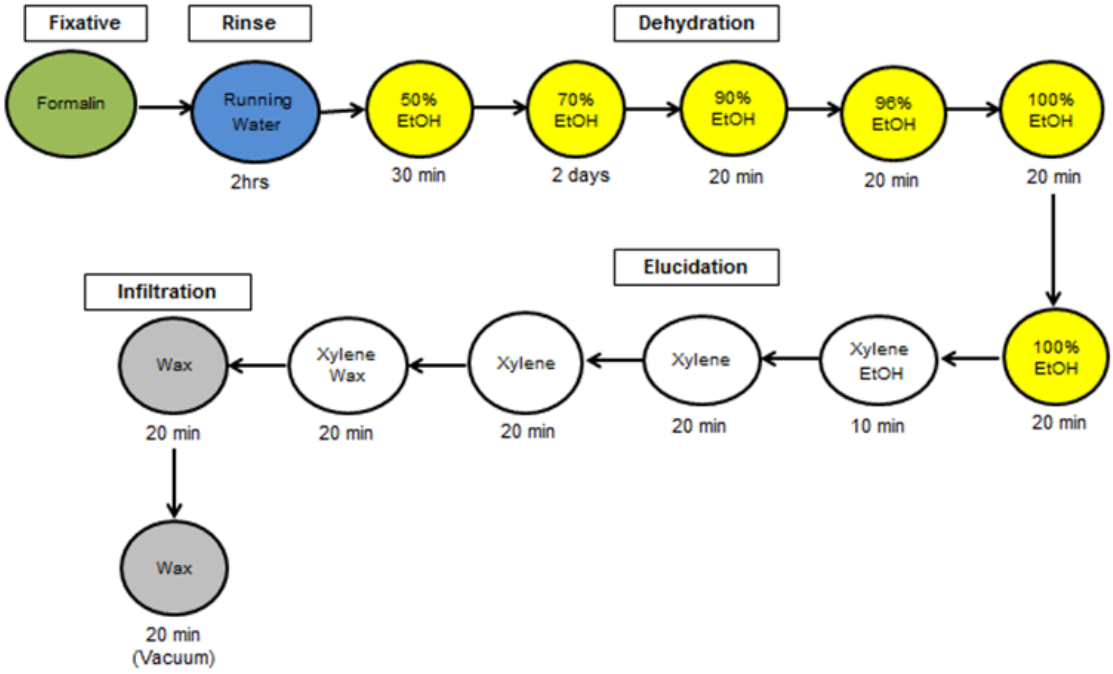

Figure 1: Tissue processing of E0771 and OVCAR-3 derived tumours for wax infiltration and embedding. Adapted with permission from Weldon (2005).

The paraffin embedded tissues were sectioned at 10 µm using Reickert-Jung 2050 automated microtome (Leica microsystems GmbH, Germany). The sections were stretched in a water bath at 40°C and mounted on a microscope slide. Thereafter, the sections were left overnight in an oven at 35°C to adhere on the slides.

For haematoxylin and eosin (H & E) staining, the tissue sections were dewaxed in xylene followed by hydration using a series of alcohol percentages, as depicted in Figure 2. After tissue hydration, the sections were stained using haematoxylin followed by eosin stain. During the staining process the sections were washed under running water to prevent cross-contamination. Following staining, the sections were dehydrated and elucidated with xylene/ethanol mixture. The slides were then mounted on the cover slips using Entellan mounting media and left overnight to air-dry.

The images were captured using a Nikon Eclipse E800microscope equipped with NIS-Elements Viewer Version D3.2 (Nikon, Japan). Interpretation of the tissue sections was done by a qualified pathologist.

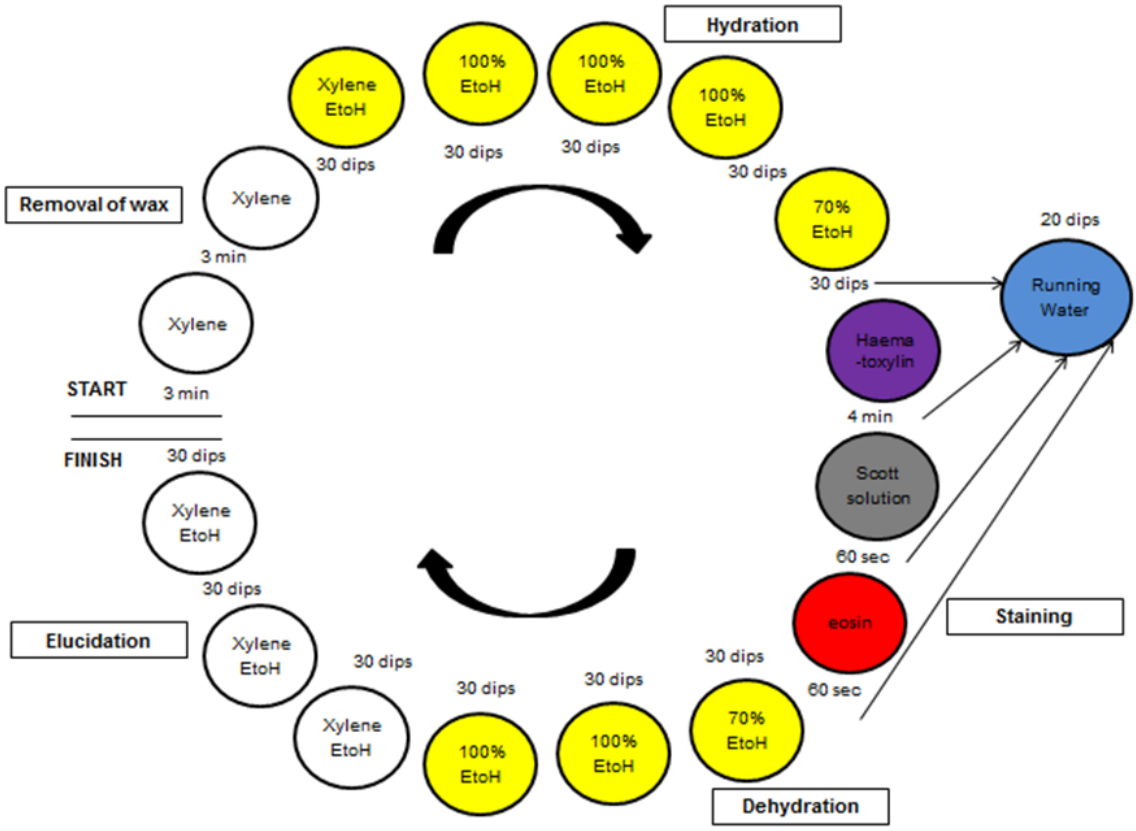

Figure 2: Staining procedure of paraffin wax embedded tumour sections of E0771 and OVCAR- 3 derived tumours with haematoxylin and eosin. Adapted with permission from Weldon (2005).

1.2.2.7 Statistical analysis

Statistical analysis of *in situ* and *ex vivo* tumour volumes was done using one-way analysis of variance (ANOVA) followed by Tukey's multiple comparison test to determine the significance of the differences within and between the groups. Unpaired student's *t*-test was used to analyse the statistical difference of tumour growth rate between two groups. A p-value of less than 0.05 was considered significant. All statistical analyses were performed using GraphPad Prism software. Data is represented as mean ± standard deviation (SD).

1.3 Results

1.3.1 E0771 derived allograft model

1.3.1.1 Tumour progression

To establish the breast tumour allograft mouse model, E0771 cells suspended in Matrigel were subcutaneously transplanted in the thoracic mammary fat pad of C57BL/6 female mice as described. For BC-G1, palpable tumours were detected within 7 days post inoculation with a tumour take rate of 6/6 animals (Figure 3). Rapid tumour growth was observed in 5/6 animals with tumour volumes greater than 300 mm^3 obtained 7 days after inoculation. The sixth animal (mouse 4) was monitored continuously but the tumour growth was slow and the volume remained <200 mm^3. At day 8 post inoculation, mouse 4 was found moribund during routine monitoring and it was euthanised immediately. Figure 4 shows the tumour progression of BC-G2 and based on the graph, tumours were detected within 10 days post inoculation. Similar to BC-G 1, tumour take rate of 6/6 animals was obtained.

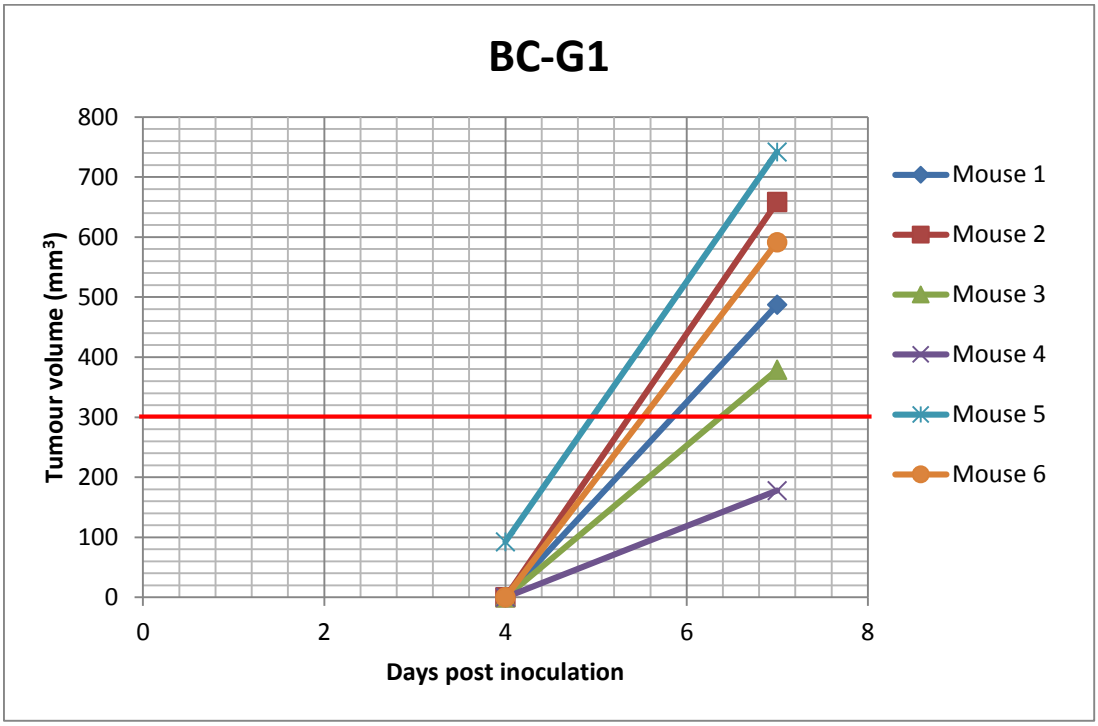

Figure 3: *In situ* tumour volume measurements for BC-G1 after inoculation of E0771 cells suspended in Matrigel (19.90 mg/ml). The red line represents the study end point (≥300 mm^3).

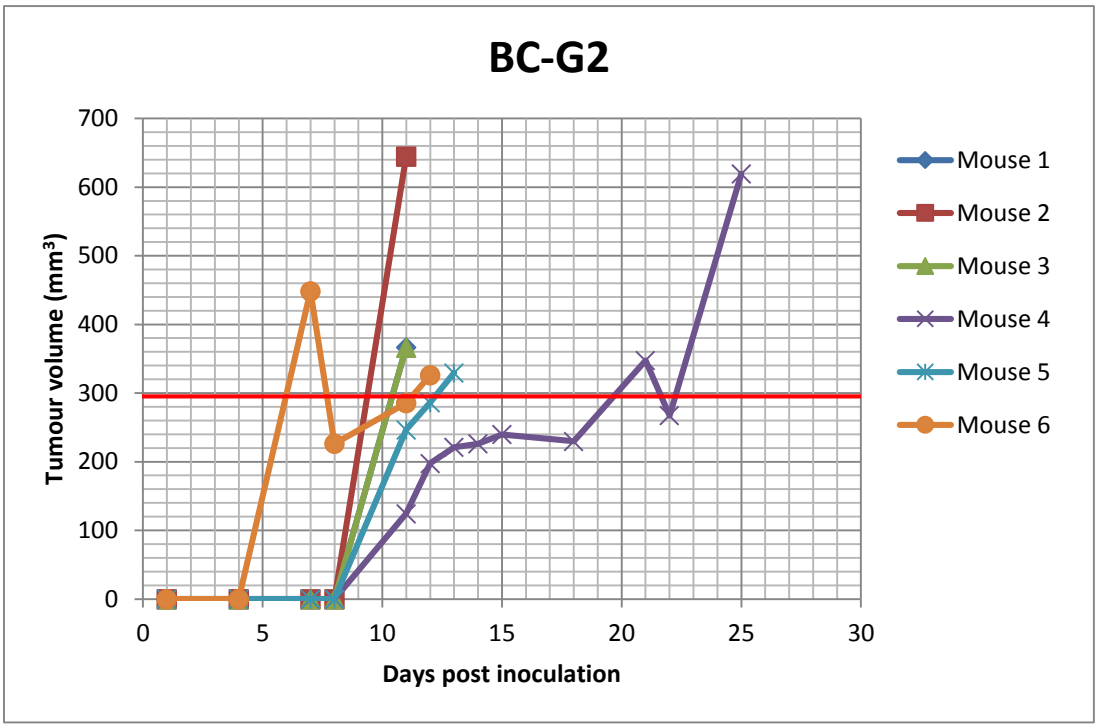

Figure 4: *In situ* tumour volume measurements for BC-G2 after inoculation of E0771 suspended in Matrigel (19.90 mg/ml). The red line represents the study end point (≥300 mm^3).

In BC-G3 (14 animals), the tumour was established by inoculation of 2.5 × 10^5 cells/ per mouse with 9.20 mg/ml diluted Matrigel. During inoculation of the first 5 (mouse 1-2, 5-7) animals, leakage of the cell suspension upon withdrawal of the needle (23 G) was a major challenge, as a result, the needle size was changed and a 25 G needle was used for the remaining 9 (mouse 3- 4, 8-14) animals with no leakage observed. As shown in Figure 5, neither the Matrigel concentration, nor the leakage and change of needle size affected the tumour onset (within 7 days after inoculation) and tumour take rate (14/14 animals).

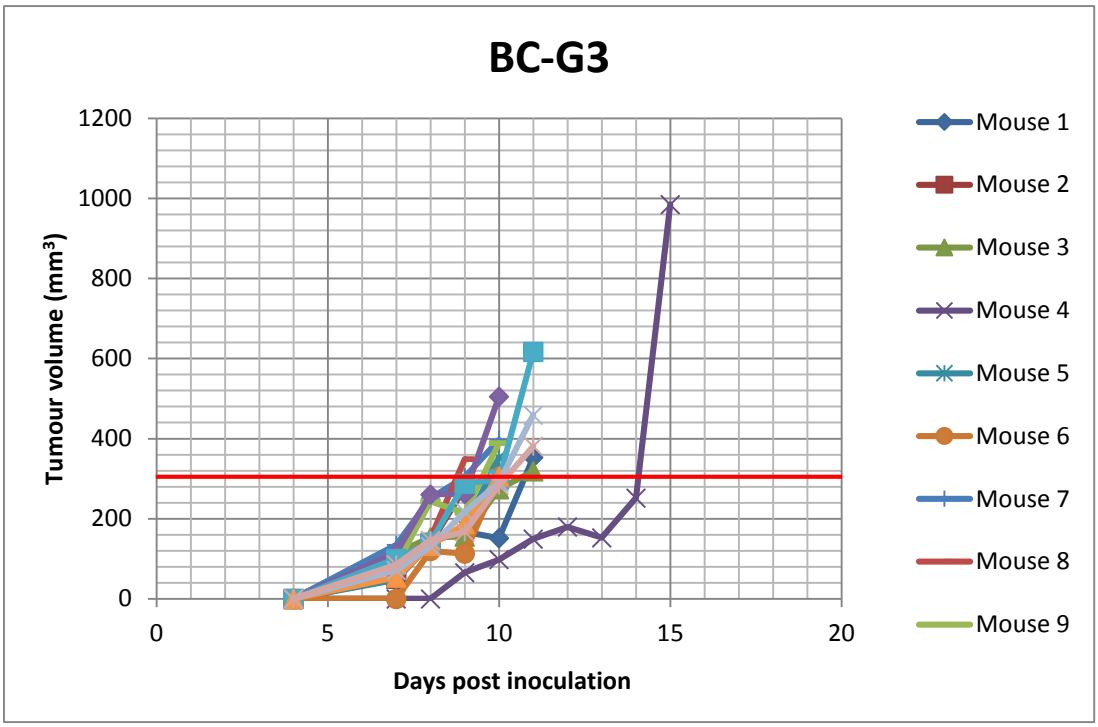

Figure 5: *In situ* tumour volume measurements for BC-G3 after inoculation of E0771 cells suspended in diluted Matrigel (9.20 mg/ml). The red line represents the study end point (≥300 mm^3).

1.3.1.2 Gross pathology

During the monitoring of tumour progression, the tumours at the site of inoculation were both palpable and visible (Figure 6A). Once the tumours reached the end point tumour volume (≥300 mm^3) the animals were euthanised and the tumour tissues (except for BC-G3 which was enrolled in a separate study), were harvested.

According to gross pathology analysis, the tumours were generally solid with no visible signs of ulceration (Figure 6B-C). The tumour from mouse 4 (BC-G1), was sent for further analysis as the animal was found moribund on day 8 after inoculation. According to the pathology report, the tumour was ulcerated and surrounded by engorged subcutaneous vessels (image not available). Based on these findings, tumour ulceration was recorded in 1/12 animals.

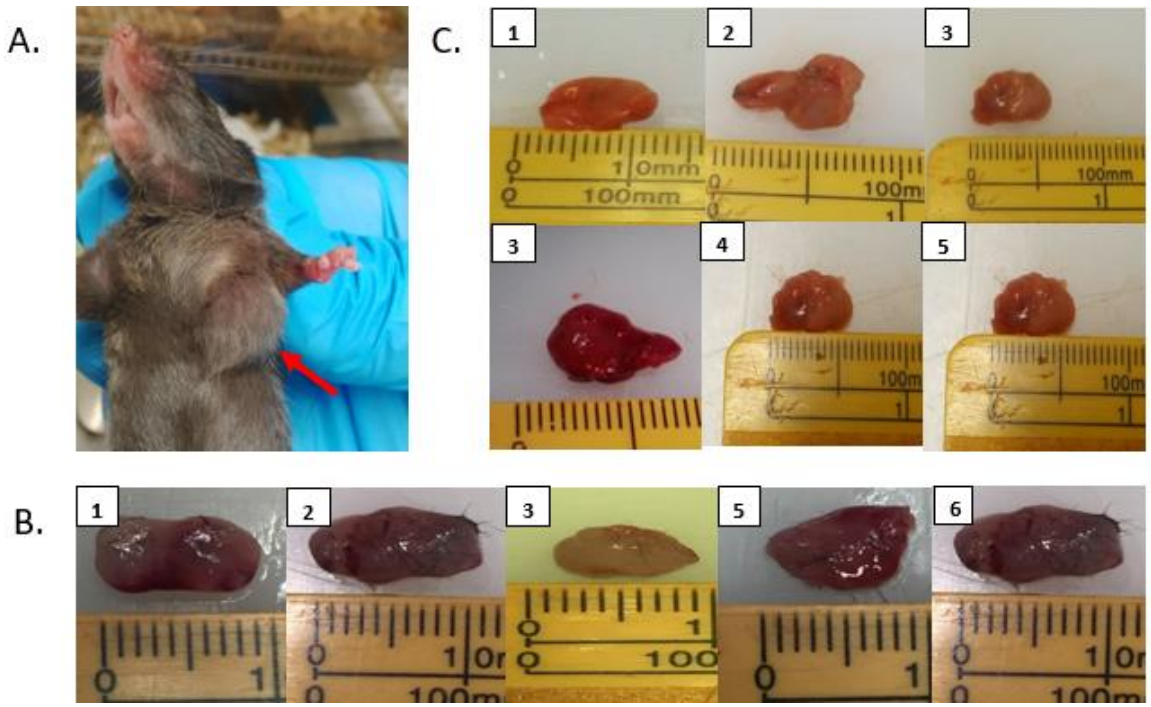

Figure 6: Breast tumours induced by subcutaneous transplantation of E0771 cells suspended in Matrigel into the thoracic mammary fat pad of C57BL/6 mice. **(A)** Image of a C57BL/6 mouse showing *in situ* tumour growth on the thoracic mammary fat pad (*red arrow).* Tumours excised from mice (**B**=BC-G1 and **C**=BC-G2). Inset numbers represent mouse number.

The ex *vivo* tumour volumes of BC-G1 and 2 were measured and a comparison was made with the final *in situ* tumour volumes (Figure 7). A one-way ANOVA revealed that *ex vivo* tumour measurements of BC-G1 were statistically smaller with intra-and inter group variability ($p<0.05$). This significant variation was due to inaccurate measurements during *in situ* tumour monitoring, which resulted in early euthanasia of the animals and excision of the tumours before the tumour volumes of ≥300 mm^3 had been reached.

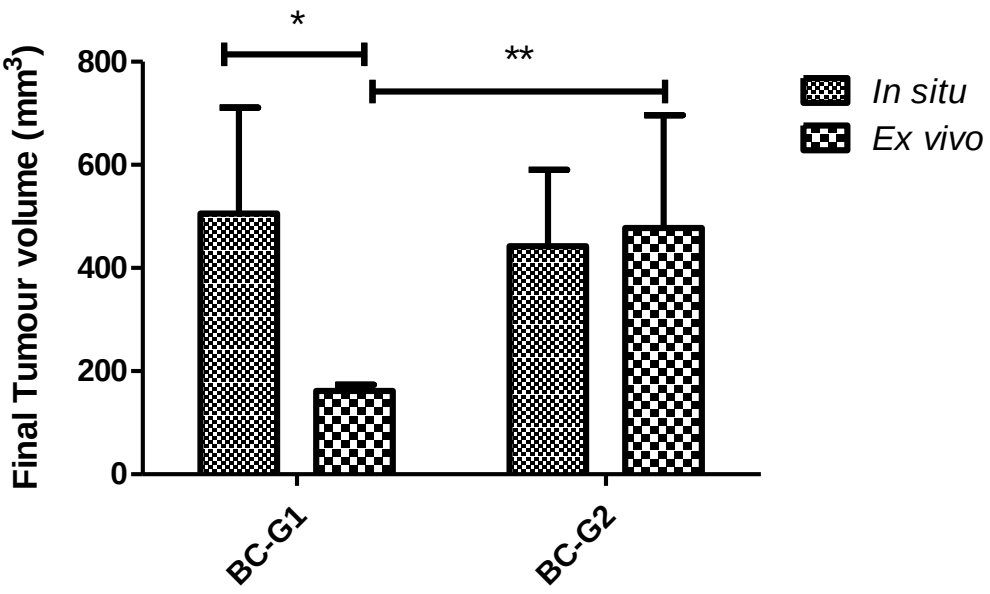

Figure 7: Average final *in situ* and *ex vivo* tumour volume measurements of tumours derived from E0771 cells suspended in Matrigel: BC-G1 (n=6), and 2 (n=6). Data represents mean ± SD. Asterisks (*) indicate significant differences within (*) and between (**) the groups ($p<0.05$).

After visual macroscopic evaluation, the tumour tissues (Groups 1 and 2) were weighed to determine tumour growth rate using Equation 3. As shown in Figure 8, the tumour growth rate of BC-G2 (0.03 g/day) seemed higher than that of the animals in BC-G1 (0.02 g/day). However, according to unpaired student's *t*-test analysis, the difference was not statistically significant ($p>0.05$).

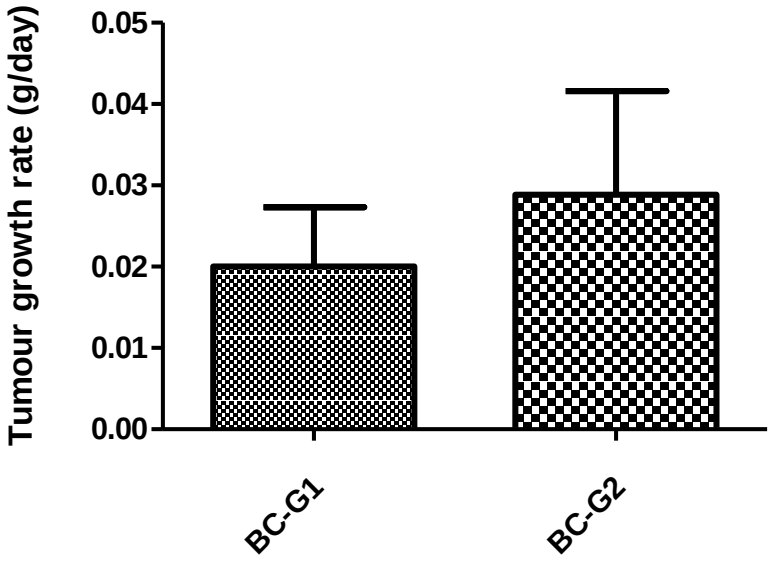

Figure 8: Average tumour growth rate of tumours derived from E0771 cells suspended in Matrigel: BC-G1 (n=6) and 2 (n=6). Data represents mean ± SD.

1.3.1.3 Histological characterisation

To confirm malignancy, the E0771 derived tumours were harvested after reaching the endpoint tumour volume (≥300 mm^3) and fixed in formalin for histological examination using H & E staining. Based on histological findings, the representative tumour was composed of highly atypical epitheliod cells with large, pleomorphic nuclei and single to multiple nucleoli. The tumour presented with malignant features such as mitotic figures (Figure 9A), necrotic foci and abundant haemorrhage (Figure 9B). Figure 9C, shows tumour cells within small blood vessel, also termed lymphovascular invasion. As mentioned previously, a palpable mass was formed at the mammary fat pad where the cells were inoculated. This site of tumour formation was histologically evident by the invasion of adipocytes between tumour cells (Figure 9A) and the presence of mammary ducts with surrounding myoepithelial layers (Figure 9D).

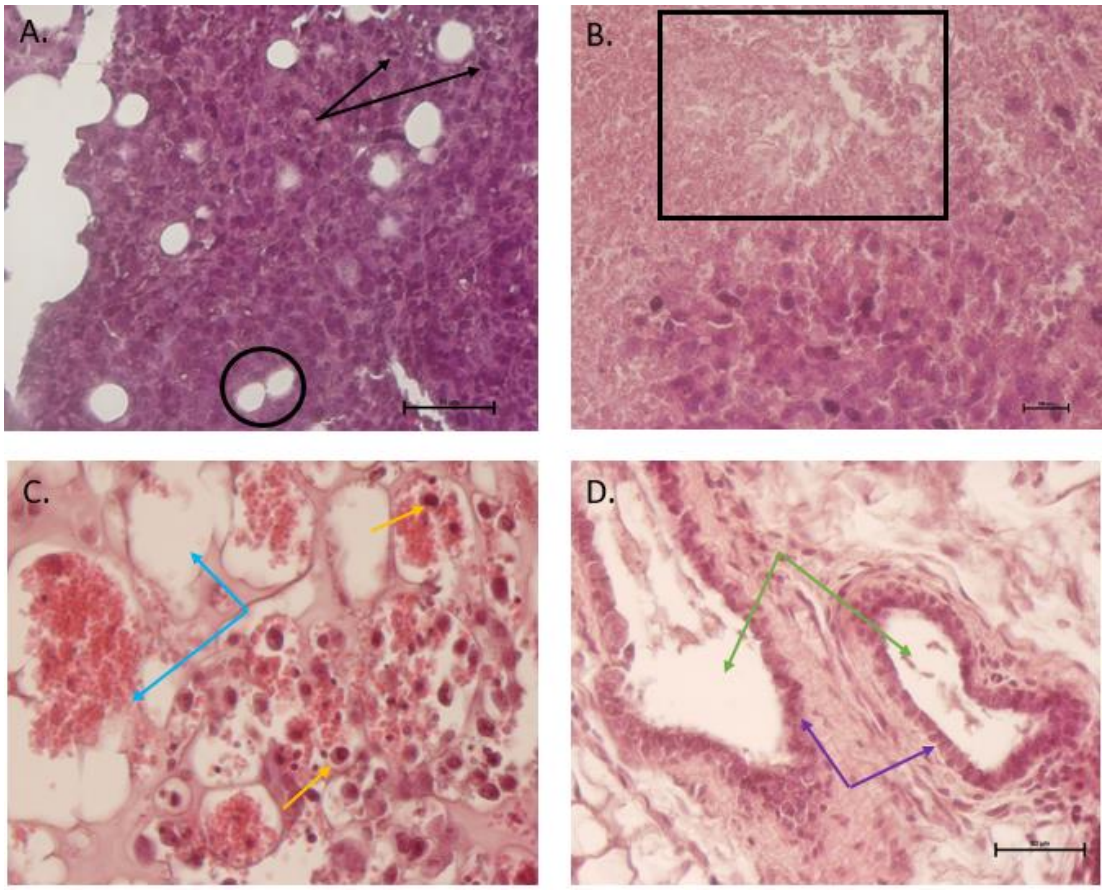

Figure 9: H & E staining of representative tumour derived from E0771 cells suspended in Matrigel showing **(A)** a sheet of tumour cells consisting of mitotic figures (*arrows*) and adipocytes (*circle*); **(B)** the tumour had area of central necrosis with visible haemorrhage (*square*); **(C)** tumour cells *(yellow arrows)* within small blood vessels *(blue arrows)* and (**D)** mammary ducts *(green arrows)* with surrounding myoepithelial layers *(purple arrows)* were also seen. All images: 40x magnification.

1.3.2 OVCAR-3 derived xenograft model

1.3.2.1 Tumour progression

To establish the ovarian cancer xenograft mouse model, OVCAR-3 cells suspended in PBS or Matrigel were subcutaneously injected above the proximal tibia in female nude athymic (nu/nu) mice. In animals inoculated with cells suspended in PBS, tumours were visible within 66 days post inoculation with a tumour take rate of 2/3 in OV-G1 (Figure 10). As shown in Figure 11, tumour take rate of 3/3 was obtained for OV-G2 with tumour onset observed within 68 days post inoculation except for mouse 5 which had a delayed tumour onset. Following these observations, an amendment was made to enhance tumour growth by co- inoculating the cells with Matrigel (OV-G3) without changing the number of cells. In comparison to the PBS inoculum (OV-G1 and 2), a more rapid tumour onset of 33 days after inoculation was observed for the Matrigel inoculum (OV-G3) with a tumour take rate of 3/4 (Figure 12).

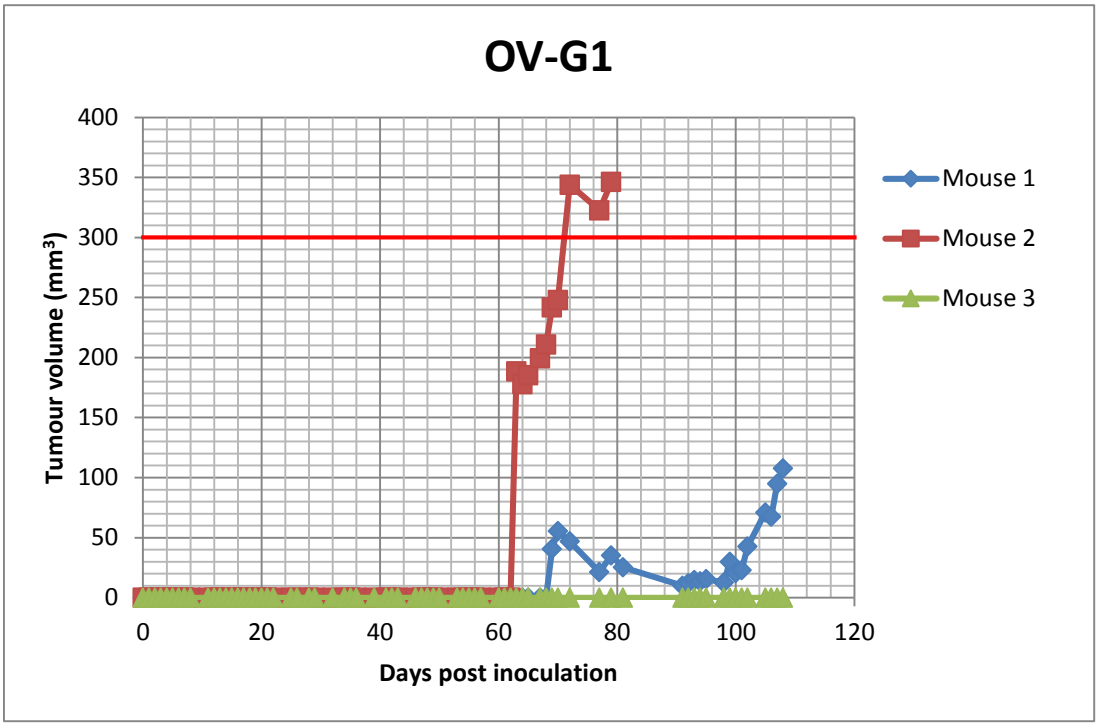

Figure 10: *In vivo* tumour growth of OVCAR-3 cells suspended in PBS. The red line represents the study end point (≥300 mm^3).

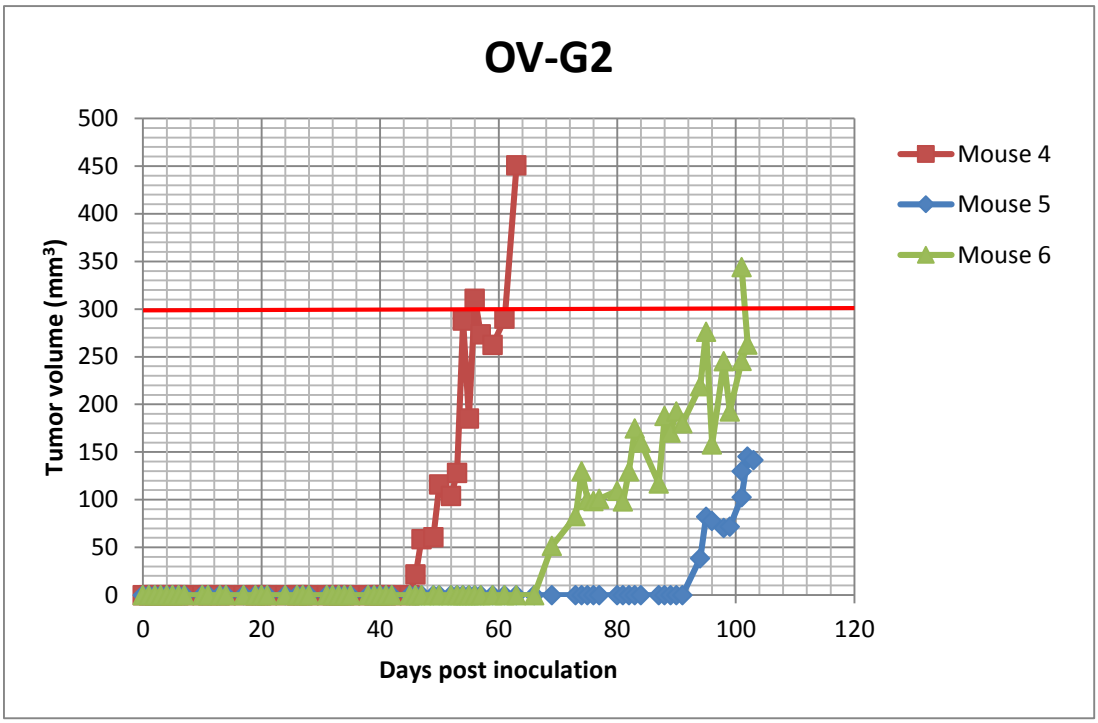

Figure 11: *In vivo* tumour growth of OVCAR-3 cells suspended in PBS. The red line represents the study end point (≥300 mm^3).

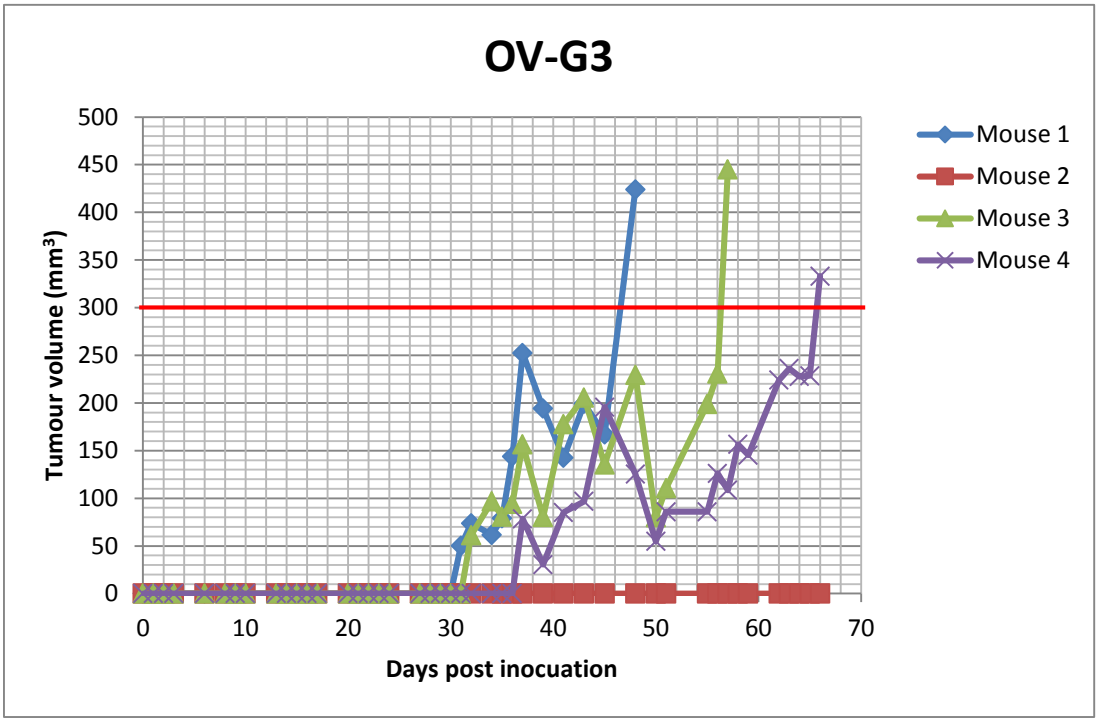

Figure 12: *In vivo* tumour growth of OVCAR-3 cells suspended in Matrigel. The red line represents the study end point (≥300 mm^3).

1.3.2.2 Gross pathology

During monitoring of the tumour growth, palpable and visible tumours were observed at the site of inoculation for both the PBS and Matrigel inoculums (Figure 13A). Once the tumours reached the study's end-point volume (≥ 300mm^3), the mice were humanely euthanised and the tumours were excised. Based on gross pathology analyses, solid tumours with no signs of ulceration were obtained (Figure 13B-C).

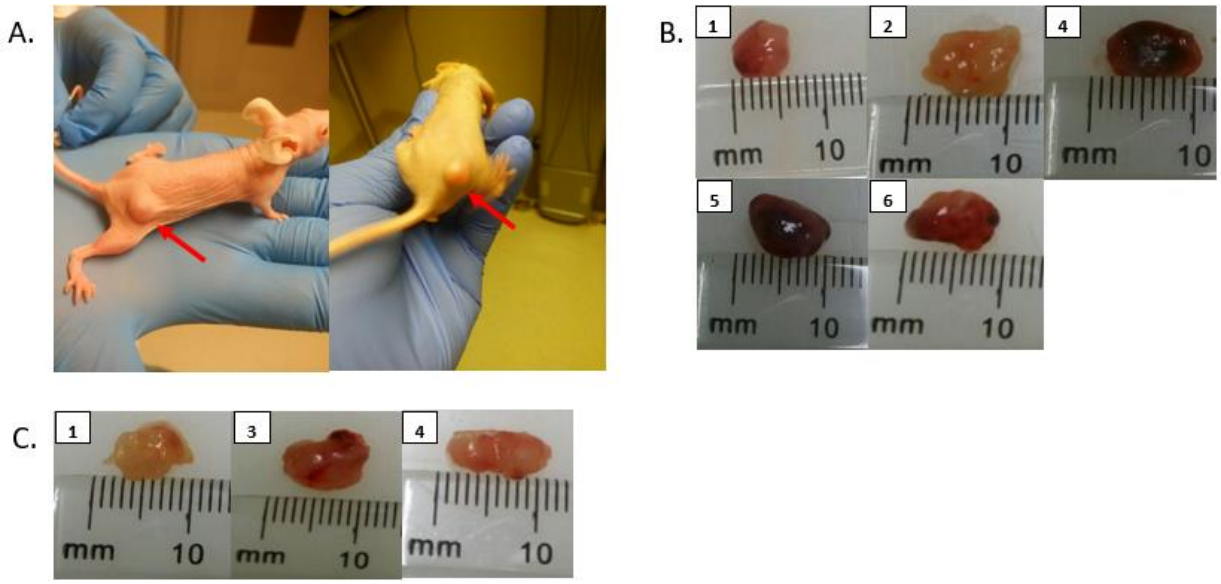

Figure 13: Ovarian tumours induced by xenotransplantation of OVCAR-3 cells subcutaneously above the flank of athymic nude (nu/nu) mice. Images of athymic nude (nu/nu) mice inoculated with OVCAR-3 cells suspended in PBS (*left*) and Matrigel (*right*) showing *in situ* tumour growth on hind quarter (*red arrows*) **(A)**. Tumours excised from mice inoculated with PBS inoculum **(B)** and **(C)** Matrigel inoculum. Inset numbers represent mouse number.

For both PBS and Matrigel inoculum the *ex vivo* tumour volumes were measured and a comparison was made with final *in situ* tumour volumes. As shown in Figure 14, inoculation with cells in PBS or Matrigel resulted in final *in situ* tumour volumes that seemed larger than *ex vivo* tumour volume measurements, however, one-way ANOVA showed no significant difference ($p>0.05$) between measurement of tumours *in situ* and *ex vivo*.

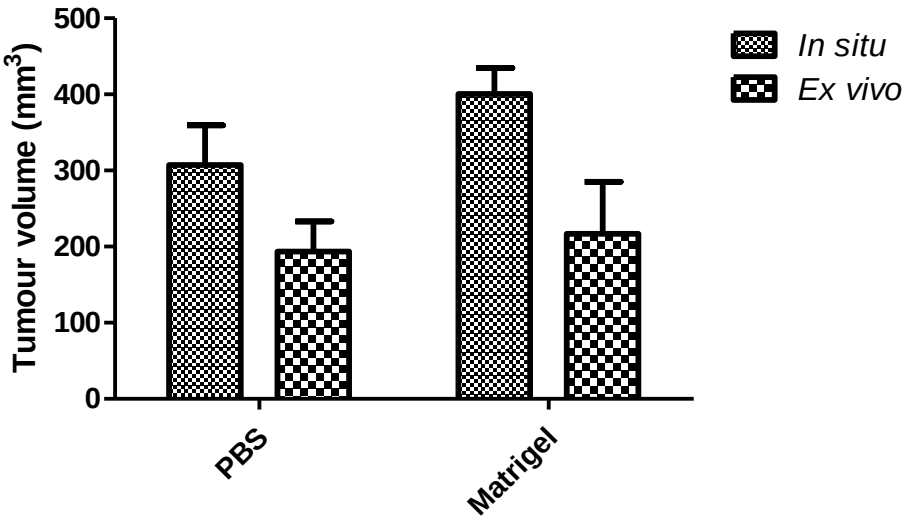

Figure 14: Average final *in situ* and *ex vivo* tumour volume measurements of OVCAR-3 cells suspended in PBS (n=5) and Matrigel (n=3). Data represents mean ± SD.

Following tumour volume measurements, the tumour tissues were weighed and the tumour growth rate was determined using Equation 3. A comparison was made between the PBS and Matrigel inoculum using unpaired student's *t*-test. As shown in Figure 15, the tumour growth rate of animals inoculated with cells in Matrigel (OV-G3) was seemingly higher than the growth rate of the animals inoculated with cells in PBS (OV-G1 and 2) but the difference was not statistically significant ($p>0.05$).

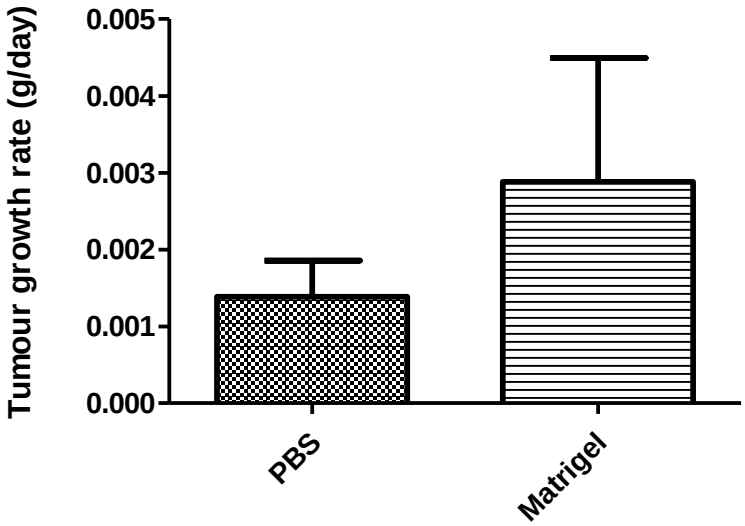

Figure 15: Average growth rate of tumours derived from OVCAR-3 cells suspended in PBS (n=5) and in Matrigel (n=3). Data represents mean ± SD.

1.3.2.3 Histological characterisation

After inoculating athymic nude (nu/nu) mice with OVCAR-3 cells suspended in either PBS or Matrigel, the tumours obtained were excised to confirm malignancy using H & E staining and to compare PBS and Matrigel inoculum. The representative tumour derived from the PBS inoculum (Figure 16A-C) was composed of pleomorphic tumour cells with vesicular to hyperchromatic nuclei and nucleoli (Figure 16A). Figure 17A-D shows a representative tumour derived from the Matrigel inoculum composed mainly of pleomorphic tumour cells with nuclear atypia and multiple nucleoli. Similarly to the PBS inoculum, histological features associated with malignancy such as mitotic figures (Figures 16B and 17A) and central necrosis (Figures 16C and 17B) were identified in tumours derived from the Matrigel inoculum. In comparison to PBS inoculum, fine vasculature traversing between the nest of tumour cells were observed with Matrigel inoculum (Figure 17C) and interestingly, sheets of foamy macrophages normally seen in early corpus albicans were also identified (Figure 17D) which indicates that the tumours reflected the site of OVCAR-3 cell origin.

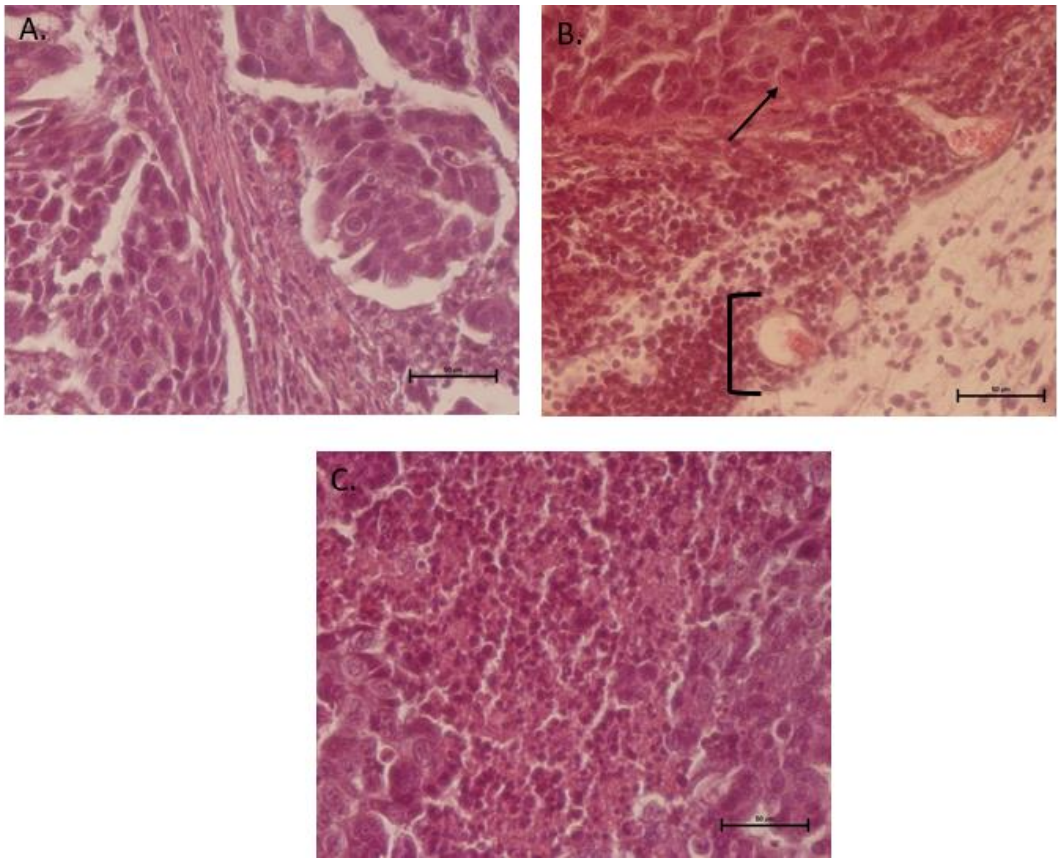

Figure 16: H & E staining of a tumour derived from OVCAR-3 cells suspended in PBS showing **(A)** a nest of tumour cells consisting of **(B)** a mitotic figure (*arrow*) with adjacent capillary (*bracket)*. **(C)** Area of central necrosis was also visible. All images: 40x magnification.

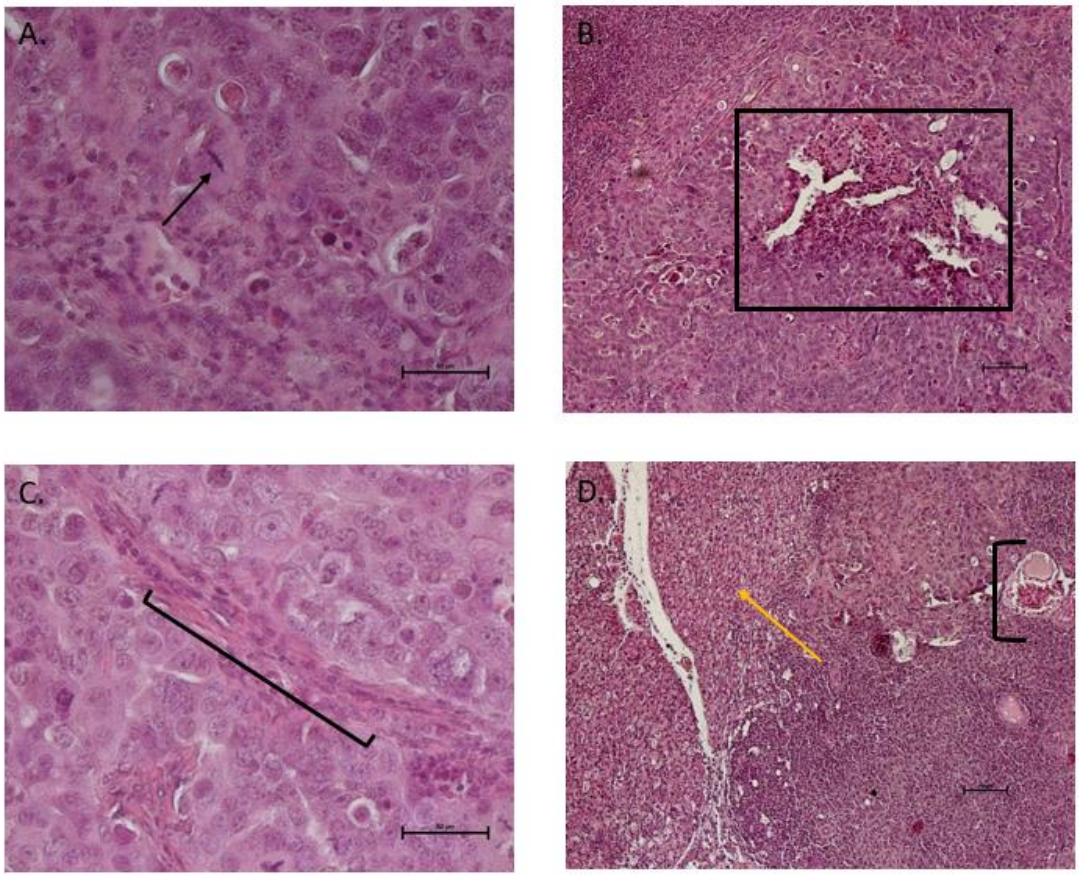

Figure 17: H & E staining of a tumour derived from OVCAR-3 cells suspended in Matrigel showing **(A)** a nest of tumour cells consisting of a mitotic figure (*black arrow*) and **(B)** area of necrosis. **(C)** Fine vasculature *(bracket*) traversing between the tumour cells and **(D)** sheets of foamy macrophages (*yellow arrow*) were visible with adjacent vasculature (*bracket*). Magnification: 40x (A and C) and 10x (B and D).

1.4 Discussion

1.4.1 E0771 derived allograft model

The E0771 cell line derived from rodent mammary adenocarcinoma has been well studied *in vitro* and has been shown to have the capability of growing *in vivo* post inoculation in immune-competent mice (Carrasco *et al.*, 2016; Ewens *et al.*, 2005; Johnstone *et al.*, 2015). In a similar study by Davis (2016), the tumours were palpable within 9 days, with a tumour take rate of 98% (47/48). The results were comparable with our findings, with a tumour take rate of 100% (26/26) obtained in the current study. In a previous study by Ewens *et al.* (2005), inoculation of E0771 cells without Matrigel resulted in slow growing tumours (reaching tumour volume ≥300 mm^3 by 50 days post inoculation) confirming that the co-injection of cells with Matrigel enhances tumour growth (Benton *et al.*, 2014).

During injection, leakage of the cell suspension from the injection site upon withdrawal of the needle was observed, however, no effect on the tumour growth and volume was found. To avoid leakage, the use of a smaller needle (size 25-30 G) was found to be preferable than a bigger needle (23G) or alternatively, the needle should be held in position for a few seconds after inoculation before withdrawal (Benton *et al.*, 2014).

Based on the tumour progression data, no difference was found between the tumour onset and tumour take rate of concentrated and diluted Matrigel. However, a study by Beyreuther *et al.* (2017) using different types of cell lines showed that concentrated Matrigel resulted in faster tumour growth and higher tumour take rate compared to diluted Matrigel. It could be that the optimum tumour growth of E0771 was reached with 9.20 mg/ml Matrigel in the current study.

In general, monitoring of tumour growth using callipers is the most commonly utilised technique because it is readily available and affordable (Girit *et al.*, 2008). However, this method is not the most accurate due to human errors and tumours with irregular shapes' making precise measurement difficult (Jensen *et al.*, 2008; Peut & Rice, 2008). Therefore, to eliminate large *in situ* and *ex vivo* tumour volume variations, as observed in the first group; measurements should be done, where possible, by the same individual throughout a study. Application of imaging techniques can be another option to overcome the shortcomings of callipers. MicroCT imaging has been shown to be more accurate than callipers and microPET imaging (Jensen *et al.*, 2008). In another study, ultrasonography was also proven to produce more accurate and reproducible measurements than callipers (Ayers *et al.*, 2010). However, taken into consideration that these techniques are labour extensive (Girit *et al.*, 2008), it is not practical to use them for daily monitoring of tumour growth. Alternatively, a structured light scanner, which is a high-throughput system for measuring subcutaneous tumours, can be utilised. In comparison to conventional

imaging techniques, the device is portable, less labour intensive and; does not require administration of radiolabelled tracers and anaesthesia (Girit *et al.*, 2008).

The macroscopic evaluation of E0771 derived tumours revealed ulceration in 1/24 (4%) animals and in a similar study tumour ulceration was reported in 4/48 (8%) animals (Davis, 2016). In another study tumour ulceration was reported in the absence of Matrigel (Ewens *et al.*, 2005), suggesting that the E0771 derived tumours are prone to develop ulceration with or without the use of Matrigel. Similarly to previous studies (Carrasco *et al.*, 2016; Ewens *et al.*, 2005), malignant features, such as mitotic figures and necrotic areas, were observed in the current study suggesting that the E0771 tumour cells were actively proliferating and malignant. Based on our data, E0771 cells grew well in C57BL/6 mice, with a tumour onset of approximately 7 days and an average tumour growth rate of 0.03 g/day obtained based on the *ex vivo* final weight. In addition, tumour take rate of 100% was obtained on three separate occasions.

1.4.2 OVCAR-3 derived xenograft model

Part of the aim of this study was to characterise the tumour growth of OVCAR-3 cells in athymic nude (nu/nu) mice. A study by Mullen *et al.* (1996) previously illustrated that the use of Matrigel was necessary to optimise subcutaneous engraftment of OVCAR-3 cells in athymic nude (nu/nu), mice with a tumour take rate of 2/6 and 0/6 reported, with and without Matrigel, respectively. In contrast, subcutaneous engraftment of OVCAR-3 cells without Matrigel was found in the current study with a tumour take rate of 5/6. The results of this study along with previous studies (Hamilton *et al.*, 1984; Mitra *et al.*, 2015) indicate that OVCAR-3 cells can grow *in vivo* with or without Matrigel. Moreover, in the current the study, the use of Matrigel resulted in earlier tumour onset within one month compared to a slow *in vivo* tumour growth of approximately two months initially observed without it.

The OVCAR-3 cell line is classified as a high-grade serous ovarian cancer (Domcke *et al.*, 2013; Mitra *et al.*, 2015), the most common histological subtype associated with low survival rate (Bowtell *et al.*, 2015; Labidi-Galy *et al.*, 2017). In the current study, histological analysis of OVCAR-3 tumour tissue revealed the presence of mitotic figures and necrotic areas, which are prominent histological features used to distinguish high-grade from low grade serous carcinoma (Vang *et al.*, 2009). No differences in histology, including degree of vascularisation were previously observed with or without the use of Matrigel (Mullen *et al.*, 1996). In this study, sheets of foamy macrophages common in early corpus albicans of the ovary were observed indicating the tumour reflected the organ of origin, even though the cells were not implanted at the area of origin. In addition, Matrigel inoculum demonstrated fine vasculature traversing between sheets of

tumours compared to PBS inoculum. Matrigel has been suggested to promote tumour vascularisation and preserve parental tumour phenotype (Benton *et al.*, 2014; Fridman *et al.*, 2012). Therefore, our findings suggest that the use of Matrigel is essential to optimise tumour growth and maintain the *in vivo* tumour microenvironment of OVCAR-3 cells

1.5 Conclusion

In summary, murine breast cancer cells were grown in C57BL/6 mice and OVCAR-3 human ovarian cells in athymic nude (nu/nu) mice in order to establish allograft and xenograft cancer models, respectively. For both models no clinical signs of tumour burden or distress to the animals were observed above the endpoint tumour volume (≥300 mm^3). The murine breast allograft model was effectively established, with reproducibility that can be used in the preclinical evaluation of novel therapeutic and diagnostic compounds, the ovarian xenograft model however requires further investigation before being established as an effective model for application.

REFERENCES

Ayers, G.D., McKinley, E.T., Zhao, P., Fritz, J.M., Metry, R.E., Deal, B.C., Adlerz, K.M., Coffey, R.J. & Manning, H.C. 2010. Volume of preclinical xenograft tumors is more accurately assessed by ultrasound imaging than manual caliper measurements. *Journal of ultrasound in medicine : official journal of the American Institute of Ultrasound in Medicine*, 29(6):891-901.

Benton, G., Arnaoutova, I., George, J., Kleinman, H.K. & Koblinski, J. 2014. Matrigel: From discovery and ECM mimicry to assays and models for cancer research. *Advanced drug delivery reviews*, 79–80:3-18.

Benton, G., Kleinman, H.K., George, J. & Arnaoutova, I. 2011. Multiple uses of basement membrane-like matrix (BME/Matrigel) in vitro and *in vivo* with cancer cells. *International journal of cancer*, 128(8):1751-1757.

Beyreuther, E., Brüchner, K., Krause, M., Schmidt, M., Szabo, R. & Pawelke, J. 2017. An optimized small animal tumour model for experimentation with low energy protons. *PLOS one*, 12(5):e0177428.

Bowtell, D.D., Böhm, S., Ahmed, A.A., Aspuria, P.-J., Bast, R.C., Beral, V., Berek, J.S., Birrer, M.J., Blagden, S., Bookman, M.A., Brenton, J., Chiappinelli, K.B., Martins, F.C., Coukos, G., Drapkin, R., Edmondson, R., Fotopoulou, C., Gabra, H., Galon, J., Gourley, C., Heong, V., Huntsman, D.G., Iwanicki, M., Karlan, B.Y., Kaye, A., Lengyel, E., Levine, D.A., Lu, K.H., McNeish, I.A., Menon, U., Narod, S.A., Nelson, B.H., Nephew, K.P., Pharoah, P., Powell, D.J., Ramos, P., Romero, I.L., Scott, C.L., Sood, A.K., Stronach, E.A. & Balkwill, F.R. 2015. Rethinking ovarian cancer II: reducing mortality from high-grade serous ovarian cancer. *Nature reviews. Cancer*, 15(11):668-679.

Bray, F., Ferlay, J., Soerjomataram, I., Siegel, R.L., Torre, L.A. & Jemal, A. 2018. Global cancer statistics 2018: GLOBOCAN estimates of incidence and mortality worldwide for 36 cancers in 185 countries. *CA: A cancer journal for clinicians*, 0(0):3-31.

Carrasco, E., Garrido, J.M., Álvarez, P.J., Álvarez-Manzaneda, E., Chahboun, R., Messouri, I., Melguizo, C., Aránega, A. & Rodríguez-Serrano, F. 2016. Meroxest improves the prognosis of immunocompetent C57BL/6 mice with allografts of E0771 mouse breast tumor cells. *Archives of medical science : AMS*, 12(5):919-927.

Davis, T.A. 2016. The role of the AHNAK protein in breast cancer: Implications for tumour metastasis and chemoresistance. Stellenbosch: SUN. (Dissertation-PhD).

Domcke, S., Sinha, R., Levine, D.A., Sander, C. & Schultz, N. 2013. Evaluating cell lines as tumour models by comparison of genomic profiles. *Nature communications*, 4:2126.

Ewens, A., Mihich, E. & Ehrke, M.J. 2005. Distant metastasis from subcutaneously grown E0771 medullary breast adenocarcinoma. *Anticancer research*, 25(6B):3905-3915.

Fridman, R., Benton, G., Aranoutova, I., Kleinman, H.K. & Bonfil, R.D. 2012. Increased initiation and growth of tumor cell lines, cancer stem cells and biopsy material in mice using basement membrane matrix protein (Cultrex or Matrigel) co-injection. *Nature protocols*, 7(6):1138-1144 (Abstract).

Fridman, R., Kibbey, M.C., Royce, L.S., Zain, M., Sweeney, T.M., Jicha, D.L., Yannelli, J.R., Martin, G.R. & Kleinman, H.K. 1991. Enhanced tumor growth of both primary and established human and murine tumor cells in athymic mice after coinjection with matrigel. *JNCI: Journal of the National Cancer Institute*, 83(11):769-774 .(Abstract).

Girit, I.C., Jure-Kunkel, M. & McIntyre, K.W. 2008. A structured light-based system for scanning subcutaneous tumors in laboratory animals. *Comparative medicine*, 58(3):264-270.

Hamilton, T.C., Young, R.C., Louie, K.G., Behrens, B.C., McKoy, W.M., Grotzinger, K.R. & Ozols, R.F. 1984. Characterization of a xenograft model of human ovarian carcinoma which produces ascites and intraabdominal carcinomatosis in mice. *Cancer research*, 44(11):5286-5290.

Jensen, M.M., Jørgensen, J.T., Binderup, T. & Kjær, A. 2008. Tumor volume in subcutaneous mouse xenografts measured by microCT is more accurate and reproducible than determined by 18F-FDG-microPET or external caliper. *BMC medical imaging*, 8(1):16.

Johnstone, C.N., Smith, Y.E., Cao, Y., Burrows, A.D., Cross, R.S., Ling, X., Redvers, R.P., Doherty, J.P., Eckhardt, B.L. & Natoli, A.L. 2015. Functional and molecular characterisation of EO771. LMB tumours, a new C57BL/6-mouse-derived model of spontaneously metastatic mammary cancer. *Disease models & mechanisms*, 8:1-15.

Kleinman, H.K. & Martin, G.R. 2005. Matrigel: Basement membrane matrix with biological activity. *Seminars in cancer biology*, 15(5):378-386.

Labidi-Galy, S.I., Papp, E., Hallberg, D., Niknafs, N., Adleff, V., Noe, M., Bhattacharya, R., Novak, M., Jones, S., Phallen, J., Hruban, C.A., Hirsch, M.S., Lin, D.I., Schwartz, L., Maire, C.L., Tille, J.-C., Bowden, M., Ayhan, A., Wood, L.D., Scharpf, R.B., Kurman, R., Wang, T.-L., Shih, I.-M., Karchin, R., Drapkin, R. & Velculescu, V.E. 2017. High grade serous ovarian carcinomas originate in the fallopian tube. *Nature communications*, 8(1):1093.

Mitra, A.K., Davis, D.A., Tomar, S., Roy, L., Gurler, H., Xie, J., Lantvit, D.D., Cardenas, H., Fang, F., Liu, Y., Loughran, E., Yang, J., Sharon Stack, M., Emerson, R.E., Cowden Dahl, K.D., V. Barbolina, M., Nephew, K.P., Matei, D. & Burdette, J.E. 2015. *In vivo* tumor growth of high-grade serous ovarian cancer cell lines. *Gynecologic oncology*, 138(2):372-377.

Mullen, P., Ritchie, A., Langdon, S.P. & Miller, W.R. 1996. Effect of Matrigel on the tumorigenicity of human breast and ovarian carcinoma cell lines. *International journal of cancer*, 67(6):816-820.

Navale, A.M. 2013. Animal models of cancer: a review. *International Journal of Pharmaceutical Sciences and Research*, 4(1):19.

Nezhat, F.R., Apostol, R., Nezhat, C. & Pejovic, T. 2015. New insights in the pathophysiology of ovarian cancer and implications for screening and prevention. *American journal of obstetrics & gynecology*, 213(3):262-267.

Peut, V.M. & Rice, A.M. 2008. A Nod/SCID model of primary human breast cancer. *Open transplant journal*, 2:1-8.

Schuh, J.C.L. 2004. Trials, tribulations, and trends in tumor modeling in mice. *Toxicologic pathology*, 32(1_suppl):53-66.

Taylor, M.R.G. 2001. Genetic testing for inherited breast and ovarian cancer syndromes: important concepts for the primary care physician. *Postgraduate medical journal*, 77(903):11-15.

Vang, R., Shih, I.-M. & Kurman, R.J. 2009. Ovarian low-grade and high-grade serous carcinoma: pathogenesis, clinicopathologic and molecular biologic features, and diagnostic problems. *Advances in anatomic pathology*, 16(5):267-282.

Weldon, C. 2005. Chytridiomycosis, an emerging infectious disease of amphibians in South Africa. Potchefstroom: NWU. (Thesis- PhD).

Workman, P., Aboagye, E., Balkwill, F., Balmain, A., Bruder, G., Chaplin, D., Double, J., Everitt, J., Farningham, D. & Glennie, M. 2010. Guidelines for the welfare and use of animals in cancer research. *British journal of cancer*, 102(11):1555.

CHAPTER 4: APPLICATION OF BREAST CANCER ALLOGRAFT MODEL IN IMAGING AND BIODISTRIBUTION STUDIES OF ^{64}CU- GLUCAB

Aim: The purpose of the study was to evaluate for the first time the *in vivo* biodistribution and tumour imaging potential of ^{64}Cu radiolabelled GluCAB, using an E0771 derived tumour-bearing mouse model.

Method: E0771 cells and E0771 derived tumours were examined for cellular membrane GLUT- 1 receptor expression using flow cytometry and immunofluorescence analysis, respectively. To determine tumour localisation and biodistribution, ^{64}Cu-GluCAB was administered to four E0771 derived allograft mice via the tail vein and microPET/CT scans were performed at 1, 2, 6 and 24 hours post-injection. After the 24-hour scan, the mice were euthanised, the organs were excised and the biodistribution of radiolabelled agent was determined.

Results: Analysis of GLUT-1 receptor expression in E0771 cells and E0771 derived tumours was inconclusive. The radioactivity from ^{64}Cu-GluCAB uptake could not be detected in the tumour using microPET/CT imaging, but a high amount of radioactivity was seen in the heart (blood pool) with an accumulation in the liver and intestines (excretion). The *ex vivo* biodistribution profile indicated a large %ID/g activity in the plasma, liver and large intestine thereby confirming the observations made from the images of the binding of ^{64}Cu-GluCAB to circulating albumin and excretion through the hepatobiliary pathway. A small amount of uptake by the tumour was also noted *ex vivo*.

Conclusion: Although ^{64}Cu-GluCAB was slightly taken up by the tumour (as measured by gamma counting), the radioactivity signal was too low to locate and visualise the breast tumour using microPET/CT imaging. GLUT-1 receptor expression on the E0771 cells and E0771 derived tumour could not be characterised due to insufficient data and so no conclusions could be made as to whether the tumour model was suitable for investigation of ^{64}Cu-GluCAB as a tumour-targeted imaging radiopharmaceutical agent.

Key words: ^{64}Cu-GluCAB, E0771, microPET/CT, GLUT-1

1.1 Introduction

Cancer can be treated effectively with a reduction in mortality, if it is detected early (Fass, 2008; Wang *et al.*, 2016). To achieve early detection, molecular imaging allows visualisation and quantification of biological processes at the cellular and molecular level (Mankoff, 2007; Pysz *et al.*, 2010). For example, positron emitting tomography (PET) is the most sensitive non-invasive molecular imaging technique that relies on positron-emitting radionuclides (Hussain & Nguyen, 2014). With the ability of computational tomography (CT) to image anatomical structure (Hu *et al.*, 2016), dual imaging of PET with a CT scan improves diagnosis by providing both physiological and anatomical information (Griffeth, 2005; Pimlott & Sutherland, 2011). For small animal imaging, microPET/CT is used (Liang *et al.*, 2007).

^{18}F-fluoro-2-deoxyglucose (FDG) is the most commonly used PET radiolabelled glucose analogue that utilises the high glucose metabolism of malignant cells facilitated by overexpression of glucose transporters, mainly GLUT-1 (Carvalho *et al.*, 2011; Griffeth, 2005; Sharma & Mukherjee, 2016). Despite the common use of ^{18}F-FDG, it is limited by poor tumour specificity (Kaira *et al.*, 2011). Therefore, more tumour specific radiopharmaceuticals should be developed to improve tumour radionuclide imaging (Chen *et al.*, 2010). Recently, the Nuclear Energy Corporation of South Africa (Necsa) developed a dual-targeting PET radiopharmaceutical called GluCAB (glucose-cyclam-albumin), which has been radiolabelled with copper-^{64}[Cu], for imaging purposes and is proposed to target the increased glucose metabolic rate and vascularisation of malignant tumours to localise in the tumour. Albumin (66.5 kDa) makes up most of the plasma proteins and is commonly used to increase the circulation and bioavailability of imaging agents at the tumour site through the enhanced permeability and retention (EPR) effect (Bhushan *et al.*, 2017; Kratz, 2008). The EPR effect describes the retention of macromolecules (>40 kDa) in tumours via leaky vasculature and impaired lymphatic system and is commonly used for tumour specific targeting (also known as passive targeting) (Danhier *et al.*, 2010; Maeda *et al.*, 2000). The ^{64}Cu-GluCAB precursor (without albumin) will be conjugated with albumin *in vivo* to bring the EPR effect into play.

Tumour-bearing animal models have been used to evaluate the potential of novel tumour target specific imaging agents (Cardinale *et al.*, 2017; Ping Li *et al.*, 2008). In comparison to spontaneously and genetically induced tumour models, tumour xenograft and allograft models are frequently used because they are easy to implement within a short period (Navale, 2013; Suggitt & Bibby, 2005). According to Killion *et al.* (1998), to achieve a tumour specific targeting, preclinical tumour-bearing models should be based on the therapeutic or imaging agent under investigation. Therefore, before testing a target-specific agent such as ^{64}Cu-GluCAB, it is important to develop a reliable tumour-bearing model by confirming the presence of the desired targeted moieties in the tumour (Kelland, 2004; Schuh, 2004), in this case GLUT-1.

Herewith, we illustrate the use of an E0771 breast tumour-bearing mouse model to determine the biodistribution and tumour imaging potential of ^{64}Cu-GluCAB. It was hypothesised that a higher uptake of ^{64}Cu-GluCAB would be visualised at the site of the tumour using microPET/CT imaging.

1.2 Materials and Methods

1.2.1 Materials

GLUT-1 antibody, DyLight 488 and fluorescein isothiocyanate (FITC) conjugated heavy and light specificity (H + L) goat anti-rabbit immunoglobulin (IgG) secondary antibody were purchased from Novus Biologicals (Littleton, CO, USA). Flow cytometry staining buffer solution (containing foetal bovine serum and sodium azide (0.09%)), immunohistochemistry (IHC)/immunocytochemistry (ICC) blocking solution and Hoechst 33258 were obtained from ThermoFisher Scientific (Waltham, Massachusetts, United States). E0771 was donated by Stellenbosch University (Western Cape, South Africa). Trypsin/EDTA, trypan blue, penicillin/streptomycin (PenStrep) a broad-spectrum antibiotic cocktail and Dulbecco's Modified Eagle's Medium (DMEM) with glutamine were purchased from Lonza (Basel, Switzerland). Phosphate-buffered saline (PBS) tablets, glycerol and histological grade xylene were bought from Sigma-Aldrich (St. Louis, MO, USA). Absolute ethanol was purchased from Merck (Darmstadt, Germany). Foetal bovine serum (FBS) was obtained from GE Healthcare HyClone (Chicago, IIlinois, United States). Isoflurane was purchased from Safeline Pharmaceuticals (South Africa).

1.2.2 Methods

1.2.2.1 Imaging and biodistribution of ^{64}Cu-GluCAB

1.2.2.1.1 Experimental animals and husbandry

Four female C57BL/6 mice bearing E0771 tumours were established as previously described in Chapter 3 (section 2.2.3.1). Once the tumours reached a palpable tumour volume of approximately 100 mm^3, the mice were transferred to Necsa and allowed to acclimatise for five days before study commencement. The mice were group-caged (two mice/cage) in individually ventilated cages (IVC) under normal conditions (22 ± 2˚C, 55 ± 10% humidity, 15 ± 5 Pa and 12 hrs light/dark cycles). Sterile standard rodent chow and water were provided *ad libitum* and the sterile corncob bedding was changed regularly. All procedures involving the animals were approved by the NWU-AnimCare REC committee (Ethics approval number: NWU-00379-16-A5).

1.2.2.1.2 Administration of test compound and microPET/CT imaging

Four mice were injected with 0.1 ml ^{64}Cu-GluCAB precursor (without albumin) directly into the tail vein. As shown in Figure 1, three of the injected animals were used for the microPET/CT imaging using a Mediso nanoScan® PET/CT system (Mediso Ltd, Budapest, Hungary), while the fourth mouse was regularly monitored in the home cage. Anaesthetisation of the mice was done in a closed induction chamber using Isoflurane at a dose of around 5% isoflurane in oxygen for induction and then 2 to 3% for anaesthesia maintenance. The imaging procedure consisted of four scans per animal at time points of 1, 2, 6 and 24 hours (hrs). ^{64}Cu has a half-life of 12 hrs therefore any scans beyond 24 hrs (two half-lives) would not yield any further information due to the radioactivity decay. The images were acquired and reconstructed using Nucline nanoScan and image analysis was done using InterView™ FUSION software (Mediso Ltd, Budapest, Hungary).

Each scan (CT with PET) lasted for a maximum of 25 minutes (min) and for the duration of the scan the temperature, heart rate and respiration of the mouse was carefully monitored by a MedisoMulticell™ rat imaging chamber and microPET/CT system (Mediso Ltd, Budapest, Hungary). After completion of the scan, the mice were placed in a warm, dry, quiet environment away from the other animals to recover. Thereafter, the mice were returned to their cages until the next scan and the process was repeated.

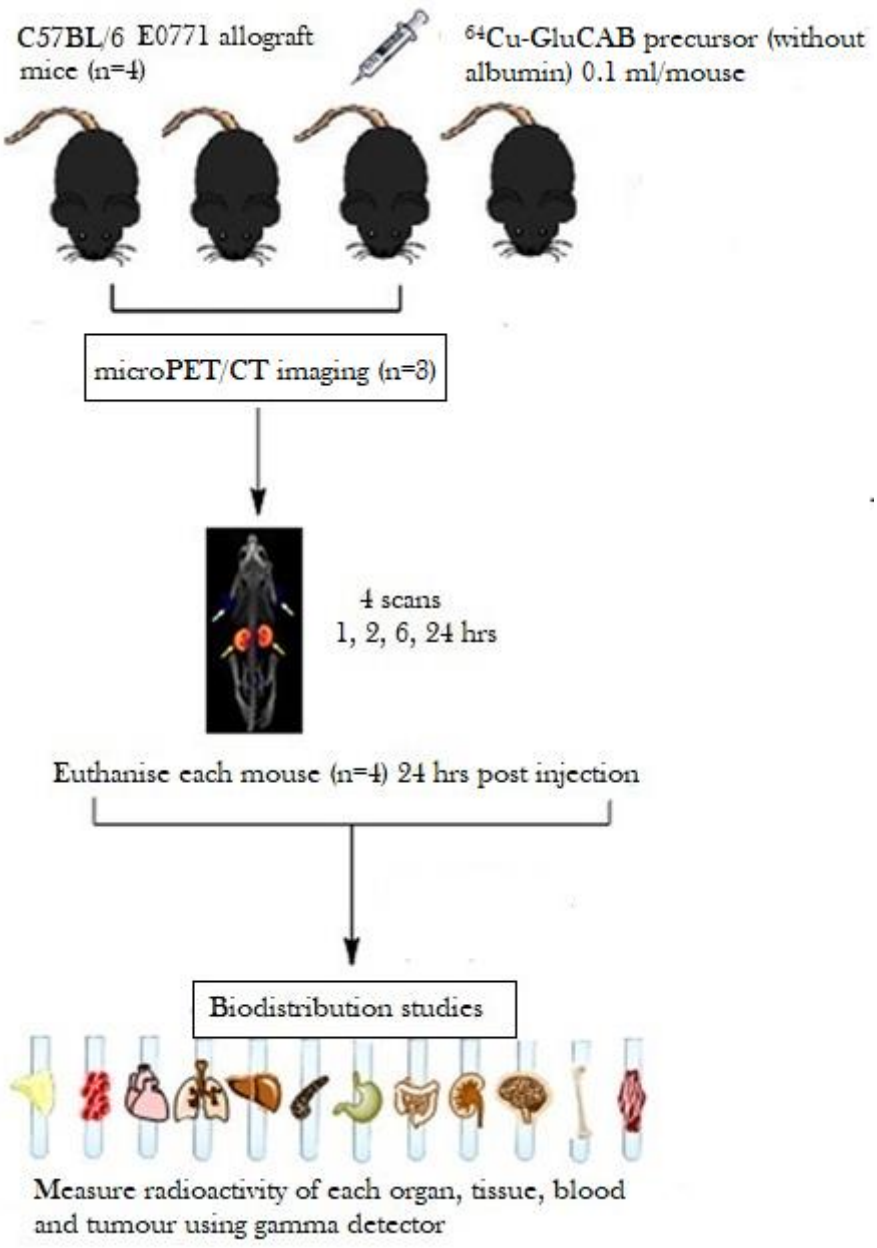

Figure 1: Study design overview for the biodistribution and microPET/CT imaging of ^{64}Cu- GluCAB using a C57BL/6 E0771 derived tumour allograft model. ^{64}Cu-GluCAB was administered via the tail vein (n=4) and the mice (n=3) were imaged at 1, 2, 6 and 24 hrs after administration. After 24 hr scan, the mice were euthanised and the organs harvested for biodistribution studies (n=4).

1.2.2.1.3 Analysis of uptake and biodistribution of ^{64}Cu-GluCAB

After the final (24hr) scan, the mice, while anaesthetised, were euthanised by decapitation and trunk blood was immediately collected into a pre-weighed vial. Following collection, the blood was immediately fractioned into plasma and erythrocyte components at 4500 rpm for 6 min using a Hettich EBA 20S centrifuge (Andreas Hettich GmbH & Co.KG, Germany), to determine the blood pool radioactivity and whether or not the administered compound was protein bound. After euthanasia, several organs and tissues (heart, lungs, liver, spleen, stomach, intestines, kidneys, brain, bladder, muscle, femur, tail, skin and ovaries) were harvested. The tumours were also collected, weighed and measured with a digital calliper to determine tumour mass and volume. A piece of the thigh muscle was collected as a background reference sample to compare the uptake of ^{64}Cu-GluCAB between different organs and the background.

For biodistribution analysis (Figure 1), the excised organs, tissues and blood fractions, as well as the tumours, were placed in pre-weighed vials to obtain the weight using a PB303 Mettler Toledo analytical balance (Mettler Toledo, United States). The radioactivity in each organ was measured using a Canberra gamma detector (CANBERRA Industries Inc, United States). The results were expressed as the percentage-injected dose per gram of tissue weight (%ID/g) for each organ to allow for comparison of compound uptake between the different organs and the tumour. The uptake ratio of organ-to-muscle was calculated using the %ID/g results. .

1.2.2.2 GLUT-1 receptor expression

1.2.2.2.1 Flow cytometry analysis of E0771 cells

E0771 cells were cultured under similar conditions as described in Chapter 3 (section 2.2.1). For cell preparation, the cells were harvested by scraping using a Costar® cell scraper (Corning Incorporated, New York, USA) once they reached 80 to 90% confluency. The cells were centrifuged at 1000 rpm for 4 min using a PLC-012 universal centrifuge (GEMMY industrial corporation, Taipei, Taiwan) and re-suspended in complete DMEM. To determine cell viability, 40 µl of cell suspension was mixed with 40 µl trypan blue, followed by manual counting of the viable cells using a haemocytometer. Following cell viability counting, the cells were then centrifuged at 1000 rpm for 4 min and re-suspended to a concentration of 1×10^6 cells/ml in staining buffer.

For GLUT-1 labelling, the cells (1×10^6 cells/sample) were incubated for 30 min on ice with GLUT- 1 antibody (1µl) diluted to 1 µg/ml using staining buffer. After incubation, the cells were washed with staining buffer (1 ml) and centrifuged at 1000 rpm for 5 min using a Z326 K universal centrifuge (HERMLE Labortechnik GmBH, Wehingen). The supernatant was discarded and the

pellet was incubated for 30 min on ice with goat anti-rabbit IgG (H + L) secondary antibody (DyLight 488) diluted to 4.6 ng/ml using staining buffer, for 30 min on ice. At the end of incubation, the cells were centrifuged (1000 rpm, 5min) to remove unbound secondary antibodies and washed twice with staining buffer (1 ml) by centrifugation at 1000 rpm for 5 min. For the blank control, E0771 cells were treated with staining buffer without antibodies under the same conditions. All the preparations were done in the dark to prevent photo bleaching of the secondary antibody. For flow cytometery analysis, using an Accuri™ C6 flow cytometer coupled with Csampler module for sample collection (BD Biosciences, California, United States), the cells were suspended in staining buffer (1 ml) and 10 000 cells/sample were obtained at a slow flow rate with fluorescence intensity measured by FL1 channel detector (488 nm). For data collection and analysis, BD Csampler™ analysis software (BD Biosciences, California, USA) was used.

1.2.2.2.2 Immunofluorescence analysis of E0771 derived tumours

After the imaging study, some of the tumours were collected and fixed in 75% ethanol. Thin (10 µm) paraffin-embedded breast tumour sections were prepared and mounted on to slides as described in Chapter 3, section 2.2.6. The sections were deparaffinised in xylene and rehydrated using graded ethanol from 100% to 70%, followed by distilled water for 5 min each step. To prevent non-specific binding, the sections were blocked with IHC/ICC blocking solution (100 µl) for 1 hr at room temperature followed by washing with PBS. The sections were then incubated with GLUT-1 primary antibody (5 µg/ml) diluted in IHC/ICC blocking solution at 4˚C in a humidified chamber overnight. The sections were washed with PBS and incubated with goat anti-rabbit IgG (H + L) secondary antibody (FITC) (5 µg/ml) in a humidified chamber for 1 hr in the dark at room temperature. For the blank control, the sections were incubated with IHC/ICC blocking solution (100 µl) without antibodies. The sections were counterstained by incubating for 10 min, at room temperature, with Hoechst nuclear stain (1 µg/ml). After counterstaining, the sections were washed with PBS and mounted with drops of glycerol. Images were captured by a Nikon D- Eclipse C1 confocal laser scanning microscope, equipped with EZ-C1 Gold Version 3.80 software (Nikon, Japan), using 60x oil immersion magnification at 408 nm and 488nm excitation wavelengths for Hoechst and FITC, respectively, detected in the emission ranges of 450-435 nm and 515-530 nm, respectively.

1.3 Results

1.3.1 Imaging and biodistribution of ^{64}Cu-GluCAB

The capability of ^{64}Cu-GluCAB to locate and image tumours *in vivo* was investigated using microPET/CT. The imaging of three E0771 tumour-bearing mice after ^{64}Cu-GluCAB administration was done at different time points using micro-PET/CT as shown in Figure 2. Based

on the microPET/CT images obtained at the different time points, the compound could not be visualised at the site of the tumour. However, radioactivity was seen in the heart, liver and intestines as an indication of the retention, accumulation and excretion of ^{64}Cu-GluCAB. The highest uptake observed following analysis of the images was at 6 hrs after administration.

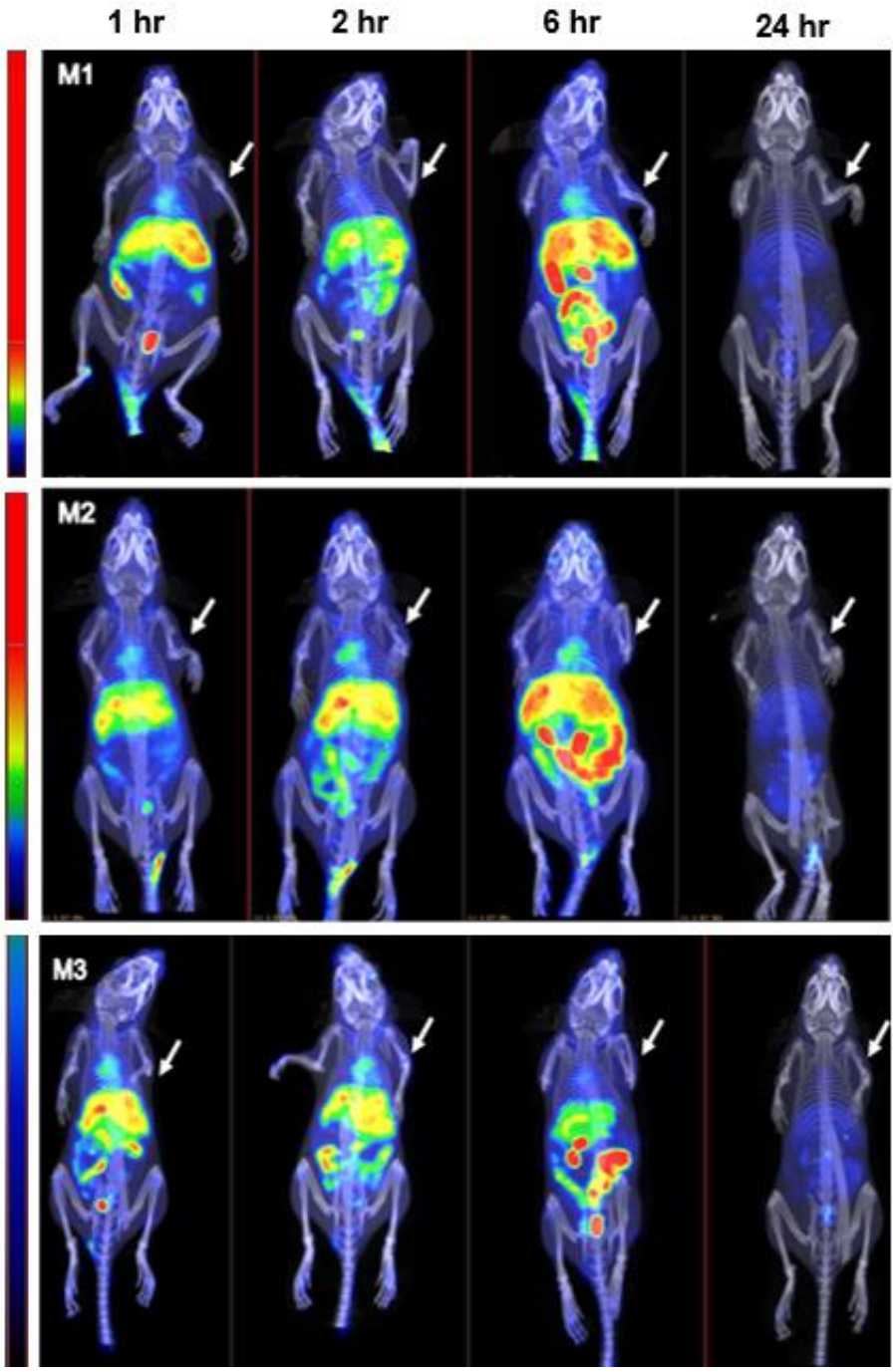

Figure 2: Maximum intensity projection (MIP) microPET/CT images of C57BL/6 mice bearing E0771 tumours at 1, 2, 6, and 24 hrs post intravenous administration of ^{64}Cu-GluCAB. The arrows indicate the E0771 derived tumour in the mammary fat pad. Inset numbers represent the mouse numbers.

Immediately after the imaging study, different organs and tissues, including the tumours, were harvested to investigate tissue distribution by measuring the radioactivity using a gamma detector. Figure 3 shows *in vivo* biodistribution of ^{64}Cu-GluCAB 24 hrs post administration. In correlation with the imaging data, high uptake was observed in the liver followed by the plasma and large intestine with 4.07 ± 0.21, 3.63 ± 0.80 and 2.82 ± 1.29 %ID/g respectively, as compared to the tumour (0.95 ± 0.30 %ID/g). Furthermore, no noticeable amount of radioactivity was detected in the brain, showing that ^{64}Cu-GluCAB does not cross the blood-brain barrier.

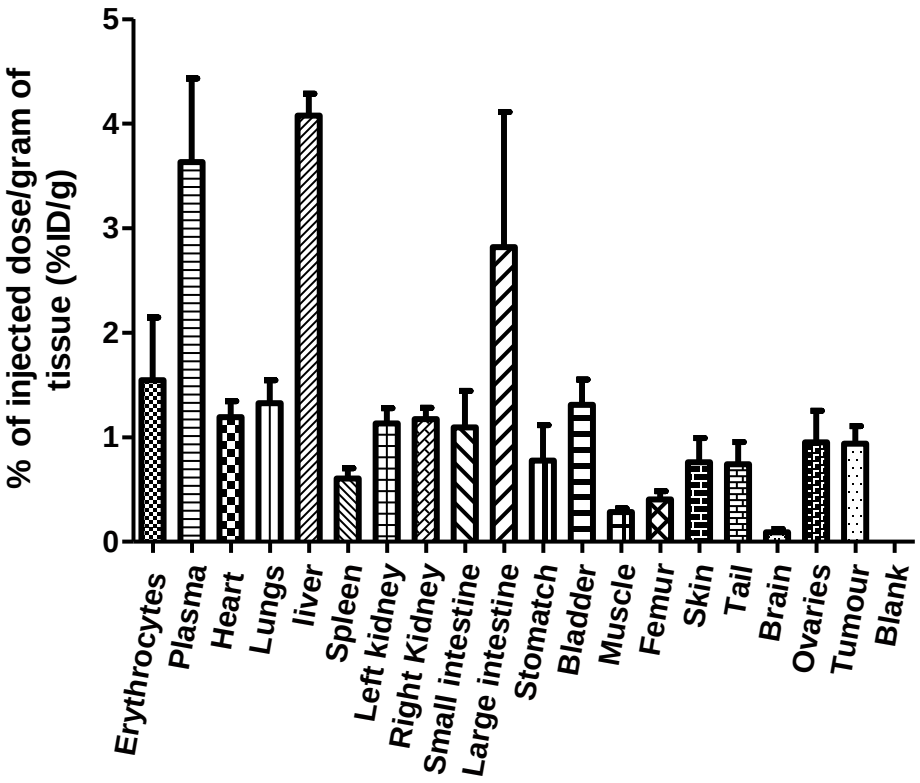

Figure 3: Biodistribution profile of ^{64}Cu-GluCAB in E0771 derived tumour mouse model (n=4) 24 hrs after intravenous administration into the tail. The data represents mean ± standard deviation (SD) of the percentage of the injected dose per gram of tissue (%ID/g).

In addition, a tumour-to-muscle uptake ratio of 0.33 ± 0.47%ID/g was found, and based on one-way ANOVA, the radioactivity was not significantly different ($p>0.05$) to uptake in the other organs, except for the liver and large intestine with organ-to-muscle uptake ratio of 1.44 ± 0.58 and 0.99 ± 3.63 %ID/g, respectively ($p<0.05$). Although tumour uptake was obtained, these results indicate that the uptake of ^{64}Cu-GluCAB was not tumour specific.

1.3.2 GLUT-1 receptor expression

1.3.2.1 Flow cytometry analysis of E0771 cells

Flow cytometry was used for quantitative and qualitative analysis of GLUT-1 receptor expression in the E0771 cells using an antibody against GLUT-1. As shown in Figure 4A, 8.2% of E0771 cells stained positive for GLUT-1 receptor with no autofluorescence of cells detected, as indicated by analysis of the control (Figure 4B). To ensure data reproducibility, the experiment was repeated four times, but based on the data as indicated in Table 1, the results were inconsistent. The optimum storage condition of GLUT1 antibody is -20˚C or -80˚C, however, from the start of the experimental period, the antibody was stored at 4˚C. The inconsistent results (as indicated in Table 1) could be because the antibody may have denatured when stored at 4˚C. However, it is apparent from the data that the antibody was still active after 3 days of storage at 4˚C, as 4.8% of the cells stained positive implying that the denaturing process was gradual.

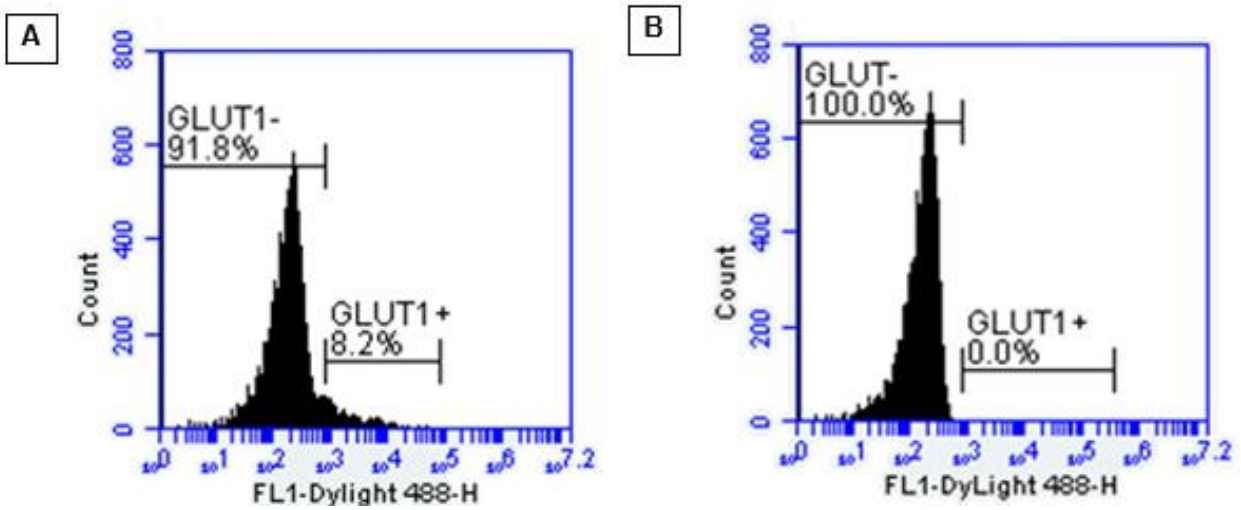

Figure 4: Representative flow cytometry analysis of GLUT-1 receptor in E0771 cells. Indirect staining of E0771 cells **(A)** with and **(B)** without (blank control) GLUT-1 antibody labelled with DyLight 488 antibody.

Table 1: Results of flow cytometry experiments performed to detect GLUT-1 receptor in E0771 cells.

Experiment day	GLUT-1	Positive cells (%)
1	+	8.2
3	+	4.8
4	-	0
4	-	0

1.3.2.2 Immunofluorescence analysis of E0771 derived tumours

After the biodistribution study, tumour tissues (n=2) derived from E0771 cells were immediately fixed in 75% ethanol GLUT-1 receptor expression using indirect immunofluorescence staining. Unfortunately, during the staining process most of the sections were lost, and therefore, only one tumour tissue was processed. The blank control, counterstained with Hoechst nuclear stain was captured in the blue, red and green channel of the confocal microscope simultaneously (Figure 5A). The cells exhibited nuclear staining detected in the blue channel, with tissue autofluorescence detected by the red and green channel. The GLUT-1 antibody used for flow cytometry was labelled with a FITC secondary antibody for detection of GLUT-1 expression. GLUT-1 is a membrane-bound receptor and as expected, the FITC fluorophore (green) (Figure 5B) was confined to the cell membrane. However, due to the use of a primary antibody that was possibly denatured and tissue autofluorescence detected in the blank control, it was concluded that the observations in Figure 5B were false-positive.

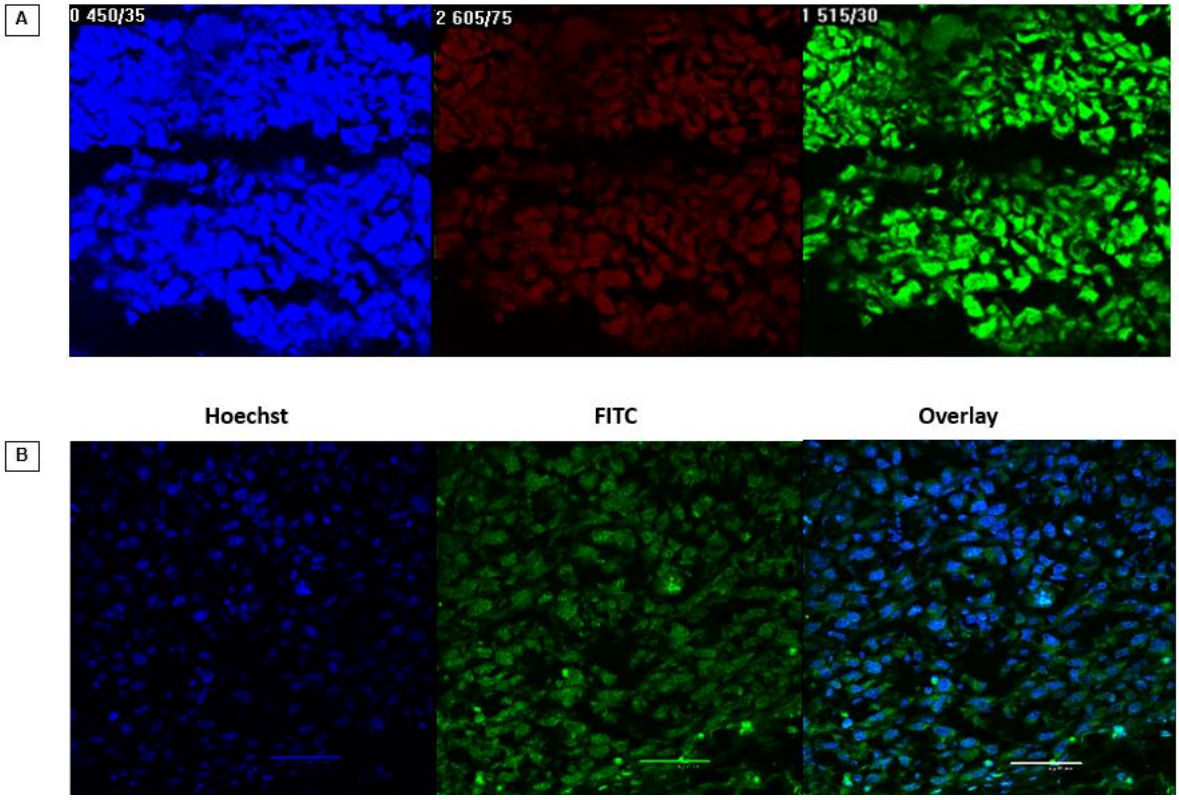

Figure 5: Indirect immunofluorescence staining of the GLUT-1 receptor in E0771 derived tumour sections. **(A).** Blank control stained with Hoechst only shown in the blue, red and green channel. **(B)**. Secondary staining of GLUT-1antibody with FITC antibody (green channel) and Hoechst counterstain is shown in the (blue channel). To localise the GLUT-1 receptor, the nucleus stain (Hoechst) was overlaid with FITC fluorophore. All images were captured at emission ranges of 450-435 nm (Hoescht) and 515-530 nm (FITC) using 60x oil immersion magnification.

1.4 Discussion

For *in vivo* imaging of a tumour, both the physical properties of the imaging radiopharmaceutical and the physiology of the tumour have an influence on tumour uptake (Zhang *et al.*, 2016). However, since the focus of this study was to investigate the application of E0771 tumour model for evaluation of ^{64}Cu-GluCAB in tumour imaging and not the physical properties of the compound, this discussion will only focus on the effect of the tumour physiology.

According to the proposed mechanism of action of ^{64}Cu-GluCAB, the precursor should first bind to albumin after administration, which will then facilitate the delivery of the compound to the site of the tumour. Albumin is the most abundant protein in plasma (Liu & Chen, 2016) and based on the biodistribution results, higher retention of the compound was obtained in the plasma. This suggests that the ^{64}Cu-GluCAB precursor (without albumin) was successfully bound to albumin,

which increased the compound's circulation time and presence in blood pool as proven by the visibility of the heart in the microPET/CT images.

The proposed targeting mechanism of ^{64}Cu-GluCAB relied mainly on the EPR effect (high and leaky vascularisation) and GLUT-1 receptor expression of the E0771 derived tumours. These two targeting approaches are rate-limiting factors, which could have compromised tumour specific delivery and uptake of the compound, and will be briefly discussed in relation to the application of the E0771 derived tumour model in preclinical evaluation of ^{64}Cu-GluCAB for tumour imaging.

With regard to the vascularisation, Mei *et al*. (2016) demonstrated that variation in tumour vascularity in different tumour-bearing mouse models had an effect on compound biodistribution, with high vascularity leading to higher tumour uptake. In this study, after administration of ^{64}Cu-GluCAB, the microPET/CT images did not show tumour radioactivity. The biodistribution profile and organ-to-muscle uptake ratio results indicated that some activity was present in the tumour, but the tumour uptake was not significantly different in comparison to other organs. These findings suggest that ^{64}Cu-GluCAB uptake was not tumour specific as expected and the radioactivity signal was too low to be clearly differentiated from the background tissue using microPET/CT imaging. Another possibility for the poor uptake is due to poor tumour vascularisation. However, based on Chapter 3, the histological analysis of E0771 derived tumour revealed infiltration of the tumours by blood vessels, but H & E staining was not applicable for quantification of vascularisation (Leung & Jensen, 2013).

Although blood flow is responsible for the delivery of the imaging compound to the tumour, the targeted receptor determines the binding and the retention of the agent by the tumour (Zhang *et al.*, 2016), hence, the other determining factor of ^{64}Cu-GluCAB biodistribution was the expression level of GLUT-1 receptors. A study by Glass *et al.* (2017) previously demonstrated the expression of GLUT-1 in E0771 tumour cells using western blot. Unfortunately, in this study, due to the denatured GLUT-1 antibody, the expression of GLUT-1 in E0771 cells and E0771 derived tumours using flow cytometry and immunofluorescence staining, respectively, could not be confirmed. In spite of this, the radioactivity of ^{64}Cu-GluCAB was shown in the biodistribution profile, possibly due to passive targeting and EPR effect. Another possible explanation could be that the minimal tumour uptake obtained was due to low expression levels of the GLUT-1 receptor, however, further investigation is required to confirm this.

Together with the biodistribution profile, the imaging data showed increased radioactivity in the liver and gastrointestinal tract. Therefore, this data suggests that ^{64}Cu-GluCAB is eliminated via the hepatobiliary excretion route as expected for a large protein/macromolecule that cannot pass through the glomerular filtration system of the kidneys (Vegt *et al.*, 2010). The liver has the highest blood perfusion compared to other organs (Anger, 2014) and in addition, GLUT-1 is moderately

expressed in the liver, with high expression of GLUT-2 found mainly in the liver, pancreas, kidney and gastrointestinal tract (Brown, 2000; Navale & Paranjape, 2016; Wood & Trayhurn, 2003). This might explain the increased hepatic accumulation observed relative to the tumour. Unfortunately, it could not be confirmed if the increased liver uptake of ^{64}Cu-GluCAB was mainly due to hepatic clearance, high blood perfusion or a higher affinity for GLUT-2 receptor compared to GLUT-1.

1.5 Conclusion

Although some uptake (as determined by *ex vivo* biodistribution) of ^{64}Cu-GluCAB was found in the tumour, it was not possible to locate and visualise the breast tumour using microPET/CT imaging. To illustrate the suitability of the breast tumour model for evaluation of ^{64}Cu-GluCAB tumour-target specificity, GLUT-1 expression was investigated. However, due to insufficient data, no conclusions could be made as to whether the tumour model was appropriate for investigation of ^{64}Cu-GluCAB.

REFERENCES

Anger, C. 2014. Physiological ranges and variability in organ blood flow in laboratory animals. https://stud.epsilon.slu.se/6673/ Date of access: 20 Oct 2018.

Bhushan, B., Khanadeev, V., Khlebtsov, B., Khlebtsov, N. & Gopinath, P. 2017. Impact of albumin based approaches in nanomedicine: imaging, targeting and drug delivery. *Advances in colloid and interface science*, 246:13-39.

Brown, G.K. 2000. Glucose transporters: Structure, function and consequences of deficiency. *Journal of inherited metabolic disease*, 23(3):237-246.

Cardinale, J., Schäfer, M., Benešová, M., Bauder-Wüst, U., Leotta, K., Eder, M., Neels, O.C., Haberkorn, U., Giesel, F.L. & Kopka, K. 2017. Preclinical evaluation of 18F-PSMA-1007, a new prostate-specific membrane antigen ligand for prostate cancer imaging. *Journal of nuclear medicine*, 58(3):425-431.

Carvalho, K.C., Cunha, I.W., Rocha, R.M., Ayala, F.R., Cajaíba, M.M., Begnami, M.D., Vilela, R.S., Paiva, G.R., Andrade, R.G. & Soares, F.A. 2011. GLUT1 expression in malignant tumors and its use as an immunodiagnostic marker. *Clinics*, 66(6):965-972.

Chen, Y., Xiong, Q.-F., Yang, X.-Q., He, L. & Huang, Z.-W. 2010. Evaluation of ^{188}Re-DTPA-Deoxyglucose as a potential cancer radiopharmaceutical. *American journal of roentgenology*, 194(3):761-765.

Danhier, F., Feron, O. & Préat, V. 2010. To exploit the tumor microenvironment: passive and active tumor targeting of nanocarriers for anti-cancer drug delivery. *Journal of controlled release*, 148(2):135-146.

Fass, L. 2008. Imaging and cancer: a review. *Molecular oncology*, 2(2):115-152.

Glass, O.K., Bowie, M., Fuller, J., Darr, D., Usary, J., Boss, K., Choudhury, K.R., Liu, X., Zhang, Z. & Locasale, J.W. 2017. Differential response to exercise in claudin-low breast cancer. *Oncotarget*, 8(60):100989.

Griffeth, L.K. 2005. Use of PET/CT scanning in cancer patients: technical and practical considerations. *Proceedings (Baylor University. Medical Center)*, 18(4):321-330.

Hu, C., Liu, C.-P., Cheng, J.-S., Chiu, Y.-L., Chan, H.-P. & Peng, N.-J. 2016. Application of whole-body FDG-PET for cancer screening in a cohort of hospital employees. *Medicine*, 95(44):e5131.

Hussain, T. & Nguyen, Q.T. 2014. Molecular imaging for cancer diagnosis and surgery. *Advanced drug delivery reviews*, 66:90-100.

Kaira, K., Oriuchi, N., Sunaga, N., Ishizuka, T., Shimizu, K. & Yamamoto, N. 2011. A systemic review of PET and biology in lung cancer. *American journal of translational research*, 3(4):383.

Kelland, L.R. 2004. Of mice and men: values and liabilities of the athymic nude mouse model in anticancer drug development. *European journal of cancer*, 40(6):827-836.

Killion, J.J., Radinsky, R. & Fidler, I.J. 1998. Orthotopic models are necessary to predict therapy of transplantable tumors in mice. *Cancer and metastasis reviews*, 17(3):279-284.

Kratz, F. 2008. Albumin as a drug carrier: design of prodrugs, drug conjugates and nanoparticles. *Journal of controlled release*, 132(3):171-183.

Leung, W.Y. & Jensen, M.B. 2013. Histological quantification of angiogenesis after focal cerebral infarction: a systematic review. *ISRN neurology*, 2013:1-5.

Liang, H., Yang, Y., Yang, K., Wu, Y., Boone, J. & Cherry, S. 2007. A microPET/CT system for *in vivo* small animal imaging. *Physics in medicine & biology*, 52(13):3881.

Liu, Z. & Chen, X. 2016. Simple bioconjugate chemistry serves great clinical advances: albumin as a versatile platform for diagnosis and precision therapy. *Chemical Society Reviews*, 45(5):1432-1456.

Maeda, H., Wu, J., Sawa, T., Matsumura, Y. & Hori, K. 2000. Tumor vascular permeability and the EPR effect in macromolecular therapeutics: a review. *Journal of controlled release*, 65(1):271-284.

Mankoff, D.A. 2007. A definition of molecular imaging. *Journal of nuclear medicine*, 48(6):18N-21N.

Navale, A.M. 2013. Animal models of cancer: a review. *International Journal of Pharmaceutical Sciences and Research*, 4(1):19.

Navale, A.M. & Paranjape, A.N. 2016. Glucose transporters: physiological and pathological roles. *Biophysical reviews*, 8(1):5-9.

Pimlott, S.L. & Sutherland, A. 2011. Molecular tracers for the PET and SPECT imaging of disease. *Chemical Society Reviews*, 40(1):149-162.

Ping Li, W., Meyer, L.A., Capretto, D.A., Sherman, C.D. & Anderson, C.J. 2008. Receptor-binding, biodistribution, and metabolism studies of ^{64}Cu-DOTA-cetuximab, a PET-imaging agent for epidermal growth-factor receptor-positive tumors. *Cancer biotherapy & radiopharmaceuticals*, 23(2):158-171. (Abstract).

Pysz, M.A., Gambhir, S.S. & Willmann, J.K. 2010. Molecular imaging: current status and emerging strategies. *Clinical radiology*, 65(7):500-516.

Schuh, J.C.L. 2004. Trials, tribulations, and trends in tumor modeling in mice. *Toxicologic pathology*, 32(1_suppl):53-66.

Sharma, P. & Mukherjee, A. 2016. Newer positron emission tomography radiopharmaceuticals for radiotherapy planning: an overview. *Annals of translational medicine*, 4(3):53.

Suggitt, M. & Bibby, M.C. 2005. 50 Years of preclinical anticancer drug screening: empirical to target-driven approaches. *Clinical cancer research*, 11(3):971-981.

Vegt, E., De Jong, M., Wetzels, J.F., Masereeuw, R., Melis, M., Oyen, W.J., Gotthardt, M. & Boerman, O.C. 2010. Renal toxicity of radiolabeled peptides and antibody fragments: mechanisms, impact on radionuclide therapy, and strategies for prevention. *Journal of nuclear medicine*, 51(7):1049-1058.

Wang, H., Naghavi, M., Allen, C., Barber, R.M., Bhutta, Z.A., Carter, A., Casey, D.C., Charlson, F.J., Chen, A.Z., Coates, M.M., Coggeshall, M., Dandona, L., Dicker, D.J., Erskine, H.E., Ferrari, A.J., Fitzmaurice, C., Foreman, K., Forouzanfar, M.H., Fraser, M.S., Fullman, N., Gething, P.W., Goldberg, E.M., Graetz, N., Haagsma, J.A., Hay, S.I., Huynh, C., Johnson, C.O., Kassebaum, N.J., Kinfu, Y., Kulikoff, X.R., Kutz, M., Kyu, H.H., Larson, H.J., Leung, J., Liang, X., Lim, S.S., Lind, M., Lozano, R., Marquez, N., Mensah, G.A., Mikesell, J., Mokdad, A.H., Mooney, M.D.,

Nguyen, G., Nsoesie, E., Pigott, D.M., Pinho, C., Roth, G.A., Salomon, J.A., Sandar, L., Silpakit, N., Sligar, A., Sorensen, R.J.D., Stanaway, J., Steiner, C., Teeple, S., Thomas, B.A., Troeger, C., VanderZanden, A., Vollset, S.E., Wanga, V., Whiteford, H.A., Wolock, T., Zoeckler, L., Abate, K.H., Abbafati, C., Abbas, K.M., Abd-Allah, F., Abera, S.F., Abreu, D.M.X., Abu-Raddad, L.J., Abyu, G.Y., Achoki, T., Adelekan, A.L., Ademi, Z., Adou, A.K., Adsuar, J.C., Afanvi, K.A., Afshin, A., Agardh, E.E., Agarwal, A., Agrawal, A., Kiadaliri, A.A., Ajala, O.N., Akanda, A.S., Akinyemi, R.O., Akinyemiju, T.F., Akseer, N., Lami, F.H.A., Alabed, S., Al-Aly, Z., Alam, K., Alam, N.K.M., Alasfoor, D., Aldhahri, S.F., Aldridge, R.W., Alegretti, M.A., Aleman, A.V., Alemu, Z.A., Alexander, L.T., Alhabib, S., Ali, R., Alkerwi, A.a., Alla, F., Allebeck, P., Al-Raddadi, R., Alsharif, U., Altirkawi, K.A., Martin, E.A., Alvis-Guzman, N., Amare, A.T., Amegah, A.K., Ameh, E.A., Amini, H., Ammar, W., Amrock, S.M., Andersen, H.H., Anderson, B.O., Anderson, G.M., Antonio, C.A.T., Aregay, A.F., Ärnlöv, J., Arsenijevic, V.S.A., Artaman, A., Asayesh, H., Asghar, R.J., Atique, S., Avokpaho, E.F.G.A., Awasthi, A., Azzopardi, P., Bacha, U., Badawi, A., Bahit, M.C., Balakrishnan, K., Banerjee, A., Barac, A., Barker-Collo, S.L., Bärnighausen, T., Barregard, L., Barrero, L.H., Basu, A., Basu, S., Bayou, Y.T., Bazargan-Hejazi, S., Beardsley, J., Bedi, N., Beghi, E., Belay, H.A., Bell, B., Bell, M.L., Bello, A.K., Bennett, D.A., Bensenor, I.M., Berhane, A., Bernabé, E., Betsu, B.D., Beyene, A.S., Bhala, N., Bhalla, A., Biadgilign, S., Bikbov, B., Abdulhak, A.A.B., Biroscak, B.J., Biryukov, S., Bjertness, E., Blore, J.D., Blosser, C.D., Bohensky, M.A., Borschmann, R., Bose, D., Bourne, R.R.A., Brainin, M., Brayne, C.E.G., Brazinova, A., Breitborde, N.J.K., Brenner, H., Brewer, J.D., Brown, A., Brown, J., Brugha, T.S., Buckle, G.C., Butt, Z.A., Calabria, B., Campos-Nonato, I.R., Campuzano, J.C., Carapetis, J.R., Cárdenas, R., Carpenter, D.O., Carrero, J.J., Castañeda-Orjuela, C.A., Rivas, J.C., Catalá-López, F., Cavalleri, F., Cercy, K., Cerda, J., Chen, W., Chew, A., Chiang, P.P.-C., Chibalabala, M., Chibueze, C.E., Chimed-Ochir, O., Chisumpa, V.H., Choi, J.-Y.J., Chowdhury, R., Christensen, H., Christopher, D.J., Ciobanu, L.G., Cirillo, M., Cohen, A.J., Colistro, V., Colomar, M., Colquhoun, S.M., Cooper, C., Cooper, L.T., Cortinovis, M., Cowie, B.C., Crump, J.A., Damsere-Derry, J., Danawi, H., Dandona, R., Daoud, F., Darby, S.C., Dargan, P.I., das Neves, J., Davey, G., Davis, A.C., Davitoiu, D.V., de Castro, E.F., de Jager, P., Leo, D.D., Degenhardt, L., Dellavalle, R.P., Deribe, K., Deribew, A., Dharmaratne, S.D., Dhillon, P.K., Diaz-Torné, C., Ding, E.L., dos Santos, K.P.B., Dossou, E., Driscoll, T.R., Duan, L., Dubey, M., Duncan, B.B., Ellenbogen, R.G., Ellingsen, C.L., Elyazar, I., Endries, A.Y., Ermakov, S.P., Eshrati, B., Esteghamati, A., Estep, K., Faghmous, I.D.A., Fahimi, S., Faraon, E.J.A., Farid, T.A., Farinha, C.S.e.S., Faro, A., Farvid, M.S., Farzadfar, F., Feigin, V.L., Fereshtehnejad, S.-M., Fernandes, J.G., Fernandes, J.C., Fischer, F., Fitchett, J.R.A., Flaxman, A., Foigt, N., Fowkes, F.G.R., Franca, E.B., Franklin, R.C., Friedman, J., Frostad, J., Fürst, T., Futran, N.D., Gall, S.L., Gambashidze, K., Gamkrelidze, A., Ganguly, P., Gankpé, F.G., Gebre, T., Gebrehiwot, T.T., Gebremedhin, A.T., Gebru, A.A., Geleijnse, J.M., Gessner, B.D., Ghoshal, A.G., Gibney, K.B., Gillum, R.F., Gilmour, S., Giref, A.Z., Giroud, M., Gishu, M.D., Giussani, G., Glaser, E., Godwin, W.W., Gomez-Dantes, H., Gona, P., Goodridge, A., Gopalani, S.V., Gosselin, R.A., Gotay, C.C., Goto, A., Gouda, H.N., Greaves, F., Gugnani, H.C., Gupta, R., Gupta, R., Gupta, V., Gutiérrez, R.A., Hafezi-Nejad, N., Haile, D., Hailu, A.D., Hailu, G.B., Halasa, Y.A., Hamadeh, R.R., Hamidi, S., Hancock, J., Handal, A.J., Hankey, G.J., Hao, Y., Harb, H.L., Harikrishnan, S., Haro, J.M., Havmoeller, R., Heckbert, S.R., Heredia-Pi, I.B., Heydarpour, P., Hilderink, H.B.M., Hoek, H.W., Hogg, R.S., Horino, M., Horita, N., Hosgood, H.D., Hotez, P.J., Hoy, D.G., Hsairi, M., Htet, A.S., Htike, M.M.T., Hu, G., Huang, C., Huang, H., Huiart, L., Husseini, A., Huybrechts, I., Huynh, G., Iburg, K.M., Innos, K., Inoue, M., Iyer, V.J., Jacobs, T.A., Jacobsen, K.H., Jahanmehr, N., Jakovljevic, M.B., James, P., Javanbakht, M., Jayaraman, S.P., Jayatilleke, A.U., Jeemon, P., Jensen, P.N., Jha, V., Jiang, G., Jiang, Y., Jibat, T., Jimenez-Corona, A., Jonas, J.B., Joshi, T.K., Kabir, Z., Kamal, R., Kan, H., Kant, S., Karch, A., Karema, C.K., Karimkhani, C., Karletsos, D., Karthikeyan, G., Kasaeian, A., Katibeh, M., Kaul, A., Kawakami, N., Kayibanda, J.F., Keiyoro, P.N., Kemmer, L., Kemp, A.H., Kengne, A.P., Keren, A., Kereselidze, M., Kesavachandran, C.N., Khader, Y.S., Khalil, I.A., Khan, A.R., Khan, E.A., Khang, Y.-H., Khera, S., Khoja, T.A.M., Kieling, C., Kim, D., Kim, Y.J., Kissela, B.M., Kissoon, N., Knibbs, L.D., Knudsen, A.K., Kokubo, Y., Kolte, D., Kopec, J.A., Kosen, S., Koul, P.A., Koyanagi, A., Krog, N.H., Defo, B.K., Bicer, B.K., Kudom, A.A., Kuipers, E.J., Kulkarni, V.S., Kumar, G.A., Kwan, G.F., Lal, A., Lal, D.K., Lalloo, R., Lallukka, T., Lam, H., Lam, J.O., Langan, S.M., Lansingh, V.C., Larsson, A., Laryea, D.O., Latif, A.A., Lawrynowicz, A.E.B., Leigh, J., Levi, M., Li, Y., Lindsay,

M.P., Lipshultz, S.E., Liu, P.Y., Liu, S., Liu, Y., Lo, L.-T., Logroscino, G., Lotufo, P.A., Lucas, R.M., Lunevicius, R., Lyons, R.A., Ma, S., Machado, V.M.P., Mackay, M.T., MacLachlan, J.H., Razek, H.M.A.E., Magdy, M., Razek, A.E., Majdan, M., Majeed, A., Malekzadeh, R., Manamo, W.A.A., Mandisarisa, J., Mangalam, S., Mapoma, C.C., Marcenes, W., Margolis, D.J., Martin, G.R., Martinez-Raga, J., Marzan, M.B., Masiye, F., Mason-Jones, A.J., Massano, J., Matzopoulos, R., Mayosi, B.M., McGarvey, S.T., McGrath, J.J., McKee, M., McMahon, B.J., Meaney, P.A., Mehari, A., Mehndiratta, M.M., Mejia-Rodriguez, F., Mekonnen, A.B., Melaku, Y.A., Memiah, P., Memish, Z.A., Mendoza, W., Meretoja, A., Meretoja, T.J., Mhimbira, F.A., Micha, R., Millear, A., Miller, T.R., Mirarefin, M., Misganaw, A., Mock, C.N., Mohammad, K.A., Mohammadi, A., Mohammed, S., Mohan, V., Mola, G.L.D., Monasta, L., Hernandez, J.C.M., Montero, P., Montico, M., Montine, T.J., Moradi-Lakeh, M., Morawska, L., Morgan, K., Mori, R., Mozaffarian, D., Mueller, U.O., Murthy, G.V.S., Murthy, S., Musa, K.I., Nachega, J.B., Nagel, G., Naidoo, K.S., Naik, N., Naldi, L., Nangia, V., Nash, D., Nejjari, C., Neupane, S., Newton, C.R., Newton, J.N., Ng, M., Ngalesoni, F.N., de Dieu Ngirabega, J., Nguyen, Q.L., Nisar, M.I., Pete, P.M.N., Nomura, M., Norheim, O.F., Norman, P.E., Norrving, B., Nyakarahuka, L., Ogbo, F.A., Ohkubo, T., Ojelabi, F.A., Olivares, P.R., Olusanya, B.O., Olusanya, J.O., Opio, J.N., Oren, E., Ortiz, A., Osman, M., Ota, E., Ozdemir, R., Pa, M., Pain, A., Pandian, J.D., Pant, P.R., Papachristou, C., Park, E.-K., Park, J.-H., Parry, C.D., Parsaeian, M., Caicedo, A.J.P., Patten, S.B., Patton, G.C., Paul, V.K., Pearce, N., Pedro, J.M., Stokic, L.P., Pereira, D.M., Perico, N., Pesudovs, K., Petzold, M., Phillips, M.R., Piel, F.B., Pillay, J.D., Plass, D., Platts-Mills, J.A., Polinder, S., Pope, C.A., Popova, S., Poulton, R.G., Pourmalek, F., Prabhakaran, D., Qorbani, M., Quame-Amaglo, J., Quistberg, D.A., Rafay, A., Rahimi, K., Rahimi-Movaghar, V., Rahman, M., Rahman, M.H.U., Rahman, S.U., Rai, R.K., Rajavi, Z., Rajsic, S., Raju, M., Rakovac, I., Rana, S.M., Ranabhat, C.L., Rangaswamy, T., Rao, P., Rao, S.R., Refaat, A.H., Rehm, J., Reitsma, M.B., Remuzzi, G., Resnikoff, S., Ribeiro, A.L., Ricci, S., Blancas, M.J.R., Roberts, B., Roca, A., Rojas-Rueda, D., Ronfani, L., Roshandel, G., Rothenbacher, D., Roy, A., Roy, N.K., Ruhago, G.M., Sagar, R., Saha, S., Sahathevan, R., Saleh, M.M., Sanabria, J.R., Sanchez-Niño, M.D., Sanchez-Riera, L., Santos, I.S., Sarmiento-Suarez, R., Sartorius, B., Satpathy, M., Savic, M., Sawhney, M., Schaub, M.P., Schmidt, M.I., Schneider, I.J.C., Schöttker, B., Schutte, A.E., Schwebel, D.C., Seedat, S., Sepanlou, S.G., Servan-Mori, E.E., Shackelford, K.A., Shaddick, G., Shaheen, A., Shahraz, S., Shaikh, M.A., Shakh-Nazarova, M., Sharma, R., She, J., Sheikhbahaei, S., Shen, J., Shen, Z., Shepard, D.S., Sheth, K.N., Shetty, B.P., Shi, P., Shibuya, K., Shin, M.-J., Shiri, R., Shiue, I., Shrime, M.G., Sigfusdottir, I.D., Silberberg, D.H., Silva, D.A.S., Silveira, D.G.A., Silverberg, J.I., Simard, E.P., Singh, A., Singh, G.M., Singh, J.A., Singh, O.P., Singh, P.K., Singh, V., Soneji, S., Søreide, K., Soriano, J.B., Sposato, L.A., Sreeramareddy, C.T., Stathopoulou, V., Stein, D.J., Stein, M.B., Stranges, S., Stroumpoulis, K., Sunguya, B.F., Sur, P., Swaminathan, S., Sykes, B.L., Szoeke, C.E.I., Tabarés-Seisdedos, R., Tabb, K.M., Takahashi, K., Takala, J.S., Talongwa, R.T., Tandon, N., Tavakkoli, M., Taye, B., Taylor, H.R., Ao, B.J.T., Tedla, B.A., Tefera, W.M., Have, M.T., Terkawi, A.S., Tesfay, F.H., Tessema, G.A., Thomson, A.J., Thorne-Lyman, A.L., Thrift, A.G., Thurston, G.D., Tillmann, T., Tirschwell, D.L., Tonelli, M., Topor-Madry, R., Topouzis, F., Towbin, J.A., Traebert, J., Tran, B.X., Truelsen, T., Trujillo, U., Tura, A.K., Tuzcu, E.M., Uchendu, U.S., Ukwaja, K.N., Undurraga, E.A., Uthman, O.A., Dingenen, R.V., van Donkelaar, A., Vasankari, T., Vasconcelos, A.M.N., Venketasubramanian, N., Vidavalur, R., Vijayakumar, L., Villalpando, S., Violante, F.S., Vlassov, V.V., Wagner, J.A., Wagner, G.R., Wallin, M.T., Wang, L., Watkins, D.A., Weichenthal, S., Weiderpass, E., Weintraub, R.G., Werdecker, A., Westerman, R., White, R.A., Wijeratne, T., Wilkinson, J.D., Williams, H.C., Wiysonge, C.S., Woldeyohannes, S.M., Wolfe, C.D.A., Won, S., Wong, J.Q., Woolf, A.D., Xavier, D., Xiao, Q., Xu, G., Yakob, B., Yalew, A.Z., Yan, L.L., Yano, Y., Yaseri, M., Ye, P., Yebyo, H.G., Yip, P., Yirsaw, B.D., Yonemoto, N., Yonga, G., Younis, M.Z., Yu, S., Zaidi, Z., Zaki, M.E.S., Zannad, F., Zavala, D.E., Zeeb, H., Zeleke, B.M., Zhang, H., Zodpey, S., Zonies, D., Zuhlke, L.J., Vos, T., Lopez, A.D. & Murray, C.J.L. 2016. Global, regional, and national life expectancy, all-cause mortality, and cause-specific mortality for 249 causes of death, 1980–2015: a systematic analysis for the global burden of disease study 2015. *The Lancet*, 388(10053):1459-1544.

Wood, I.S. & Trayhurn, P. 2003. Glucose transporters (GLUT and SGLT): expanded families of sugar transport proteins. *British journal of nutrition*, 89(1):3-9.

Zhang, L., Bhatnagar, S., Deschenes, E. & Thurber, G.M. 2016. Mechanistic and quantitative insight into cell surface targeted molecular imaging agent design. *Scientific reports*, 6:25424.

CHAPTER 5: RESEARCH OUTCOMES, LIMITATIONS AND FUTURE RECOMMENDATIONS

1.1 Research outcomes

- The E0771 derived breast cancer allograft mouse model and OVCAR-3 derived human ovarian cancer xenograft mouse model were successfully developed. Growth patterns of each cell line were determined *in vivo*. Furthermore, it was demonstrated that co-injection of cells with Matrigel optimises proliferation of slow growing cells like OVCAR-3, post inoculation.

- The histological characterisation of E0771 and OVCAR-3 derived tumours provided evidence that the tumours were malignant and actively proliferating.

- The expression of GLUT-1 receptor in E0771 cells and E0771 derived tumour sections, for tumour targeting of ^{64}Cu-GluCAB was investigated. However, the results were inconclusive.

- Application of the E0771 breast tumour model in the evaluation of ^{64}Cu-GluCAB as a potential PET/CT radiopharmaceutical for cancer diagnostics was demonstrated. It was hypothesised that higher uptake of ^{64}Cu-GluCAB will be visualised at the site of the tumour using a microPET/CT scan. Although the biodistribution results obtained using gamma detection indicated tumour uptake of ^{64}Cu-GluCAB, tumour imaging was not successful.

1.2 Research limitations

- Both the negative and the positive control were not included for flow cytometry and Immunofluorescence analysis.

- ^{64}Cu-GluCAB is a complex dual-targeting imaging radiopharmaceutical compound proposed to target tumour vascularity and overexpression of GLUT-1 receptor. The investigation of GLUT-1 receptor expression in E0771 cells and E0771 derived tumour sections was hampered by the use of the denatured GLUT-1 antibody. The experiments could not be repeated due to resource limitations. The H & E analysis did not provide enough data about the degree of tumour vascularisation. Taken together, no conclusions could be made on whether the tumour model was appropriate for ^{64}Cu-GluCAB investigations

- Another possible limitation was the influence of the physical properties of ^{64}Cu-GluCAB on *in vivo* biodistribution. However, since the main focus of the current study was not on the compound we were unable to carry out further investigations.

- This is the first study to evaluate the application of ^{64}Cu-GluCAB for tumour imaging. Therefore, taking the study limitations into consideration, it was difficult to confirm whether the failure of ^{64}Cu-GluCAB to visualise the tumour *in vivo* was due to the limitations in the model or the influence of the compound's physical properties on *in vivo* biodistribution.

1.3 Future recommendations

- E0771 derived tumours exhibited lymphovascular invasion, which is an indicator of high risk of metastasis (Mohammed *et al.*, 2013). It would be interesting to investigate the E0771 cell line for modelling metastasis *in vivo*.

- Further optimisation of the *in vivo* growth of OVAR-3 cells could be carried out by increasing the number of cells.

- Flow cytometry and immunofluorescence staining should be repeated with viable GLUT- 1 antibody to confirm the expression of GLUT-1 receptor in E0771 cells and E0771 derived tumours.

- To optimise the flow cytometry and immunofluorescence staining protocols the following controls should be included:

    - Positive control: Human epithelial colorectal adenocarcinoma cells (Caco-2 cells), known to have high expression of GLUT-1 receptor (Harris et al., 1992) could be used.

    - Negative control: Follow the same procedure without the GLUT-1 primary antibody.

- For quantification of tumour vascularity, protein markers, such Von Willebrand factor, cluster of differentiation 31 (CD31) and vascular endothelial growth factor (Poncelet *et al.*, 2002), could be used.

- *In vitro* binding studies using ^{64}Cu-GluCAB could be used to select other suitable cell lines with high expression of the GLUT-1 receptor, which could be further used to develop tumour-bearing models for animal testing.

- ^{64}Cu-GluCAB should be further investigated to enhance tumour accumulation and uptake.

REFERENCES

Harris, D.S., Slot, J.W., Geuze, H.J. & James, D.E. 1992. Polarized distribution of glucose transporter isoforms in Caco-2 cells. Proceedings of the National Academy of Sciences, 89(16):7556-7560.

Mohammed, Z.M., McMillan, D.C., Edwards, J., Mallon, E., Doughty, J.C., Orange, C. & Going, J.J. 2013. The relationship between lymphovascular invasion and angiogenesis, hormone receptors, cell proliferation and survival in patients with primary operable invasive ductal breast cancer. *BMC clinical pathology*, 13(1):31.

Poncelet, C., Madelenat, P., Feldmann, G., Walker, F. & Darai, E. 2002. Expression of von Willebrand's factor, CD34, CD31, and vascular endothelial growth factor in uterine leiomyomas. *Fertility and sterility*, 78(3):581-586.

ANNEXURE 1: CONFERENCE PRESENTATIONS

ORAL PRESENTATIONS

Palesa C Koatale, Ambrose Okem, Kobus Venter, Anne Grobler and Rose Hayeshi. Establishment and characterisation of a mouse xenograft model of human ovarian cancer. The South African Society of Biochemistry and Molecular Biology (SASBMB) and the Federation of African Societies of Biochemistry and Molecular Biology (FASBMB) Conference. North-West University, Potchefstroom, South Africa: 8-11 July 2018.

POSTER PRESENTATIONS

Palesa C Koatale. Ambose Okem, Vusani Mandiwana, Rose Hayeshi, Cor Bester and Anne Grobler. Establishment of novel syngeneic and xenograft rodent mode. The South African association for laboratory animal science (SAALAS) International Conference. Cape Town, South Africa: 1-3 November 2017.

Rose Hayeshi, Riaan Van Wyk, Ambrose Okem, **Palesa C Koatale**, Cor Bester, Kobus Venter and Anne Grobler. Precinical technologies at the DST/NWU preclinical drug development platform in South Africa. World Preclinical Congress. Boston, MA: 18-21 June 2018.

Palesa C Koatale, Ambrose Okem, Kobus Venter, Antoinette Fick, Cor Bester and Rose Hayeshi. Establishment and characterization of allograft and xenograft cancer rodent models. Drug Safety Africa Conference. North-West University, Potchefstroom, South Africa: 20-22 November 2018.

ANNEXURE 2: JOURNAL PERMISSIONS FOR RE-USE OF FIGURES

THE NEW ENGLAND JOURNAL OF MEDICINE

If you have questions about using the RightsLink service, please contact:

RightsLink® Customer Support
+1-877-622-5543 (toll free)
+1-978-777-9929
Email: customercare@copyright.com

For general questions about NEJM Permissions, email permissions@nejm.org.

Permission for Authors

If you are the author of an article that has been published in NEJM, see Author Permissions.

Reuse of Content Within a Thesis or Dissertation

Content (full-text or portions thereof) may be used in print and electronic versions of a dissertation or thesis without formal permission from the Massachusetts Medical Society (MMS), Publisher of the *New England Journal of Medicine*.

The following credit line must be printed along with the copyrighted material:

> Reproduced with permission from (scientific reference citation), Copyright Massachusetts Medical Society.

Third-Party Content

Grants of permissions apply only to copyrighted materials that the MMS owns and not to copyrighted texts or illustrations from other sources.

Prohibited Uses

The *New England Journal of Medicine* (and its logo design) are registered trademarks of the Massachusetts Medical Society. NEJM does not grant permission for its logo, cover, or brand identity to be used in materials. Permission will not be granted for photographs depicting identifiable individuals.

Rights and Permissions (https://www.bioscience.org/rights-and-permissions)

Educational Use

Frontiers in Bioscience grants permission to all authors, readers and third parties of educational nature to reproduce and use published material and online resources as part of another publication or entity. This permission is granted free of charge provided that:

1. There is no charge, submission fee, royalty, honorarium, or any other monetary rewards for the use of the figure by the author, user, website, publisher, organizer or any other entity using the material.
2. The material is properly credited by including citing the source within the text or legend and including the full citation of the article in the reference section of educational material. When available, the DOI link should also be provided. If reproduced in CD format, the reference should be included in the same page that the material is included. If reproduced on a website, the reference should be linked to the article published in the Frontiers in Bioscience. Users who do not know the URL of the link can request it by providing the citation in an email to fbs@bioscience.org.
3. If used online, the use should be for a timeline not longer than 1 month. The educational use includes, for example, the use of a figure, table or text in a presentation, another article, a book chapter, newsletter, thesis, dissertations, classroom material, academic course, academic conference material, training material or posting of an abstract on a website. If your use complies with the above guideline, you do not need to obtain permission from Frontiers in Bioscience for the use of material.

However, if in doubt or if the use does not comply with the above guideline, please proceed below to the commercial use form.

Commercial Use

If the use of the material does not fall within the guidelines provided above (as “educational use”), then, the use requires a license and payment of an assessed fee. The license enables the user to reproduce the material. If your use falls within this category, please fill out the following form:

THE ROYAL SOCIETY OF CHEMISTRY

Thank you for your order!

Dear Ms. Palesa Koatale,

Thank you for placing your order through Copyright Clearance Center's RightsLink® service.

Order Summary

Licensee:	Ms. Palesa Koatale
Order Date:	May 17, 2018
Order Number:	4351420753904
Publication:	Dalton Transactions
Title:	Metallic radionuclides in the development of diagnostic and therapeutic radiopharmaceuticals
Type of Use:	Thesis/Dissertation
Order Total:	0.00 USD

View or print complete details of your order and the publisher's terms and conditions.

Sincerely,

Copyright Clearance Center

How was your experience? Fill out this survey to let us know.

Tel: +1-855-239-3415 / +1-978-646-2777
customercare@copyright.com
https://myaccount.copyright.com

ANNEXURE 3: LANGUAGE EDITING CERTIFICATE

Gill Smithies

Proofreading & Language Editing Services

59, Lewis Drive, Amanzimtoti, 4126, Kwazulu Natal

Cell: 071 352 5410 E-mail: moramist@vodamail.co.za

Work Certificate

To	Palesa Koatale
Address	DST/NWU Preclinical Drug Development Platform, Potchefstroom Campus, North West University
Date	09/11/2018
Subject	Establishment and characterisation of tumour bearing mouse models for evaluation of biodistribution of a radiopharmaceutical
Ref	GS/PK/01

I, Gill Smithies, certify that I have proofed the following dissertation, Establishment and characterisation of tumour-bearing mouse models for evaluation of biodistribution of a radiopharmaceutical, to the standard as required by NWU, Potchefstroom Campus.

Gill Smithies

09/11/2018